2020

Self-Assembled Metal Nanoparticle/Polymer Nanocomposites as Nanoreactors for One-Pot Reactions

Andrew Harrison
Virginia Commonwealth University

Self-Assembled Metal Nanoparticle/Polymer Nanocomposites as Nanoreactors for One-Pot Reactions

A dissertation submitted in partial fulfillment of the requirements for the degree of Doctor of Philosophy in Chemical Engineering at Virginia Commonwealth University

By

Andrew Harrison

Advisor

Christina Tang, Ph.D., Department of Chemical and Life Sciences Engineering

Advisory Committee

Everett E. Carpenter, Ph.D. M.B.A., Department of Chemistry

Carlos E. Castaño Londono, Ph.D., Department of Mechanical and Nuclear Engineering

Thomas D. Roper, Ph.D., Department of Chemical and Life Sciences Engineering

Vamsi Yadavalli, Ph.D., Department of Chemical and Life Sciences Engineering

Virginia Commonwealth University

Richmond, Virginia

August 24, 2020

Acknowledgements

First, I'd like to thank my parents and my family. You've been there every step of the way with support, encouragement, and love. Special thanks to Nana for making me complete summer workbooks during K-12. Though I hated working on them at the time, you were persistent in making sure that I continued learning and I attribute all of my subsequent academic opportunities and successes to you.

Thank you to my friends for providing comedic relief and, most of all, motivation. You're a beautiful group of overachievers.

To my committee members, thank you for your support and feedback throughout this process. I deeply appreciate your generosity with your expertise and genuine interest in my professional development.

I'd also like to specifically thank my advisor, Dr. Christina Tang, for giving a new graduate student with no background in chemical engineering a chance in her research lab. While it hasn't been easy, for either of us, you stuck with me and I've learned so much in the past 4 years under your patient guidance. I have genuinely appreciated your advice, and especially your foresight.

Finally, I'd like to thank my wife. We met at the beginning of this doctorate journey, you were the first person I got to share the news of my acceptance into the program, and throughout this entire process you have never wavered in your belief in me, even when I did. I love you. (Does THIS count as a mushy thing?)

Table of Contents

List of Figures

List of Tables

Abstract

Polymer nanoreactors incorporating gold nanoparticle catalysts were self-assembled via Flash Nanoprecipitation. The incorporated gold nanoparticles maintained catalytic activity, which was evaluated using reduction of 4-nitrophenol with sodium borohydride as a model reaction. The diffusion coefficient for 4-nitrophenol was determined by NMR and used to calculate the second Damköhler number, which indicated that the systems were not diffusion limited. Despite similar diffusion coefficients, catalytic performance was strongly affected by the co-precipitant. For example, the apparent reaction rate per surface area using castor oil was over 8-fold greater than polystyrene. Thus, we measured the partition coefficient of 4-nitrophenol between water and castor oil or toluene (to mimic polystyrene). The core material:water partition coefficient for castor oil was 7.81 ± 0.16 compared to 0.09 ± 0.01 for toluene. Including the partition coefficient in the Langmuir-Hinshelwood model, the intrinsic rate constants were comparable. Overall, the increase in apparent catalytic performance could be attributed to differences in reactant solubility rather than differences in mass transfer or intrinsic kinetics. Finally, the polymer nanoreactor were applied to the one-pot condensation of benzaldehyde with 4-nitrophenol performed in water at ambient conditions. The product spontaneous precipitated from the reaction mixture; the nanoreactors were stable in dispersion whereas citrate-stabilized gold and PEG-coated gold precipitated with the product. The product (analytically pure by NMR) was extracted from the precipitate with acetone resulting in a yield of 66%. Overall, these results demonstrate proof-of-principle that multiple reactions can be performed in one-pot and the product can spontaneously phase separate from the nanoreactor dispersion.

Chapter 1 : Review of Micellar Nanoreactors for Aqueous Catalysis with Metal Nanoparticles

1.1. Significance

The amount of waste and relative cost for the production of fine chemicals and pharmaceuticals ranks among the highest within chemical processing industries. This relative waste can be quantified by considering the E-factor, which is the mass of waste generated per the mass of product. Ideally, the E-factor would be zero (zero waste). The E-factor for the production of fine chemicals and pharmaceuticals compared to other industries is provided in Table 1.1. Much of this is due to the processing that takes place to produce and isolate the compounds of interest [1]. Organic solvents generally make up the majority of this waste, with first generation production of the common pharmaceutical sildenafil reportedly generating organic solvent waste around 1700 L kg^{-1} of product over a nine-step synthesis [1]. Assuming an organic solvent density around 1 g/mL that results in an E-factor of 1700. New technology is needed to shift the field away from organic solvents, including their use for reaction solutions and extraction techniques [2]. Drastic improvement in waste generation is possible, as evidenced by second generation synthetic processes for sildenafil production reducing waste to just 7 L kg^{-1} of product [1].

Table 1.1: E-Factors for various chemical industries

Industry	Product (tons)	E-factor (kg waste/kg product)
Oil	10^6 - 10^8	< 0.1
Bulk Chemicals	10^4 - 10^6	1 - 5
Fine Chemicals	10^2 - 10^4	5 - 50
Pharmaceutical	10 - 10^3	25 - 100

The use of aqueous reaction mixtures is highly desirable to reduce the harmful waste associated with organic solvents. Micellar structures are known to facilitate traditionally organic phase reactions in a bulk aqueous environment due to the stabilization of confined hydrophobic regions which promote the reaction [3–8]. This effectively reduces the amount of organic "solvent" necessary to perform a reaction from a milliliter or liter scale down to attoliter volumes. While this quality of micelles is highly beneficial for reducing organic solvent dependency, the ability to tailor the nanoreactor reaction environment is a significant challenge.

Further reduction of organic solvent use could be achieved by performing multiple reactions in a "one pot" reaction which would eliminate the need to perform extractions to isolate compounds of interest at intermediate steps [9–11]. Given the nature of chemical syntheses, multiple reactions are often required to produce the desired compound, with product isolation between each step. Performing multiple reactions within a single reaction solution reduces the need for wasteful organic solvent extractions. However, this often requires the use of multiple catalysts in order to perform each reaction independently [8,12]. Core-shell polymer nanoparticles and micelles have demonstrated the ability to perform such cascade and domino reactions in aqueous solutions, often reducing organic solvent waste by orders of magnitude [13–15].

1.2. Micellar Nanoreactors

Small molecule amphiphiles have been used to facilitate a wide range of reactions. For example, Lipshutz and co-workers have developed a series of "designer surfactants" for aqueous micellar catalysis. Using several generations of PEG based amphiphilic surfactants they have demonstrated nanoreactor applicability to a wide range of organic reactions such as cross-couplings [16–18], oxidations [19], reductions [20], and peptide synthesis [21] all in bulk aqueous solutions with high yield.

For aqueous Suzuki-Miyaura cross couplings, Lipshutz employed Pd homogenous catalysts and micellar nanoreactors formed using either polyoxyethanyl α-tocopheryl sebacate (PTS) [16], α-tocopheryl

poly(ethylene glycol) succinate (TPGS) or Triton-100 [17], among others [18] in 2% wt/wt aqueous solutions. TPGS and Triton-100 formed roughly 15 nm micelles in solution while PTS formed slightly larger 25 nm micelles. PTS micelles showed the most favorable reaction yields for iodoanisole couplings, nearly quantitative, and even allowed the coupling of 4-chlorobenzonitrile with 2,4-difluorophenylboronic acid in 96% yield [17]. The improvement in yield seen using PTS instead of the similar TPGS was attributed to the difference in the length of the lipophilic tails of the amphiphiles, with PTS supporting a larger hydrophobic micellar volume providing a hydrophilic lipophilic balance [16]. Drastic improvements in Heck couplings were noted with the addition of salt, also resulting in a 4-fold diameter increase for PTS micelles [18]. Recycling of the PTS micelles was carried out by extracting the aqueous reaction solution with ethyl acetate to remove the reagents/products. The aqueous reaction solution could then be reused with addition of more reagents and catalyst, for up to 10 times without noticeable loss of reagent conversion.

Benzylic alcohol oxidation to the corresponding aldehyde was also accomplished using micellar nanoreactors [19]. TPGS-750-M micelles were engineered to form larger micelles than previous studies [16–18], around 50 nm in diameter in order to take advantage of previously demonstrated benefits of larger micelles for reactions and the reported greater solubility of oxygen in organic solvents than aqueous environments [19]. Oxidation of 3-nitrobenzyl alcohol was carried out in a 2 wt% TPGS-750-M solution with catalytic amounts of CuBr (5 mol%), TEMPO (5 mol%), 2, 2-bipyridine (5 mol%), and N-methylimidazole (10 mol%) at room temperature in water. Complete conversion was achieved after 24 hours. Generally, greater than 80% isolated yields were achieved for primary alcohols, while secondary alcohols required heating to around 45°C to achieve similar yields. Benzylic alcohols were found to preferentially oxidize over aliphatic alcohols at room temperature. Recycling of the micelles was achieved with selective product extraction and reuse of the aqueous phase. Greater than 85% yield was achieved

after 5 recycles with a reported E-factor of 2.2. However, the calculation did not consider excess reagents or loss of catalyst.

Likewise, reductions were also studied using the TPGS-750-M micellar system using Fe/ppm Pd nanoparticle catalysts [20]. A variety of nitroarenes were reduced including those with halogen, cyano, ester, methylmercapto, hydroxyl, or carboxylic acid substituent groups. Generally, greater than 85% isolated yield was witnessed using sodium borohydride as the reducing agent in aqueous media at room temperature. One-pot tandem reactions were considered with reduction of the nitro- group and Boc protection of the resulting amine, resulting in yields greater than 90%. Another tandem reaction involving post-reduction oxidative cyclization was carried at 80°C using O_2 as the oxidant, resulting in the benzimidazole product with 94% yield. Recycling was possible with extraction of the product using ethyl acetate, neutralization of the aqueous media with HCl, and addition of sodium borohydride to activate the catalyst. Finally, sequential one-pot reactions were carried out involving reduction of a nitroarene followed by amidation with a carboxylic acid. E-factors were reported around 5-6 when considering only the use of the organic solvent.

Gold catalysts have also been employed in micellar reaction systems [22]. Cyclizations of allenes and allenols were catalyzed with gold bromide in either PTS or TPGS-750-M micellar solutions at room temperature. Again, TPGS-750-M solutions are shown to produce greater yields than comparable reactions utilizing PTS micelles and this is attributed to the increased size of TPGS-750-M micelles. Recycling was carried out on PTS solutions without loss of yield (~85%) for up to 4 runs, though some decreased activity is noted resulting in a longer reaction time. Catalyst leaching was observed, resulting in loss of 0.29% catalyst mass over 4 runs.

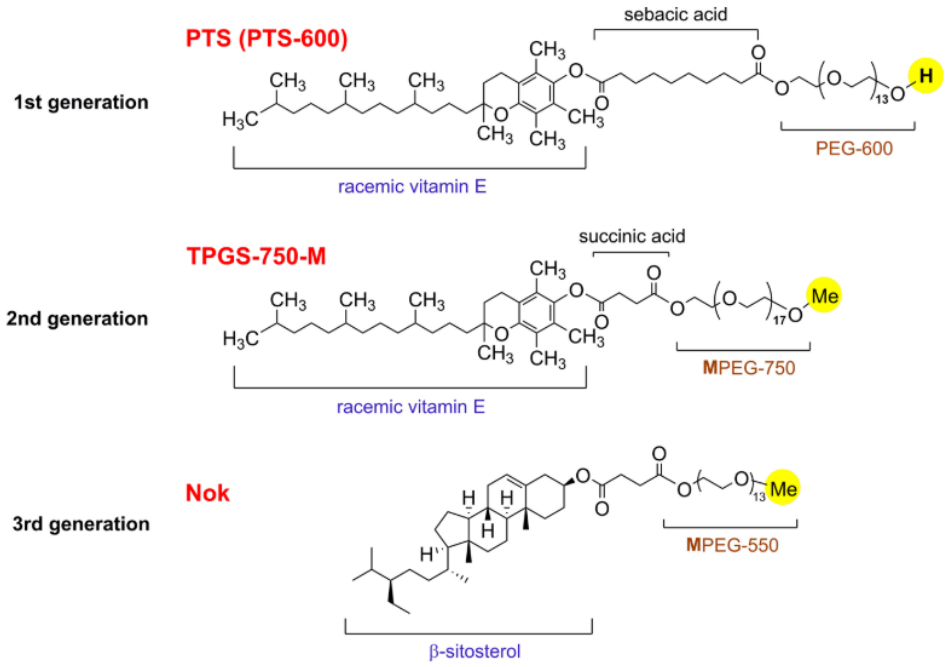

Figure 1.1: Generations of designer-surfactants for micellar catalysis in water [23].

Size and hydrophobicity are central elements when designing surfactants for micellar nanoreactors. By designing a surfactant molecule (shown in Figure 1.1) with a longer PEG portion and a shorter carbon linker between vitamin E and PEG, the generated micelles were larger and faster reactions were observed [23] in various transition metal-catalyzed reactions (e.g. Suzuki-Miyaura, cross metathesis, amination, C-H activation, borylation, silylation, etc.). Theoretically, the larger micelles have more volume to house chemical reagents, thereby improving reaction rates [23].

Changing the hydrophobic portion of the PTS surfactant from vitamin E to β-sitosterol decreased the conversion of cross metathesis reactions using Grubbs' catalyst [23,24]. Compared to TPGS 1000 (another Vitamin E based surfactant), the improved reaction conversions were attributed to more lipophilic tendencies based on the hydrophobic-lipophilic balance profile. However, both the β-sitosterol containing PSS and TPGS-1000 micelles are notably smaller than the PTS micelles, with diameters of 10-15 nm and 23 nm, respectively [25]. β-sitosterol based surfactants were found to be superior in transition-metal catalyzed

couplings compared to vitamin E based surfactant micelles, even with similar diameters of roughly 45 nm [25].

Surfactants with polar sulfone components within the nonpolar, hydrophobic cores used to facilitate peptide synthesis have recently been reported [21]. It is important to note that the design of these systems has generally involved syntheses of libraries of new amphiphilic molecules and screening their reactivity [21,25].

Macromolecular amphiphilic nanoreactor systems have also been considered, with improved stability compared to self-assembled small molecule amphiphilic systems [26,27]. For example, O'Reilly and co-workers incorporated 4-(N,N-dimethylamino)pyridine, a nucleophilic catalyst for a number of reactions including esterifications, into the hydrophobic block of an amphiphilic block copolymer using reversible-addition fragmentation chain (RAFT) polymerization which self-assembled into kinetically frozen micelles.

Kinetically frozen micelles differ from traditional micelles in that the surfactants do not freely exchange with surrounding system in a dynamic equilibrium. This difference is largely due to the increased molecular weight of the hydrophobic portion of the amphiphile which presents a significantly greater entropy barrier to solubilize in the aqueous solution [8,28,29]. This results in the need for reagents to partition into the micelles instead of a guided transport via surfactant exchange and generally prevents the exchange of molecules between kinetically trapped micelles (Figure 1.2).

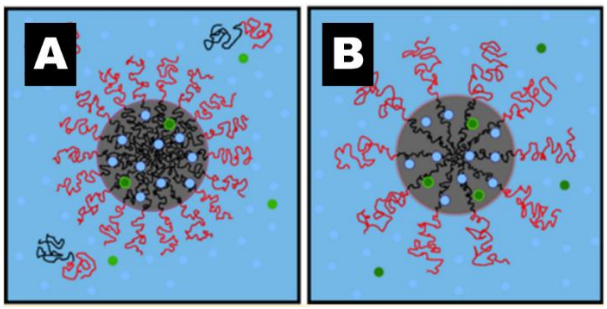

Figure 1.2: Representative illustration of A) dynamic micelle and B) kinetically-trapped micelle. Dynamic micelles show dynamic exchange of the amphiphile which can guide and transport small molecules while

the kinetically-trapped micelle micelle does not undergo dynamic exchange of the amphiphile requiring partitioning of small molecules [30].

The stable, kinetically-trapped, micellar nanoreactors catalyzed the competitive esterification between multiple anhydrides. More hydrophobic substrates resulted in higher conversions. Further, the hydrophobicity of the substrate could also be used to modify selectivity [26,27]. In other work, L-proline, a chiral organocatalyst for the aldol reaction, was incorporated into the hydrophobic block of an amphiphilic block copolymer via reversible-addition fragmentation chain (RAFT) polymerization [31]. Upon self-assembly in water, core-shell micellar nanoreactors with catalytic hydrophobic cores were achieved that were significantly more efficient than the unsupported catalyst [31] which was attributed to the hydrophobic microenvironment of the micelle core [32]. The catalyst loading and core hydrophobicity affected the turnover number but the effects could not be decoupled from micelle swelling.

1.3. Aqueous Gold Nanoparticle Catalysis

A key component of many of the polymer nanoreactors that have been discussed is the use of a catalyst to facilitate the desired reaction. Aqueous catalysis is an important class of reaction for ongoing development in green chemistry [1,2]. Many studies have turned towards gold nanoparticles as an inexpensive and efficient catalyst for a wide variety of reactions [33–36]. The reduction of 4-nitrophenol has become the standard model reaction for analyzing the performance of new gold nanoparticle catalysts in water (Table 1.2) [36].

Table 1.2: TOF's of Gold Nanoparticle Systems for Aqueous Reduction of 4-Nitrophenol.

Entry	System	AuNP diameter (nm)	$NaBH_4$ (mM)	4NP (mM)	k_{app} (s^{-1})	TOF (h^{-1})	Reference
1	$NaBH_4$	3.2 ± 0.8	50	0.5	$9.0x10^{-3}$	9000	[37]
2	Citrate	5.6 ± 1.4	13	0.067	$5.7x10^{-3}$	1794	[34]
3	TiO_2 supported AuNP	5.8 ± 1.8	13.2	0.067	$6.67x10^{-3}$	1700	[34]
4	PVP stabilized Hollow AuNP	80	13.2	0.01	$7.47x10^{-3}$	94	[38]
5	PVP stabilized AuNP	6	13.2	0.01	$3.72x10^{-3}$	46	[38]
6	TRZ terminated MPEG	6.2 ± 0.5	12	0.15	$5.2x10^{-3}$	2570*	[39]
7	N-Substituted PEGylated TRZ	2.7 ± 0.5	48	0.15	$1.65x10^{-2}$	600*	[40]
8	TRZ containing PEO stabilized Iron Nanoparticle	<2	48	0.15	$4.2x10^{-3}$	200*	[41]
9	PS@P5	2.77	100	0.1	$1.46x10^{-2}$	927	[42]
10	H40-PEI-PEG	6.85 ± 0.82	50	0.1	$4.27x10^{-3}$	1500*	[43]
11	Polyanion H40-COONa and	8.0 ± 3.9	50	0.1	$8.5x10^{-3}$	3180	[44]

Entry	System	AuNP diameter (nm)	$NaBH_4$ (mM)	4NP (mM)	k_{app} (s^{-1})	TOF (h^{-1})	Reference
	polycation PEG-b-(PCL-g-PEI)						
12	dendritic PEI@PS	8.5 ± 1.8	66	0.06	$6.3x10^{-3}$	0.72	[45]
13	dendronized amphiphilic copolymer	2.1 ± 1.5	13.2	0.132	$2.8x10^{-3}$	26470	[46]

*Turnover frequency was calculated from the reported reaction methods and kinetic data

Gold nanoparticle catalysts are often evaluated for their activity in reducing 4-nitrophenol to 4-aminophenol using sodium borohydride. The reaction is considered a model reaction because the kinetics are well understood and the reaction does not result in side-products. A brief variety of systems are summarized in Table 1.2 including supported and dispersed gold nanoparticles. Generally, the activity of gold nanoparticles is size dependent [47,48] which can make comparison between studies difficult. To compare across various systems, the turnover frequency can be used as a measure of catalytic performance and is calculated as:

$$TOF = \frac{n_{4NP}}{n_{cat} * t} \tag{1.1}$$

where TOF is the turnover frequency, n_{4NP} is the moles of 4-nitrophenol consumed in the reaction, n_{cat} is the moles of catalyst used in the reaction, and t is the time of reaction duration. For catalysis via gold nanoparticles, the moles of catalyst has generally referred to the moles of gold nanoparticles in the reaction solution [46].

1.3.1. Single Gold Nanoparticle Systems

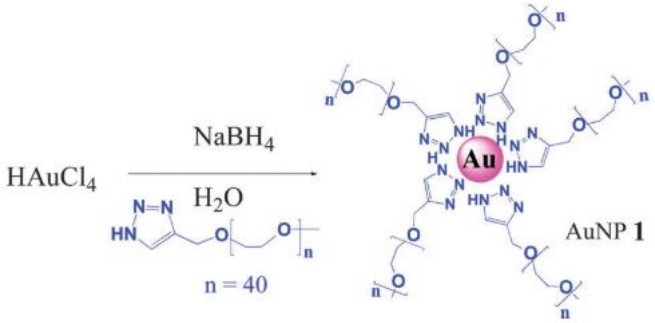

Figure 1.3: Gold nanoparticles stabilized with triazole-terminated MPEG [39].

Nanoreactor systems designed around a single gold nanoparticle generally fall into the category of ligand-stabilized nanoparticles (Figure 1.3). The baseline for such systems would be gold nanoparticles without any stabilizing ligand [49]. These ligand-free gold nanoparticles were synthesized by laser ablation of a gold target in an aqueous environment. Ballauff used these particles as a reference catalyst for other gold nanoparticle systems, analyzing the kinetics using the Langmuir-Hinshelwood model.

Sodium borohydride is commonly used to reduce auric acid and synthesize gold nanoparticles, but it can also act as a stabilizing ligand for the generated nanoparticle [37]. Due to the degradation of borohydride in aqueous solutions the hydride and/or borohydride ligand is not permanent and deteriorates rapidly in acidic solutions. However, Astruc et al. found that such systems are highly active for the reduction of 4-nitrophenol with sodium borohydride, with a reported turnover frequency of 9000 h^{-1} (entry 1, Table 1.2) [37].

Citrate is another simple ligand which is well known for its ability to stabilize gold nanoparticles. Kitchens et al. investigated 5.6 nm citrate-stabilized gold nanoparticles and compared that colloidal system (entry 2, Table 1.2) to a supported system consisting of similarly sized gold nanoparticles supported on TiO_2 (entry 3, Table 1.2) [34]. The citrate-stabilized gold nanoparticles demonstrated slightly faster kinetics than the supported system with reported turnover frequencies of 1794 h^{-1} and 1700 h^{-1}, respectively.

Kitchens et al. also demonstrated that ligand packing on the catalyst surface influences catalyst activity [50]. While citrate is a weak ligand which can readily dissociate from the catalyst surface, thiol-ligands covalently bind to the gold surface resulting in active site blocking which can lead to decreased catalytic performance. Kitchens demonstrated this effect, which ultimately led to complete inhibition of the catalyst at 2.5 molecules/nm^2 HS-PEG packing density. The length of the PEG chain was found to influence the packing of the ligand on the surface, with longer chains leading to lower packing densities and faster reactions.

Strategic choice of ligand composition and packing densities led to the ability to recycle gold nanoparticle catalysts with changes in pH [51]. Thiolated poly(acylicacid) (SPAA) undergoes a conformation change in neutral to acidic conditions leading to reversible aggregation and precipitation from aqueous solutions. In previous studies, shorter pH-responsive ligands led to irreversible aggregation of the gold nanoparticles after 3 recycles due to desorption of the ligand from harsh reagents such as sodium borohydride [52]. However, the longer SPAA ligand was proven to be more stable under reaction conditions, allowing the catalyst to be recycled up to 5 times. Increasing the ligand density on the catalyst surface resulted in less activity loss after each recycle, however the rate constants were still nearly 5-fold less than the lower ligand density catalysts after 5 recycles.

Another interesting ligand system consisted of poly(vinyl pyrrolidone) (PVP) stabilized hollow, porous gold nanoparticles which were formed through reduction of gold on a silver chloride template in the presence of PVP followed by dissolution of the silver chloride with ammonium hydroxide (entry 4, Table 1.2). Despite a nominal diameter of 70 nm, well outside the range of traditionally active solid-gold nanoparticles [47], the hollow gold nanoparticle (stabilized by a PVP shell) demonstrated a TOF two-fold faster than that of 6 nm solid gold nanoparticle cores stabilized by PVP shells (entry 5, Table 1.2) [38].

Polyethylene glycol (PEG) with a triazole (TRZ) end groups were studied for stabilizing catalytically active gold nanoparticles (Figure 1.3) [39,40]. The ligands were prepared through click-chemistry and the

gold nanoparticles were synthesized by reducing a solution of auric acid with sodium borohydride in the presence of the different ligands. TRZ ligands stabilizing roughly 6 nm diameter gold nanoparticles were the most active, with a reported turnover frequency of 2570 h^{-1} (entry 6, Table 1.2) [39]. When TRZ moiety was N-substituted with 4-carboxylic phenyl the turnover frequency fell to 600 h^{-1} (entry 7, Table 1.2) [40].

1.3.2. Systems Containing Multiple Gold Nanoparticles

1.3.2.1. Ligand Stabilized Gold Nanoparticles

Zhao et al. reported an interesting system in which multiple gold nanoparticles were ligand-stabilized on the shell of a pre-formed iron oxide nanoparticle (Figure 1.4) [41]. Oleic acid stabilized iron oxide nanoparticles (Fe_3O_4) underwent ligand exchange with triazole ligands, synthesized through click-chemistry, containing a carboxylic acid and polyethylene oxide fragment at opposing termini (entry 8, Table 1.2) [41]. The carboxylic acid ligand coordinated with the iron oxide surface and the poly(ethylene oxide) (PEO) stabilized the iron nanoparticles in the aqueous solution. The resulting structures had an iron oxide nanoparticle core surrounded by a PEO shell with TRZ moieties near the surface of the iron nanoparticle. $HAuCl_4$ was then dissolved in the nanoparticle dispersion and reduced by dropwise addition of sodium borohydride. Thus, gold nanoparticles were synthesized in the iron nanoparticle solution near stabilizing interactions occurring in both the PEO layer and at the TRZ moieties located at the iron nanoparticle surface (Figure 1.4). The formed gold nanoparticles were less than 2 nm in diameter and were dispersed throughout the structure. The reported turnover frequency of 200 h^{-1} is notably lower than the other TRZ containing polyethylene oxide ligand systems (entries 5 and 7, Table 1.2) [39,40] which reached a maximum TOF of 2570 h^{-1}. Notably, these alternative systems did not utilize an iron nanoparticle system but relied solely on the coordination of the triazole ligands to individual gold nanoparticles.

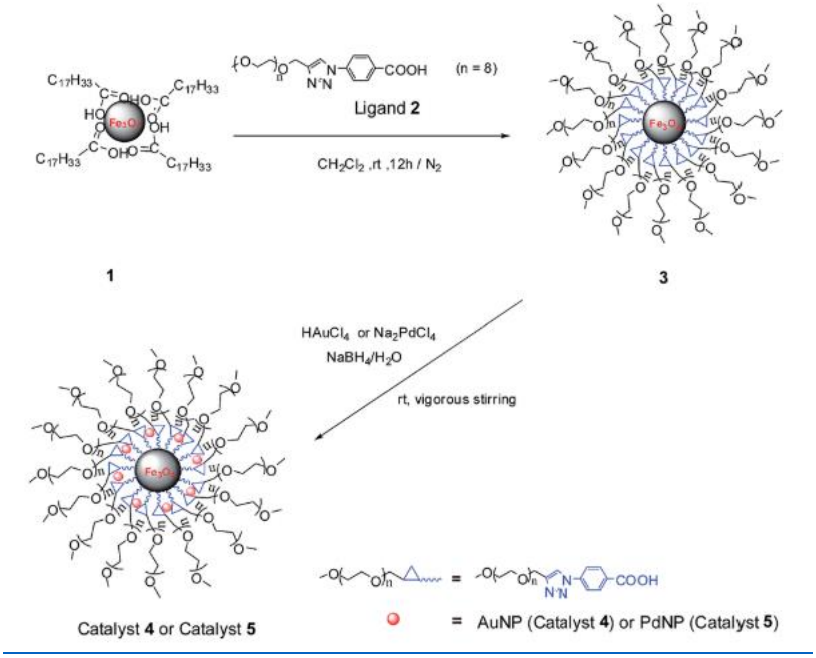

Figure 1.4: Magnetically recoverable gold nanoparticle catalyst [41].

1.3.2.2. Amphiphilic Systems

Amphiphilic polymers can be used to form many nanostructures including micelles, vesicles, polymersomes, and hyperbranched polymer particles making them a diverse group to study for use in gold nanoparticle stabilization and use in catalysis [7,53]. For example, 8-hydroxyquinoline-containing thermoresponsive diblock copolymers of poly(N-isopropylacrylamide) (PNIPAm) and polystyrene or PNIPAm and polymethacrylate (PMMA) amphiphiles were prepared through RAFT-polymerization. Triblock copolymers of PNIPAm-b-(P(MMA-co-MQ)-St were also prepared. The hydroxyquinoline functionalities were dispersed in the hydrophobic, hydrophilic, or interfacial regions through copolymerization techniques. In water, the block copolymers self-assembled into micelles. Gold precursor was reduced with sodium borohydride in the presence of the aqueous block copolymer dispersion. The hydroxyquinoline was used as a coordination site for the gold nanoparticles. Generally, the amphiphilic micelles approached 80 nm hydrodynamic diameter by DLS with 3-4 nm gold nanoparticles distributed in

the micelle core. The hydroxyquinoline moieties were necessary for stabilizing the gold nanoparticles and achieving high catalytic activity. The hydroxyquinoline containing triblock copolymer was found to stabilize active gold nanoparticles with a TOF of 927 h^{-1} (entry 12, Table 1.2) whereas amphiphilic copolymer PS-b-PNIPAm without hydroxyquinoline moieties had a much lower TOF of 156 h^{-1} (entry 9, Table 1.2) [42].

Hyperbranched amphiphilic polymers (H40-PEI-PEG) were synthesized using commercially available hyperbranched aliphatic polyesters after modification of hydroxyl groups with succinic anhydride allowed conjugation of PEG chains and azide groups which could then be used to connect poly(ethyleneimine) (PEI) through azide-alkyne click-chemistry. Gold nanoparticles were then synthesized in the aqueous polymer solution through reduction of the gold salt with sodium borohydride. The nitrogen groups of the H40-PEI-PEG provided coordination sites for the gold atoms, stabilizing the resulting nucleated gold nanoparticles within the polymer structure. Fast turnover frequencies were reported (1500 h^{-1}) for the reduction of 4-nitrophenol using 7 nm gold nanoparticles core stabilized by a polymer shell (entry 10, Table 1.2) [43].

Another example of an amphiphilic polymer use for encapsulation of catalytic gold nanoparticles is PEG-b-(PCL-g-PEI), which is a polyion complex that self-assembles in water forming micelles with a PCL/PEI core and PEG shell (entry 11, Table 1.2). Gold nanoparticles were formed in the micelle core in situ by adding chloroauric acid to a dispersion of micelles which interacts with the PEI segment of the polymer. The gold precursor is then reduced with sodium borohydride resulting in gold nanoparticles dispersed in the micelles core. The resulting gold nanoparticles were 8.0 ± 3.9 nm in diameter. The resulting polymer shell-gold nanoparticle shell catalyst was used to facilitate the aqueous reduction of 4-nitrophenol, with a reported turnover frequency of 3180 h^{-1} [44].

1.3.2.3. Dendrimer Systems

Dendrimers offer a unique structure similar to a micelle or core-shell nanoparticle except it is composed of a single, branched, molecular chain. One example of dendrimer use for supporting gold nanoparticle catalysts prepared the dendritic amphiphile by alkylation of branched poly(ethylenimine) with a polystyrene epoxide in chloroform (entry 2, Table 1.2). Chloroauric acid was then added to the dendritic amphiphile solution and allowed to stir for 24 hours in order to allow the tertiary amine groups of PEI to reduce the gold ions and form gold nanoparticles. The gold nanoparticles were situated near the PEI core of the dendritic amphiphiles. Polymer monolith supports were then created with the gold nanoparticle-bearing dendritic amphiphiles (Au-DA) by emulsion polymerization in which the role of the Au-DA was to stabilize the emulsion. The high internal phase emulsion (HIPE) polymerization was accomplished by dropwise addition of water to a stirring solution of Au-DA, 2,2-azobisisobutyronitrile, and divinylbenzene in toluene. In the emulsion, the Au-DA stabilized the water-oil interface. The resulting emulsion was heated at 70°C for 2 days, washed with water and ethanol and dried under vacuum. Upon drying, the solvent removal leaves open cells resulting in gold (8.5 ± 1.8 nm) supported on a porous polymer monolith. Similar structures could be created in one-pot with simultaneous in-situ synthesis of gold nanoparticles by using chloroauric acid and dendritic amphiphile instead of Au-DA in the HIPE solution. The Au-DA-HIPE structure was able to catalyze the reduction of 4-nitrophenol with a TOF of 0.72 h^{-1}, and could be recycled up to 7 times. By Increasing the Au-DA N:Au ratio, smaller gold nanoparticles could be achieved, resulting in higher apparent catalytic activities. For example, monoliths with gold nanoparticles that were 4.0 ± 1.5 nm had a turnover frequency of 13.51 h^{-1} [45].

As an alternative to dendrimers, dendrons can also be used as stabilizing ligands for gold nanoparticles. For example, an amphiphilic dendronized diblock copolymer with dendronized ferrocene-containing hydrophobic segments and hydrophilic triethylene glycol containing amphiphilic segments was

prepared by ring-opening metathesis polymerization and self-assembled in water to form a hydrophobic core and hydrophilic shell. Gold nanoparticles was produced in situ by adding gold precursor to the self-assembled polymer structure and reducing the gold. The gold nanoparticles were dispersed throughout the hydrophobic core and hydrophilic shell. The size of the gold nanoparticle was affected by the reducing agent used. The highest turnover frequency was observed was 26470 h^{-1} (entry 13, Table 1.2) which was attributed to the well distributed gold nanoparticles throughout the polymer structure which resulted in large amounts of gold surface area. Further, the stabilization of gold nanoparticles with weakly interacting, amphiphilic triazole functionalities, which sterically stabilize the colloidal gold particle without blocking active sites on the gold surface, could play a role in the observed turnover frequency [46]. Notably, the hydrophobic microenvironment generated by the amphiphiles may also play a role in promoting the reaction [46].

1.4. Kinetics of 4-Nitrophenol Reduction with Gold Nanoparticles

The reduction of 4-nitrophenol as a model reaction provides a framework for analyzing the performance of novel gold nanoparticle catalysts. While turnover frequencies are a common metric for gold nanoparticle catalytic performance it is a reaction condition specific metric and can be affected by catalyst size as well as 4-nitrophenol and sodium borohydride reactant concentrations. The intrinsic rate constant described in the Langmuir-Hinshelwood kinetic model provides an independent measure of performance.

Ballauff et al. conducted analysis of the 4-nitrophenol reduction under pseudo-first order rate kinetics and demonstrated the relationship between sodium borohydride concentration and reaction rate constant vary proportionally until pseudo-first order kinetics are reached at which point the reaction rate no longer varies with increasing sodium borohydride [54,55]. Ballauff reported that for gold nanoparticle decorated dendrimers pseudo-first order kinetics were reached at 10 mM sodium borohydride, a 100-fold

excess to 4-nitrophenol. From Table 1.2 it is clearly seen that there are a variety of reaction conditions used with sodium borohydride excess ranging from 10 to 100-fold, indicating the sodium borohydride concertation may be an important consideration when evaluating catalytic performance of nanoreactor systems.

Further, Ballauff demonstrated that the 4-nitrophenol reduction catalyzed by gold nanoparticles fits the Langmuir-Hinshelwood kinetic model [54]. Under Langmuir-Hinshelwood kinetics, molecules compete for a fixed number of active sites on the catalyst surface. Molecules adsorb and desorb from the surface, or can undergo the desired reaction if the requisite conditions are met. As such, for reactions requiring two or more reagents catalyst active sites can effectively be blocked by one species if a sufficient concentration difference exists. Therefore, the Langmuir-Hinshelwood model takes into consideration the concentrations of the different species in the reaction, the adsorption constants for those species and the catalyst surface, the catalyst surface area, and finally the intrinsic rate constant. The intrinsic rate constant described by the Langmuir-Hinshelwood model is therefore an unbiased metric of catalyst performance because it is independent from reagent concentrations or even catalyst surface area.

1.5. One-Pot Cascade Reactions

Colloidal metal nanoparticles are promising nanoreactors for performing multiple reactions in a "one pot" reactions. Such capabilities could significantly reduce organic solvent waste by eliminating the need for isolation of the intermediates. There are multiple approaches to performing "one pot" reactions. For example, cascade, or domino, reactions take place in a single reaction vessel, generally with addition of all reagents simultaneously. This is often difficult due to the need for multiple catalysts or reagents that can inhibit each other when used together in bulk [8,12]. Polymer nanoreactors can combat this outcome by compartmentalization of different reactions within isolated regions within the structure [56–59]. Alternatively, tandem reactions are a subset of one-pot reactions where, unlike cascade reactions, reagents

are added in a step-wise fashion, allowing one reaction step to proceed before the addition of reagents for the second reaction [60].

1.5.1. Gold Nanoparticle Catalysts Used in Cascade Reactions

García-Verdugo et al. utilized polymeric ionic liquids to stabilize gold nanoparticles for aqueous cascade reactions. Polymer ionic liquids were formed through RAFT polymerization of p-chloromethylstyrene followed by further chemical modification [61]. Gold nanoparticles were synthesized by reduction with sodium borohydride either before, or after, modification of the polymer with 1-butylimidazole which formed the polymeric ionic liquid. These alternate methods produced gold nanoparticle composites in which the gold nanoparticles were mainly stabilized by thiol-ligands (before modification of the polymer) or stabilized through loose coordination with the ionic liquid units (after modification of the polymer). The gold nanoparticles were roughly 4 nm in diameter. Analysis of the gold nanoparticle-polymeric ionic liquid composites for the reduction for 4-nitrophenol indicated that the thiol-ligand stabilized composites were half as catalytically active as the coordination stabilized composites, likely because of the active site blocking which occurs with thiol-ligand binding [50]. This suggests that differences in the microenvironment can influence reaction outcome. The gold nanoparticle composites were used to facilitate a Knoevenagel condensation reaction between p-nitrobenzaldehyde and ethyl cyanoacetate followed by reduction of the nitro and C=C double bond. With 20 equivalents of sodium borohydride as reductant and allowing the reaction to progress for 20 hours, 100% yield was achieved with the thiol-ligand stabilized gold nanoparticle composite [61].

AuPd-Fe_3O_4 nanoparticles were prepared through a hydrothermal procedure using sodium borohydride as a reductant and stabilized in a solution with polyvinylpyrillodone [62]. The alloy nanoparticles were able to facilitate the cascade reaction of nitrophenyl reduction and reductive amination of benzaldehyde. The cascade reaction was carried out at room temperature under a molecular hydrogen

atmosphere in methanol. Au-Fe_3O_4 particles lacking the Pd component could not catalyze the reaction, unlike Pd-Fe_3O_4 particles which catalyzed the reaction but produced a variety of side products. The AuPd-Fe_3O_4 particles produced the desired product with 93% yield within 3 hours. Due to the iron component, the particles were easily separable with a magnet. Therefore, the particles were magnetically recovered and recycled with addition of fresh reagents. The particles were cycled up to 20 times, with no change in catalytic activity until the 13th cycle. The activity decreased until the 16th cycle, at which point the reaction was allowed to proceed for 6 hours and the yield recovered to 93% desired product.

Grande et al. synthesized PS-b-PLA copolymers in order to form porous structures to attach catalytic gold nanoparticles [63]. The PS-b-PLA was spin-coated on Si wafers, followed by an acid wash in trifluoroacetic acid to cleave the PLA block which was washed away with ethanol. The porous PS was functionalized with a primary amines which served as anchors for gold nanoparticles synthesized *in-situ* via sodium borohydride reduction. The gold nanoparticle incorporated structure was then placed in an ethanol reaction solution containing 3-nitrobenzeneboronic acid and K_2CO_3. The homo-coupling reaction was carried out at 65 °C for 24 hours. The reaction solution was cooled to room temperature, sodium borohydride added, and the reduction of the nitro-group took place over the following 24 hours. The sample was analyzed by NMR to determine purity of the product as evidenced by shifts in the aromatic protons. Recycling was carried out for three cycles with no loss of activity reported, however the yield decreased to 90% by the third recycle.

1.5.2. Reduction Based Cascade Reactions

Li et al. prepared polymer nanoreactors incorporating palladium nanoparticles in the core and acidic catalysts in the shell by a seeded polymerization technique. Poly(acrylamide) (core) was polymerized first in the presence of palladium ions (chloroplatinic acid) followed by the addition of an AMPS (shell) solution. The palladium ions coordinated with the amine groups in the core of the nanoreactor so that when the

palladium was reduced by sodium borohydride the resulting palladium nanoparticles were synthesized in the core of the polymer nanoreactors. The core-shell architecture, as well as the presence of platinum nanoparticles in the core, was confirmed with TEM. Bis(2,4-dinitrophenyl)oxalate was both hydrolyzed and reduced by the bifunctional nanoreactor in PBS solution. Hydrolysis occurred at the acidic AMPS sites in the shell followed by reduction by the palladium nanoparticles in the core (Figure 1.5). Kinetic tracking via UV-vis demonstrated that the hydrolysis and reduction occurred at the different catalytic regions of the nanoreactor simultaneously. Spatio-temporal analysis of the reaction corresponded with theoretical models of catalysis in a core-shell nanoreactor following Fickian diffusion thereby demonstrating the efficacy of compartmentalization for tandem reaction processes [64].

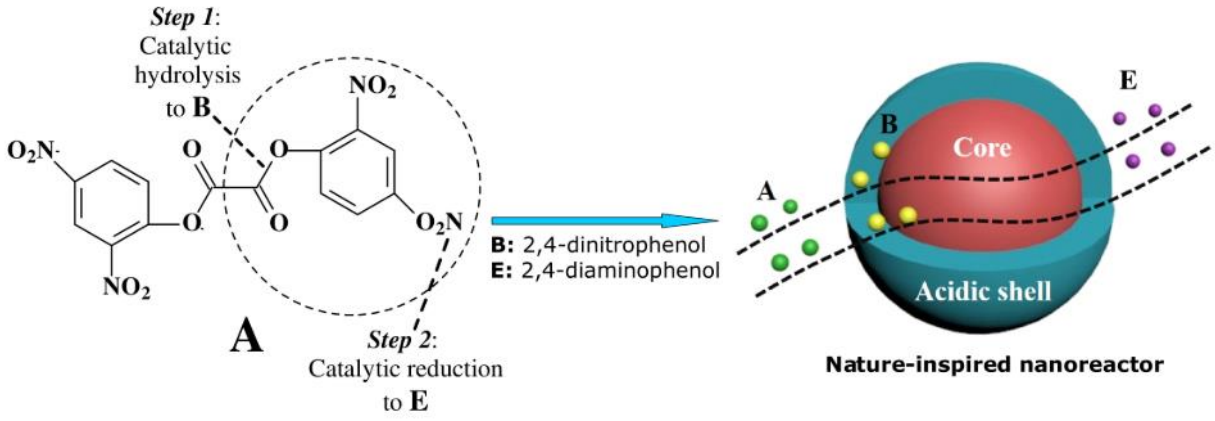

Figure 1.5: Tandem hydrolysis and reduction by core-shell nanoreactors [64].

Li et al. also prepared poly(2-acrylamido-2-methylpropane- sulfonic acid) (PAMPS) polymer nanoreactors through inverse-emulsion polymerization to create the core first, followed by polymerization of the shell with incorporation of silver ions. After complete polymerization, the silver ions were reduced with sodium borohydride to produce silver nanoparticles which were distributed throughout the shell of the nanoreactors as indicated by TEM. The overall structure was about 100 nm in diameter with a 13 nm thick shell. Tandem reduction and hydrolysis of bis(2,4-dinitrophenyl)oxalate (DNPO) was accomplished in a PBS solution, without mutual engagement of the catalysts as inferred from kinetic tracking via UV-Vis.

This "undisturbed" tandem reaction was attributed to the spatiotemporal separation of the catalysts within the shell and core regions of the nanoreactor. Greater than 80% conversion of the DNPO was achieved in 1 hour of reaction [56]. While the polymer nanoreactors with silver nanoparticles did catalyze the reaction faster, conversion was significant in even the control experiments [56].

Nickel acetate was added to a solution of nanocellulose and reduced with sodium borohydride to form nickel nanoparticles [65]. Interaction between the nickel ions and the carboxyl groups of the nanocellulose led to nickel boride nanoparticles that were stable in aqueous solution. The catalyst was found to efficiently reduce nitro compounds in the presence of sodium borohydride. Tandem reactions involving nitro group reduction and either BOC protection of the amine or epoxide ring opening to form amino alcohols. The complete tandem reaction with BOC protection was generally completed within 4 hours, while amino alcohol synthesis took as long as 24 hours. High yields were achieved in both cases (>95%). Recyclability studies were carried out with reduction nitrobenzoic acid. The reaction solution was extracted with diethyl ether leaving the catalyst in the aqueous phase to be reused. Five recycles were performed with yields exceeding 95%, but longer reaction times were required for each subsequent reaction with an order of magnitude increase over the 5 reactions [65].

1.5.3. Reductive Amination Cascade Reactions

Integrated yolk shell (IYS) nanoreactors were prepared by nanocasting aminostyrene on preassembled crosslinked polystyrene sulfuric acid on silicon oxide microspheres (CLPS-SO3@SiO2) [66]. After polymerization of the aminostyrene, the SiO_2 was removed via etching, leaving an acid-base bifunctional yolk-shell nanoreactor. Pd nanoparticles were incorporated throughout the nanoreactor. The roughly 300 nm nanoreactors were able to catalyze the cascade reaction of 4-nitrobenzaldehyde to 2-(4-aminophenyl)-^{1}H-benzimidazole through reductive amination with the acid catalyst and catalytic hydrogenation with Pd nanoparticles. Benzimidazole derivatives have antiviral, antiulcer, and anticancer properties making them

an attractive intermediate target. The cascade reaction yielded 97% of the desired product and no aggregation of Pd NP was observed after 5 catalytic cycles.

1.5.4. Coupling based Cascade Reactions

TPGS-750-M, a PEG based surfactant, is used to form a micellar support on which Fe/Pd nanoparticles are stabilized [15]. Reagents were added to a TPGS-750-M solution and partition to the micelles cores at higher than bulk concentrations. This solution is then added to the Fe/Pd NP solution for the reaction to progress. A large variety of Sonogashira coupling reactions are studied, even completing double and triple couplings in the same reaction solution. These reactions are generally heated and span reaction times of 5-72 hrs. Multi-step one-pot reactions are effectively completed by protection of an alkyne prior to coupling, followed by deprotection and subsequent coupling. Another cascade route using Sonogashira reactions was completed by utilizing bromo- and iodo- moieties to control reactivity. This allowed the iodo- region to be coupled at lower temperatures while protecting the bromo-group for a subsequent reaction. No separation, purification, or additional catalyst was necessary to complete a 5 step one-pot synthesis with 75% overall yield. Recycling can be achieved through extraction of the reaction solution with ethyl acetate, removing the product while leaving the catalyst in the aqueous solution. After completing 5 different reactions with recycling after each, the E-factor of the process was determined to be 4.1, which was noted as an order of magnitude reduction in waste generation from a traditional reaction carried out in organic solvent.

Fe with ppm Pd + Ni NP's were prepared by reduction with methylmagnesium chloride. The active catalyst was formed with addition of $NaBH_4$ to remove the methyl ligands [13]. The metal nanoparticle catalysts were then added to a solution of TPGS-750-M micelles. Rates of nitro group reduction were found to improve with the addition of a THF as a co-solvent (10%). A 3-step one-pot domino reaction was performed with reduction of a 4-chloronitrobenzene to the aniline compound, SnAR addition to the amine

with 2,4,5-trichloropyrimadine, followed by Suzuki-Miyaura coupling. The coupling reaction took place with added $Pd(OAc)_2$ at an elevated temperature of 45C. Greater than >90% yield was recovered with extraction by MTBE. Recycling studies were conducted with the reduction of 4-chloro-3-(trifluoromethyl)nitrobenzene, again utilizing extraction with MTBE. The micellar catalyst aqueous solution was recycled 4 times. To maintain functionality after product extraction from the aqueous phase, addition nanoparticles catalysts were added prior to the subsequent reaction. The overall process had a reported E-factor of 3.9.

1.5.5. Oxidation Based Cascade Reactions

Polymer incarcerated metal nanoclusters were formed by reducing platinum in the presence of a triblock copolymer of polystyrenes with alcohol and epoxy moieties [67]. After metal cluster formation hexane was added to the polymer solution to induce precipitation of the polymer incarcerated nanoclusters. The clusters were then heated to induce crosslinking of the alcohol and epoxy groups producing an insoluble catalyst. Those clusters were then introduced to a solution with hollow-center spherical carbon black and addition triblock polymer. The nanoclusters coordinated with the carbon black spheres, and the solution was heated to further crosslink polymer around the supported cluster system. The secondary carbon black support prevented aggregation of the clusters. The polymer incarcerated carbon black (PICB) particles showed excellent activity for catalyzing a wide range of reaction including direct oxidative esterification and oxidative amide and imine formations. The catalysts were found to be recyclable up to four times, but only upon heating the filtered and dried catalyst to 170 °C for 5 hours under an argon atmosphere. Without heating, significant loss of activity was noted. Sequential catalysis of aerobic oxidation and Michael addition was then performed with the PICB catalyst in DCM at room temperature over 20 hours. Excellent yields of greater than 95% were reported.

1.6. Conclusion

Liquid phase chemical processing generates large amounts of organic solvent waste. This waste is associated with use of organic solvent for the reaction as well as large amounts of solvent for isolation of the product. Generally, production of the desired product requires multiple reaction and separation steps. Thus, the amount of waste is 10-100 fold times greater than the mass of product. Metal nanoparticles stabilized by polymer structures have been widely studied their ability to conduct traditionally organic phase reactions in a bulk aqueous phase. Proven benefits of conducting aqueous reactions through the use of polymer micelles and core-shell structures are increases in reaction rate [31], conversion [18], and selectivity [26,27] as well as significantly lower generated waste [3,15,20,68]. They have been broadly applied variety of reactions including oxidations, reductions, and couplings. In a handful of studies, they have been used for performing "one pot" cascade and tandem reactions. While these results are promising, systematic studies of nanoreactor design and composition on catalytic performance is limited, largely due to the necessity to synthesize specific amphiphiles and surfactants or dendritic polymers which can involve laborious synthetic methods [18,25,42,69,70].

Chapter 2 : Project Overview

2.1. Project Purpose

The purpose of this project is to demonstrate the applicability of kinetically-trapped filled polymer micelles, self-assembled through Flash Nanoprecipitation, to function as nanoreactors in performing multiple reactions steps in one pot using water as the bulk solvent. Flash Nanoprecipitation offers a rapid, tunable, and flexible method to self-assemble kinetically-trapped micelles with controllable size and composition [71–73]. Thus, this strategy provides an effective route to systematically study the effect of those nanoreactor properties on nanoreactor performance in parallel with achieving multiple reactions steps in one pot.

First, the ability of the Flash Nanoprecipitation method will be investigated for the ability to tailor polymer nanoreactor size, composition, and catalyst loading. The catalytic activity of the nanoreactors will be investigated using the 4-nitrophenol reduction as a model reaction. The Langmuir-Hinshelwood kinetic model will be used to describe the intrinsic kinetic parameters of gold nanoparticles incorporated within different polymer nanoreactors (Figure 2.1C), while accounting for nanoreactor composition-dependent differences in localized reagent concentrations. The application of the polymer nanoreactors to facilitate the oxidation of benzyl alcohol will be discussed. Finally, the ability of the polymer nanoreactors to perform a two-step reaction in one pot with spontaneous precipitation of the product will be presented.

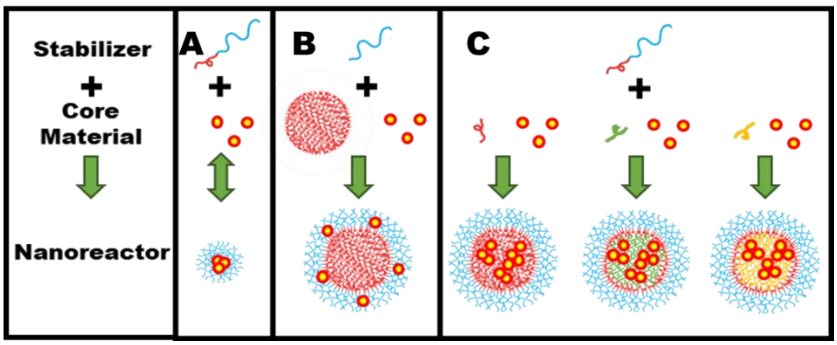

Figure 2.1: Illustrations of structural differences between A) thermodynamically stable micelles, B) spherical brush polymers, and C) kinetically-trapped core-shell nanoreactors. Only kinetically-trapped core-shell structures result in gold nanoparticles (yellow circle) that are core-localized with modular core-material.

2.2. Background

Performing catalyzed, organic phase reactions has been achieved by a wide range of colloidal dispersions. For example, aqueously dispersed surfactant micelles support organic, homogenous metal, and metal nanoparticle catalysts while providing a shielded hydrophobic environment for a variety of reactions (Figure 2.1A) [3–5]. The confinement of the reaction to the hydrophobic microenvironment has even lead to improvements in apparent reaction kinetics as well as yield and selectivity when compared to traditional organic solvents [5–8].

Polymer micelles, specifically, are promising for nanoreactor design due to the ability to functionalize the amphiphilic polymer molecule with metal nanoparticle catalysts, homogenous catalysts, and various acid/base moieties [8,31,32,74]. The variety of amphiphilic block copolymers available is also nearly limitless, and the choice of polymer can bestow unique characteristics, such as thermoresponsive permeability, onto the formed nanoreactor [69,75]. However, amphiphilic polymers can be expensive and often require tedious synthesis and purification.

Another class of colloidal dispersions used for catalysis have been core-shell nanoreactors composed of dendritic polymers or spherical polyelectrolyte brushes (SPB) used to support catalysts (Figure 2.1B) [36,54]. These structures generally require multiple chemical synthetic steps. For example, in the case of SPB's the polystyrene latex core is produced by emulsion polymerization of styrene and N-isopropylacrylamide (NIPA) using SDS as a stabilizer. The latex cores are purified by ultrafiltration using 10-fold the initial volume of water. The shell is then grafted onto the polystyrene latex core by seeded emulsion polymerization. These systems generally exhibit improved stability to harsh reaction conditions compared to thermodynamically stable micelles due to being composed of a single polymer molecule. Interestingly, metal nanoparticle catalysts have been selectively attached to the shell of the SPB nanoreactor, in contrast to the hydrophobic core [54,76,77]. Reaction kinetics were comparable to micellar systems with core-localized catalysts.

While SPB nanoreactors benefit from improved stability, functionalization of the nanoreactor core with metal nanoparticle catalysts is very difficult post-polymer synthesis and would require *in-situ* synthesis of the metal nanoparticle catalyst in order to successfully be incorporated throughout the core-shell structure. This effectively limits the ability to investigate catalyst reaction environments to the shell of the nanoreactor. Changes to that environment in an attempt to improve reaction kinetics, selectivity, or catalyst incorporation would require a completely different polymer, perhaps even a novel polymer synthesis. This drawback is similar to thermodynamically stable micelles, which require different amphiphilic polymers in order to change the composition of the nanoreactors core/shell.

To date, the effect of nanoreactor material on microenvironment characteristics has usually been exploited for the development of novel amphiphiles for micellar self-assembly using an ad hoc approach [3–5]. With thermodynamically stable micelles and dendritic polymers, this is a necessity as either structure is comprised of the single molecular species. Spherical brush polymers could be modularly produced,

however they generally require a polymer bead to begin assembly and often rely on chemically linking the stabilizing molecule.

Alternatively, kinetically trapped micelles can stabilize hydrophobic cores composed of completely separate materials from the amphiphilic stabilizer through a bottom up-assembly process (Figure 2.1C). Therefore, these systems could allow for fundamental studies of nanoreactor microenvironments without the need for complex organic synthesis of amphiphilic polymers.

2.3. Approach

A directed self-assembly process known as Flash NanoPrecipitation offers a method to rapidly and tunably produce kinetically trapped polymer nanoreactors through directed self-assembly [73,78]. In Flash NanoPrecipitation, a water-miscible organic solvent stream solubilizes the nanoparticle materials. For a kinetically trapped micelle these would include an amphiphilic polymer, a hydrophobic co-precipitate, and a hydrophobic material of interest such as a catalyst. The water-miscible organic solvent stream containing the nanoparticle materials is then rapidly mixed against water. Solvent quality degradation resulting from the increased volume fraction of water induces precipitation of the hydrophobic materials. The hydrophobic precipitates aggregate to reduce unfavorable interaction with water and the nucleates grow in size until growth is arrested by stabilization with the amphiphilic polymer. This process is unique because by tuning the relative time scales of block copolymer self-assembly and core material precipitation, the size and relative composition of the nanoreactor can be tuned.

2.4. Specific Aims

Therefore, in this work Flash NanoPrecipitation will be used to create polymer nanoreactors incorporating gold nanoparticles as a model system. The size and catalyst loading can be systematically tuned. Furthermore, modular co-precipitate selection will facilitate investigation of the effects of

nanoreactor composition on reaction kinetics. The versatility of the nanoreactors in oxidation and "one pot" cascade reactions will be examined.

The specific aims of this work are to:

Aim 1: Use Flash Nanoprecipitation to self-assemble polymer nanoreactors and understand the interplay between mass transfer and reaction kinetics within the reaction system. The reduction of 4-nitrophenol will be used as a model reaction. To study potential diffusion limitations, the diffusion coefficient of 4-nitrophenol will be measured through Pulsed Field Gradient NMR with a combination of scaling analysis. When appropriate, the Langmuir-Hinshelwood kinetic model can be used to study intrinsic kinetics.

Aim 2: Through modular selection of the co-precipitate, understand the effect of nanoreactor microenvironment on reaction kinetics. Investigated if the reagent partition coefficients in the nanoreactors affecting localized reagent concentrations influence apparent reaction kinetics. Based on the partition coefficients, study the intrinsic kinetics when using nanoreactors with various co-precipitants.

Aim 3: Demonstrate the application of polymer nanoreactors by performing a one-pot cascade reaction. Reduction of 4-nitrophenol will be combined with condensation of benzaldehyde with the resulting 4-aminophenol as a model reaction. The effect of reducing agent and various one-pot reaction strategies will be investigated. Green chemistry metrics such as E-factor will be evaluated.

Completion of these aims will demonstrate the novel application of the Flash Nanoprecipitation method of self-assembly for producing kinetically-trapped polymer nanoreactors with tunable size, composition, and gold loading. This would allow systematic study of nanoreactor structure with a first-of-its-kind demonstrable impact on reagent concentrations leading to differences in reaction kinetics. Successful application of the polymer nanoreactors to the aqueous one-pot condensation of benzaldehyde

with 4-nitrophenol would demonstrate proof-of-concept use toward cutting-edge green chemical synthesis.

2.5. Overview of Dissertation

The first objective of this study was to use Flash Nanoprecipitation to self-assemble gold nanoparticle/polymer nanocomposite nanoreactors with tunable size and gold loading in order to understand the mass transfer and intrinsic kinetics within the nanoreactors (Figure 2.2A). Next, the Flash Nanoprecipitation formulation composition was varied to create polymer nanoreactors with different hydrophobic core microenvironments in order to study the effects of composition on localized reagent solubility and catalytic performance (Figure 2.2B). Finally, we demonstrate the application of the nanoreactors to green chemical synthesis by performing an aqueous one-pot cascade reaction (Figure 2.2D).

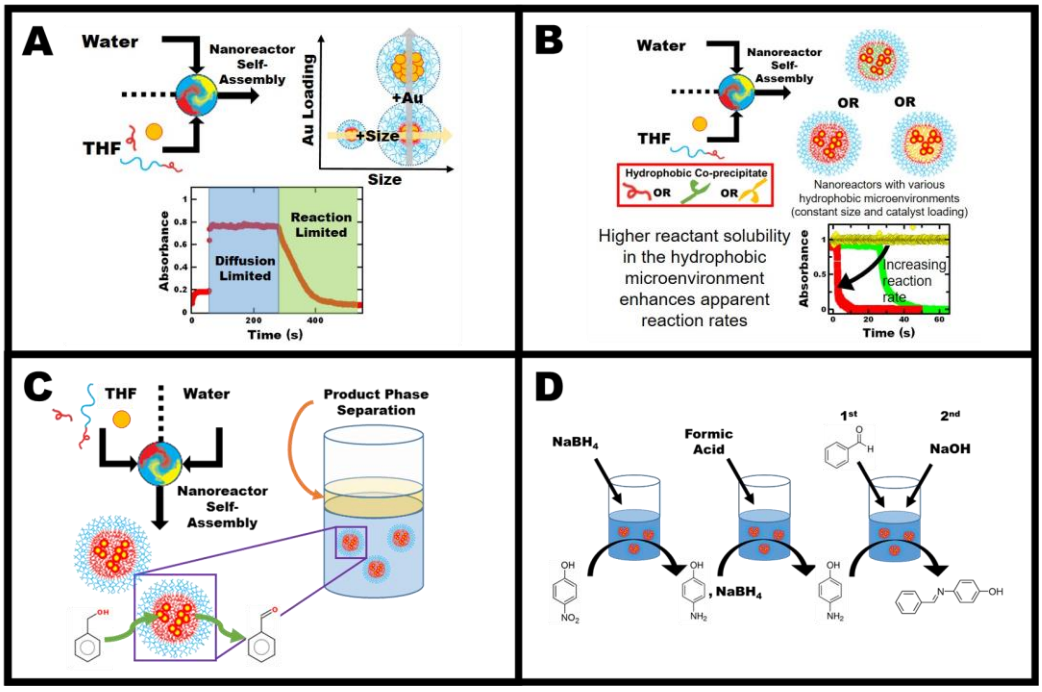

Figure 2.2: Overview of dissertation work. A) Self-assembly of polymer nanoreactors with independent tuning of size and gold loading. B) Accelerated reaction rates within self-assembled polymer nanoreactors with tunable hydrophobic microenvironments. C) Application of self-assembled polymer nanoreactors

towards the oxidation of benzyl alcohol. D) Self-assembled polymer nanoreactors for the one-pot condensation of benzaldehyde with 4-nitrophenol.

The first aim was to understand mass transfer, in regards to reagents, and reaction kinetics within the nanoreactor system. For this purpose, nanoreactors were produced using Flash Nanoprecipitation a directed self-assembly method. In the proposed nanoreactor system, the gold nanoparticle catalysts are expected to be directed within the core of the nanoreactor through hydrophobic interactions during the precipitation event and are kinetically trapped in that arrangement without covalent linkage. For a polystyrene core system this would mean that there are two layers of polymer between the catalyst and the bulk solvent (PEG shell and PS core). In order to achieve this goal of understanding any mass transfer implications on a reaction, stable nanoreactors must be formulated with the ability to independently adjust the size and catalyst loading of the nanoreactors using polystyrene as a model system. The diffusion component was considered using a combination of NMR experiments to measure the diffusion coefficient of the reactant, the apparent reaction rate, and scaling analysis. When appropriate, the Langmuir-Hinshelwood kinetic model was used in order to determine the inherent rate kinetics for comparison to other systems from literature. These results are discussed in Chapter 3.

Solvents play a critical role in reactions not only in the ability to solubilize reagents but also to influence the behavior of the reaction. Within nanoreactors, the core material acts as the solvent for the reaction and can dictate reaction kinetics accordingly [3–8]. Building on the foundation of catalytically active nanoreactors, which could provide a reasonable support for organic phase reactions in aqueous solutions, we next examined the effect of co-precipitate (acting as the local microenvironment for the catalyst/solvent for reaction) on catalytic performance. Flash Nanoprecipitation was used with modular selection of the hydrophobic core material of the nanoreactor and constant size and gold loading in the dispersion. Core materials that interact with gold are beneficial for improving incorporation efficiency of the gold nanoparticles into the nanocomposite nanoreactor during self-assembly but decrease catalytic

performance. For the non-interacting core materials, the catalytic performance is strongly affected by the hydrophobicity as indicated by the Hansen Solubility Parameters. Specifically, the apparent reaction rate per surface area using castor oil (CO) is over 8-fold greater than polystyrene (750 g/mol, PS 750). The increase in apparent catalytic performance can be attributed to differences in reactant solubility rather than differences in mass transfer or intrinsic kinetics; higher reactant solubility enhances apparent reaction rates. These results are discussed in Chapter 4.

We next wanted to explore the versatility of the nanoreactors to other classes of reactions. The oxidation of alcohols to aldehydes and ketones is an important class of chemistry used throughout industrial chemical syntheses, especially in the pharmaceutical industry. While these oxidations are traditionally performed in organic solvents at high temperature, using gold to catalyze the reaction can facilitate the reaction in water to reduce solvent waste. We examined the use of nanoreactors for oxidation of benzyl alcohol. Three oxidants were considered: air, hydrogen peroxide, and sodium hypochlorite. Sodium hypochlorite was the only effective oxidant; conversion of 70 ± 9% of benzyl alcohol was observed to a combination of benzaldehyde and benzyl benzoate. However, the reactors were not stable under the reaction conditions. These results are discussed in Chapter 5.

Finally, we demonstrated ability to perform multiple reactions "one-pot" using the nanoreactors building on the reduction of 4-nitrophenol reaction. Specifically, we examine one-pot, aqueous condensation of benzaldehyde with nitroarenes using polymer stabilized gold nanoparticles. The reduction of 4-nitrophenol to 4-aminophenol followed by the condensation with benzaldehyde was used as a model reaction. The reducing agent selection was examined. One-pot cascade reactions are an attractive approach to green chemistry because they negate the need for intermediate compound isolation, which generally requires organic solvent extractions. This would further reduce the amount of organic solvent necessary during the use of polymer nanoreactors to perform organic phase reactions, and provide

further basis for their use in green chemistry approaches. Therefore, the E-factor was evaluated. These results are discussed in Chapter 6. Conclusions and Future work are presented in Chapter 7.

Chapter 3 : Rapid Self-Assembly of Metal/Polymer Nanocomposite Particles as Nanoreactors and their Kinetic Characterization

Published in Nanomaterials 2019, 9, 318; doi:10.3390/nano9030318

Abstract

Self-assembled metal nanoparticle-polymer nanocomposite particles as nanoreactors are a promising approach for performing liquid phase reactions using water as a bulk solvent. In this work, we demonstrate rapid, scalable self-assembly of metal nanoparticle catalyst-polymer nanocomposite particles via Flash NanoPrecipitation. The catalyst loading and size of the particles can be tuned independently. Using nanocomposite particles as nanoreactors and reduction of 4-nitrophenol as a model reaction, we study the fundamental interplay of reaction and diffusion. The induction time is affected by the sequence of reagent addition, time between additions, and reagent concentration. Combined, our experiments indicate the induction time is most influenced by diffusion of sodium borohydride. Following the induction time, scaling analysis and effective diffusivity measured using NMR indicate that the observed reaction rate are reaction- rather than diffusion-limited. Furthermore, the intrinsic kinetics are comparable to ligand-free gold nanoparticles. This result indicates that the polymer microenvironment does not de-activate or block the catalyst active sites.

3.1 Introduction

Self-assembled amphiphilic molecules, both small molecules and macromolecules, that confine catalysts to micelle, vesicle, and Janus particle nanoreactor systems have proven to offer an efficient approach to perform organic reactions using water as a bulk solvent [26,74,79]. Using Janus particles, catalysts can be incorporated into a portion of the nanocomposite particle and the other portion imparts stability to the system. Asymmetric catalyst loading can facilitate particle motion driven by a chemical reaction [79]. In other nanoreactor systems, surfactant micelles that incorporate organic, metal

(homogeneous), and metal nanoparticle catalysts have been used for a wide range of coupling reactions in water [5,68,80]. Confining catalyzed organic reactions to the nanoreactor environment can be leveraged to speed up various chemical reactions [6,7]. Improved yield and selectivity when compared to traditional organic solvents has been reported [5,8].

Core-shell polymer systems have also been considered. Polymeric micelles have been used for several reactions, such as asymmetric aldol reactions catalyzed by L-proline [69], acylation [31], hydroaminomethylation of octane catalyzed by Ru-based nanoparticles [81], to name a few, with extensive reviews available elsewhere [32]. Another approach has been to immobilize gold nanoparticles within polyelectrolyte-brushes synthesized on a polystyrene core [55]. The polymer microenvironment of these systems can lead to increased local concentrations of reactants, which can accelerate reactions, facilitate reactions of otherwise non-reactive species [8,69,82–84], temperature or pH dependent catalytic activity [85], and/or provide specificity based on hydrophobicity [82].

Generally, these promising approaches have involved design and synthesis of amphiphiles, block copolymers, or polyelectrolytes that contain catalyst or ligand for covalent attachment of the catalyst. Additionally, nanoreactor properties, such as catalyst loading and nanoreactor size, are related to the molecular properties of the synthesized material. Thus, varying the nanoreactor properties would require additional syntheses. Approaches to metal nanoparticle catalyst-polymer nanocomposite particle fabrication would facilitate (1) modular material (off-the-shelf polymer, catalyst) selection, (2) tunable properties (size and catalyst loading), and (3) rapid, scalable production, which would be beneficial to expanding their potential application.

Flash NanoPrecipitation (FNP) is a rapid, scalable method of polymer self-assembly that may be useful for producing nanoreactors. In Flash NanoPrecipitation, an amphiphilic block copolymer and hydrophobic core material are dissolved in a water miscible organic solvent and rapidly mixed against water using a confined impinging jet mixer. Upon mixing, the rapid decrease in solvent quality causes the hydrophobic

core material to precipitate and the block copolymer to micellize directing formation of the overall nanocomposite particle. This particle assembly ends when the hydrophobic block of the block copolymer adsorbs on the precipitating core material preventing further growth, while the hydrophilic block sterically stabilizes the nanoparticle. Given the molecular weight of the block copolymer, dynamic exchange of the block copolymer does not occur [8,28,29], so the resulting structure is kinetically-trapped.

Hydrophobic, inorganic nanoparticles have been incorporated into nanocomposite particles by dispersing the nanoparticles with the dissolved block copolymer and then mixing. Upon mixing, colloidal aggregation and block copolymer self-assembly occurs, due to the decrease in solvent quality. Nanocomposite particle assembly is complete when sufficient hydrophobic blocks of the block copolymer adsorb to the nanoparticle clusters to prevent further aggregation. For example, Gindy et al. demonstrated fabrication of polymer nanostructures containing colloidal gold using Flash NanoPrecipitation [78]. More recently, Pinkerton et al. encapsulated iron oxide nanoparticles for medical imaging applications [73]. For medical imaging, ~100 nm composite nanostructures with tunable inorganic nanoparticle loading were achieved. These studies suggest that Flash NanoPrecipitation is a suitable method for nanoreactor fabrication. However, the ability to independently tune inorganic nanoparticle loading and nanocomposite particle size has yet to be demonstrated.

Other important considerations when using the nanocomposite particles as nanoreactors are the reaction and diffusion within the system. In small molecule micelle systems that are thermodynamically stable, there is constant molecular exchange between the bulk solvent, and the confined hydrophobic mesophase facilitates reaction [5,8]. In the kinetically-trapped systems produced by Flash Nanoprecipitation, reactants and products reach the catalyst by partitioning from the bulk and diffusing through the nanoreactor structure [84]. The potential mass transfer limitations and the effect of incorporation into the nanocomposite particle on reactivity of the catalyst need to be established.

In this work, we use Flash NanoPrecipitation for rapid and scalable self-assembly of hybrid metal nanoparticle catalyst-polymer nanocomposite nanoreactors. Independently tuning the nanoreactor properties, namely size and gold loading, is investigated. We focus on fundamental understanding of reaction and diffusion using the reduction of 4-nitrophenol as a model reaction. Kinetic and scaling analysis following the induction time are also discussed.

3.2 Materials and Methods

3.2.1 Materials

Citrate stabilized 5 nm gold nanoparticles were purchased from Ted Pella. Polystyrene (PS, M_W 800-5000 g/mol) was purchased from Polysciences, Inc. Sodium borohydride and 4-nitrophenol were purchased from Sigma Aldrich (St. Louis, MO, USA). Dodecanethiol (DDT) stabilized 5 nm nanoparticles, tetrahydrofuran (tetrahydrofuran (THF), HPLC grade), ethanol (ACS reagent grade), and diethyl ether (ACS reagent grade) were purchased from Fisher Scientific (Fairmont, NJ, USA). Environmental Grade Hydrochloric Acid 30-38% and Environmental Grade Nitric Acid 70% were purchased from GFS Chemicals (Columbus, OH, USA). The ^{1}H-NMR solvent D_2O with 4,4-dimethyl-4-silapentane-1-sulfonic acid DSS as an internal standard was purchased from Cambridge Isotope Lab, Inc (Andover, MA, USA). These chemicals and materials were used as received. Polystyrene-b-polyethylene glycol (PS-b-PEG, PS_m-b-PEG_n where m = 1600 g/mol and n = 5000 g/mol) was obtained from Polymer Source (Product No. P13141-SEO). Prior to use, PS-b-PEG was dissolved in THF (500 mg/mL) and precipitated in ether (~1:20 v/v THF:ether). The PS-b-PEG was recovered by centrifuging, decanting, and drying under vacuum at room temperature for 2 days.

3.2.2 Nanoreactor Assembly

For self-assembly, the gold nanoparticles should be dispersed in THF (a water-miscible solvent) with molecularly dissolved block copolymer. To disperse the gold nanoparticles in THF, the as-received dodecanethiol stabilized gold nanoparticles in toluene (1 mL) were precipitated into ethanol (45 mL) and filtered using a Buchner funnel. The filtered nanoparticles from the filter cake were resuspended in THF and concentrated via evaporation at room temperature overnight to achieve a nominal concentration of around 20 mg/mL. The final concentration was confirmed by inductively coupled plasma optical emission spectroscopy using an Agilent 5110 (ICP-OES, Santa Clara, CA, USA). UV spectra collected on an Ocean Optics FLAME-S-UV-VIS with a HL-2000-FHSA light source (Largo, FL, USA) were compared before and after the solvent switch to confirm processing did not significantly affect gold nanoparticle size.

For nanoreactor self-assembly, typically, PS-b-PEG (6 mg), dodecanethiol stabilized 5 nm gold nanoparticles (0.5 mg), and PS homopolymer (co-precipitate, 5.5 mg) were added to 0.5 mL of tetrahydrofuran (THF) and sonicated at 55 °C for 30 minutes. Using a manually operated confined impinging jet mixer with dilution (CIJ-D) [71,86] with achievable Reynolds' numbers > 1,300, the resulting THF mixture was rapidly mixed against 0.5 mL of water into a stirring vial of water (4 mL). The resulting dispersion (5 mL total) was stored at room temperature for further characterization and analysis without purification. The nanocomposite particle properties were tuned by adjusting the total solids concentration or the relative amounts of gold nanoparticles and the co-precipitate at a constant total mass or a constant total core volume based on the bulk density of gold and co-precipitate.

3.2.3 Nanoreactor Characterization

Nanoreactor size was measured after mixing using a Malvern Zetasizer Nano ZS (Westborough, MA, USA) with a backscatter detection angle of 173°. Size distributions are reported using the average of four measurements of the intensity weight distributed with normal resolution. The reported size is the peak 1

mean intensity. The polydispersity index (PDI) is defined from the moment of the cumulant fit of the autocorrelation function calculated by the instrument software (appropriate for samples with PDI < 0.3) and is reported as a measure of particle size distribution. UV absorbance spectra (300 to 1200 nm) of the nanoparticle dispersions were measured at room temperature with an Ocean Optics FLAME-S-UV-VIS with a HL-2000-FHSA light source (Largo, FL, USA). For visualization by TEM, samples were submerged in a dilute dispersion of nanoreactors (10-fold dilution with water) for one hour and dried at ambient conditions overnight. Samples were imaged using a Zeiss Libra 120 TEM (Oberkochen, Germany) using an accelerating voltage of 120 kV. To determine the gold nanoparticle concentration, nanoreactor dispersions were dissolved in THF and digested in aqua regia (1:3 nitric acid:hydrochloric acid by volume) and diluted to 5% v/v aqua regia. Gold concentration of the digested sample was measured using inductively coupled plasma optical emission spectroscopy measurements with an Agilent 5110 (Santa Clara, CA, USA).

3.2.4 Kinetic Analysis

The catalytic performance of the nanoreactors was evaluated using the reduction of 4-nitrophenol with sodium borohydride as a model reaction using well established procedures [25,26]. Briefly, gold nanoreactors (AuNR) (150 uL) produced using FNP were diluted with water (2.275 mL) in a quartz cuvette with a stir bar. The reaction was monitored under stirring with an Ocean Optics FLAME-S-VIS-NIR-ES using an HL-2000-FHSA light source (300-1200 nm), with a CUV-UV cuvette holder (Ocean Optics) placed on a stir plate. The spectrometer was blanked to the reaction mixture. Typically, 4-nitrophenol (25 uL of 0.01M solution) was added to the reaction mixture, and data collection began. After 1 minute, sodium borohydride (50 uL of a 5 M solution) was added to the stirring reaction mixture. Scans were taken every millisecond and averaged over 100 scans with data recorded every quarter-second. The reaction was tracked by monitoring the change in intensity of 4-nitrophenol peak at 425 nm. Absorbance at 425 nm as a function of time was smoothed using a five data point centered moving average to correspond to every

second of the experiment. Similar to previous studies [54], the induction time and apparent reaction rate were determined from the absorbance as a function of time. The final reaction mixture contained less than 0.01 vol% THF. The values of K_{app} and induction time are the averages (± standard deviations) of at least 3 trials of each experiment.

3.2.4.1. Induction Time

Initially, the spectra of the polymer nanoreactor dispersion was recorded as a reference to be subtracted from subsequent spectra as background. The 4-nitrophenol was added resulting in an increase in absorbance at 425 nm. The increase in absorbance due to the addition of 4-nitrophenol occurs within 30 seconds. After 1 minute, the sodium borohydride is added, which results in a further increase in absorbance at 425 nm due to formation of the 4-nitrophenolate ion. The initiation of the reaction corresponding to the start of the induction period was defined as the time at which the absorbance at 425 nm increased to at least 10% of the maximum absorbance of the preceding plateau. The induction time is characterized by a slow decrease (0.002 Abs/s) in absorbance that is followed by a sharp (> 0.01 Abs/s) decline in absorbance indicating beginning of the reduction reaction, which signifies the end of the induction period. Changes in the slope of the absorbance vs. time was used to quantitatively determine the induction time. Specifically, the absorbance vs. time during the induction time was presumed to be adequately described by a line calculated from fitting the initial ~20% of the induction period. For example, if the induction period lasted roughly 300 seconds based upon visual inspection, the linear fit of the induction time was based on the first 60 seconds of the induction time. The end of the induction time was determined to be the time at which the experimental data deviated from the predicted value for induction time. Specifically, the first occurrence of three consecutive experimental absorbance values that were greater than 5% lower than the fitted line was classified as the end of the induction period and the beginning of the catalytic reaction.

3.2.4.2. Apparent Reaction Rate Constant

For analysis of the reaction rate, the data was normalized to the absorbance value at the end of the induction period. The natural log of the normalized absorbance over time was plotted and regions of two distinct slopes were observed. The first region has been attributed to formation of an intermediate [54]. In order to avoid analysis of the intermediate reaction, the apparent reaction rate was calculated from the second region corresponded to when the normalized absorbance fell below 0.67. Data corresponding to a 15% conversion was analyzed when determining apparent reaction rate. The induction time and apparent reaction rate are reported as the average ± standard deviation of three experimental trials.

Because the reaction was carried out with a large excess of sodium borohydride compared to 4-nitrophenol, the reaction kinetics can be described by pseudo-first-order kinetics. For heterogeneous catalysts, the apparent rate constant is assumed to be proportional to the surface of the catalyst described by [47,49]:

$$-\frac{dc}{dt} = k_{app}c = k_1 Sc \tag{3.1}$$

where c is the concentration of 4-nitrophenol at time (t), k_{app} is the apparent rate constant, k_1 is the rate constant normalized to surface area of gold nanoparticles per unit volume of the reaction. Experimentally, k_1 is determined by the change in 4-nitrophenol concentration after the induction period and the mass of gold measured by ICP (surface area calculated assuming 5 nm spherical particles).

3.2.5 Langmuir-Hinshelwood Kinetics

For more detailed kinetic analysis, we performed full kinetic analysis considering the two-step reaction mechanism previously established [54]. Full kinetic analysis is described by the reaction rate of each step and the Langmuir adsorption constants of 4-nitrophenol, borohydride, and the stable intermediate. We determined the rate constants for both steps by solving the coupled rate equations using

the numerical method previously described and fitting the experimental data (average of three experimental trials) [54].

The Langmuir Hinshelwood Kinetic Analysis is influenced by the data available at the end of the induction time and start of the reaction. Therefore, we used a more precise method to define the induction time. Prior to the addition of 4-nitrophenol or sodium borohydride, a background spectra of the polymer nanoreactors was taken in order to adjust the reaction data. With the addition of 4-nitrophenol, the absorbance at 425 nm could be seen to rise from the initial absorbance of zero. A plateau in absorbance occurs within 30 seconds after the addition of 4-nitrophenol, which is disturbed by the addition of sodium borohydride. The resulting pH change and presence of the 4-nitrophenolate ion spikes the measured absorbance 10% over the maximum absorbance of the preceding plateau, which begins the period of induction time. A slow decrease (0.002 Abs/s) in absorbance is then noted over the following induction period, after which a sharp decline in absorbance indicates the beginning of the reduction reaction and the termination of the induction period.

The slope of absorbance was calculated over a centered 11-point data range. Noise in the calculated slope was determined to be 10% of the maximum peak absorbance change prior to the beginning of the induction time. The first negative slope change that had a magnitude greater than the defined noise and was consistent over the following two data points was considered the beginning of the reduction reaction and the termination of the induction time. All of the data was then normalized to the absorbance value at the time point, marking the end of the induction period. The reaction data immediately following the induction period was fit to the Langmuir Hinshelwood model.

The reduction of 4-nitrophenol catalyzed by metal nanoparticles model is fully described considering two intermediates: 4-nitrosophenol and 4-hydroxylaminophenol. Since 4-hydroxylaminophenol is the first stable intermediate, there are three compounds that adsorb and desorb during the reaction cycle (reactant, intermediate, and product) and compete for a fixed number of sites on the surface of the nanoparticle

catalysts. The surface coverage is modeled as a Langmuir-Freundlich isotherm following previous reports [54]. The reaction is modelled using two steps: (A) the reduction of 4-nitrophenol to 4-hydroxylaminophenol and (B) the reduction of 4-hydroxylaminophenol to 4-aminophenol and step B is rate limiting. The resulting coupled rate equations are solved numerically to fully model the concentration of 4-nitrophenol as a function of time to fit experimental data (normalized after the induction time for conversions up to 30%) as described previously [54].

3.2.6 NMR Measurements

Saturation transfer difference (STD) spectroscopy is commonly used in biological molecular interaction studies to analyze ligand-protein interactions [87]. These interactions are probed with and without irradiating the sample by utilizing a very selective pulse, typically a Gaussian pulse with a long pulse duration, at a frequency identical to the resonance frequency the host molecule that is in close spatial proximity to the ligand molecule of interest. Moreover, due to spin diffusion, the signals from the ligands associated with the host molecule will be attenuated as well. A peak subtraction is pursed between the spectra obtained with and without the selective irradiation. The interacting ligands are then probed from the difference spectrum.

To evaluate effective transport of the 4-nitrophenol, ^{1}H-NMR spectroscopy and pulsed field gradient (PFG) NMR were performed using a Bruker Avance II 800 MHz NMR with a 5-mm coil 1H-X-Y TBI solution state cryo-NMR probe (Billerica, MA, USA) operating at a narrow-bore and 18.8 T magnet with 50 G/cm gradient along the z-direction. Nanoreactor samples in D_2O and 4-nitrophenol were equilibrated for 100 minutes prior to the PFG-NMR experiment. The self-diffusion coefficients D were determined from the proton spin-echo intensities measured as a function of gradient pulse strength using a standard DOSY sequence:

$$ln(I/I_0) = -D\gamma^2 g^2 \delta^2 \left(\Delta - \frac{\delta}{3} - \frac{\tau}{2}\right) \quad (3.2)$$

where I_0 is the signal amplitude after the PFG pulse sequence with minimal gradients applied, γ the gyromagnetic ratio, g the gradient strength applied, δ is the gradient pulse duration (1 ms), Δ is the diffusion time, and D the self-diffusion coefficient of the mobile species. Parameters employed in our experiments were: g = 46.99 G/cm; Δ = 0.1 s; δ = 1 ms; τ = 514 μs. A standard solution (1% H_2O/99% D_2O, doped with 0.1 mg $GdCl_3$) with established diffusion coefficient (1.872×10^{-9} m^2/s at 298 K) was used for calibration.

Combined saturation transfer difference (STD) spectroscopy and PFG NMR were used to isolate the solute molecules associated with the nanoreactors. Selective saturation of the reactor was achieved by a train of Gaussian-shaped pulses of 30 ms, saturating a bandwidth of about 20 Hz, at 6.88 ppm (where the nanoreactor has signals, but the solute does not) for a saturation time of approximately 3 s to ensure full saturation of the nanoreactor. A reference spectrum and PFG spectra were obtained by irradiating at 0 ppm spectrum. A difference spectra between 0 ppm and 6.8 ppm was obtained (0 ppm spectrum –6. 88 ppm spectrum) to analyze the solute molecules that are within the reactor. Using the PFG spectra, the solute peak intensity as a function of gradient strength was plotted and the diffusion coefficient was determined from the slope of the linear fit. Since nanoreactors diffuse in free solution at least 3 orders of magnitude slower than molecules, the measured diffusion coefficient was considered the effective diffusion coefficient of the solute within the nanoreactor [88–90].

3.2.7 Leaching Studies

To confirm that the observed catalytic activity is associated with the nanoreactors, we compared the nanoreactors to the nanoparticles that were added to polystyrene nanoparticles made via FNP under rigorous stirring with multiple reuses. For reuse following the reaction, nanoreactors were recovered using an Amicon Ultra 2 mL 50K centrifugal filter according to manufacturer's instructions. The filtrate was collected and the retentate containing nanoreactors was diluted with DI water to the original volume. The

recovered nanoreactors were diluted with water to their initial nominal concentration. Finally, the 4-nitrophenol reduction was performed again. This process was carried out three times. For analysis of catalyst leaching, the cumulative filtrate collected for a single sample over multiple recycling steps was dissolved in aqua regia and analyzed with ICP-OES.

3.3 Results and Discussion

3.3.1 Nanoreactor Self-Assembly

To perform Flash NanoPrecipitation, dodecanethiol stabilized 5 nm gold nanoparticles were dispersed in THF with the molecular dissolved, PS and PS-b-PEG, and rapidly mixed with water using a hand-operated confined impinging jet mixer. The entire formation process was accomplished in less than a second; further, the process can be performed continuously at large scales [86,91,92]. Due to their hydrophobic nature and particle aggregation during assembly, the gold nanoparticles are expected to be in the hydrophobic core of the nanoreactor [78,79], forming a nanoparticle-macromolecular system [29,93]. Due to the high molecular weight of the polystyrene block, no dynamic exchange of the block copolymer is expected [20]. The resulting nanoreactors were ~130 nm indicated by a single Gaussian peak with PDI <0.2 on DLS. The dispersions were stable when stored at room temperature for at least 2 months as there was no significant change in size or size distribution by DLS (Figure 3.1), and no macroscopic precipitation of unencapsulated gold was observed.

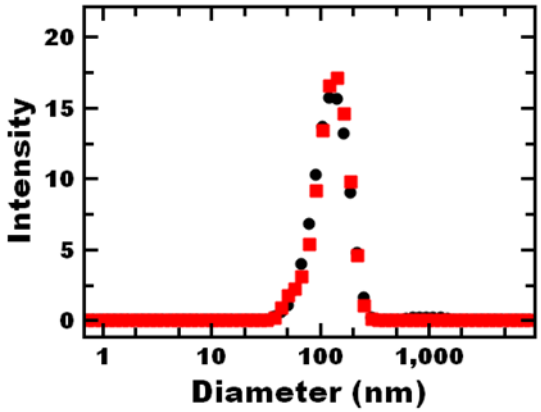

Figure 3.1: Nanoreactor stability at room temperature. No significant change in hydrodynamic size or PDI was observed by DLS after 8 weeks of storage (red squares) compared to the initial size distribution (black circles). Intensity reported is a Malvern reported average of four measurements per sample.

We further characterized the nanoreactors using UV-Vis spectroscopy. Prior to Flash NanoPrecipitation, the dodecanethiol-stabilized nanoparticles dispersed in toluene showed a peak absorbance at 495 nm (as received and after switching solvents). The nanoreactors showed a peak absorbance of 520 nm (Figure 3.2b). The peak shift could occur due to differences in hydrophobicity of the surrounding environment [94]. Since the polystyrene microenvironment should have similar hydrophobicity as toluene, we attribute the red-shift to plasmonic coupling due to close proximity of the encapsulated gold nanoparticles, which has been previously observed with polymer-gold nanocomposite particles [95].

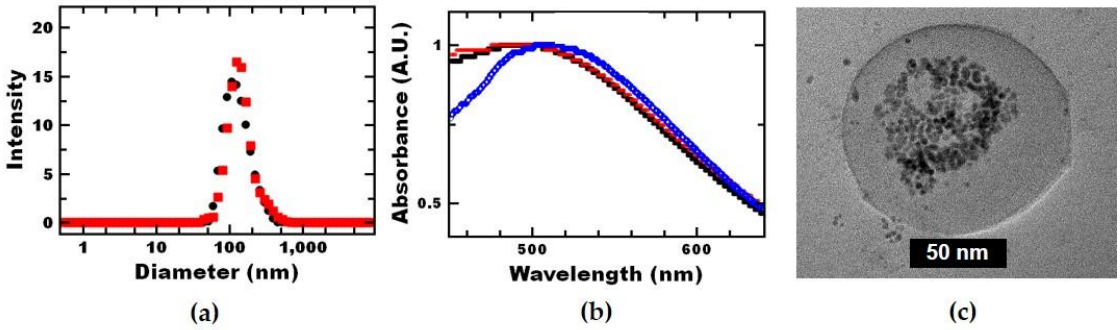

Figure 3.2: Polymer nanoreactors were fabricated via self-directed assembly. (a) DLS confirms the uniform size distribution of the ~130 nm self-assembled polymer nanoreactors (black circles) and confirms that the size is the same after the reduction of 4-nitrophenol (red squares). Intensity reported is a Malvern reported average of four measurements per sample. (b) UV-vis analysis shows that the absorbance of the gold nanoparticle remains unchanged through the solvent switch from toluene (black filled circles) to tetrahydrofuran (THF) (red open circles). A red-shift is seen upon encapsulation within polymer nanoreactors (blue open diamonds) due to close proximity of the encapsulated gold nanoparticles. Absorbance reported is an average of ten measurements per sample. (c) TEM imaging demonstrates that multiple gold nanoparticles were encapsulated within the core of the nanoreactors.

The structure of the nanocomposite particles was visualized using TEM. Based on TEM imaging, clustering of the gold nanoparticles during assembly resulted in multiple catalytic gold nanoparticles per nanoreactor. The majority of the gold nanoparticles appear to be in the nanoreactor core, although multiple polymer layers are not visible on TEM due to low electron density. This result is consistent with previous reports of encapsulated gold nanoparticles via FNP [78,96]. Based on TEM, some of the gold may also be associated with the PEG-layer of the nanoreactors whereas unassociated gold would be expected to precipitate out of the dispersion as well as affect the size distribution measured by DLS. Since we do not observe gold precipitate from the dispersion, and the size of the TEM size is consistent with DLS with PDI <0.2, we assume all the gold in the dispersion is associated with the nanoreactors. Finally, we confirmed

the amount of gold by ICP-OES. We found the polystyrene nanoreactors retained 74% of the gold from the THF-gold nanoparticle solution and the loss can be attributed to the hold-up volume during mixing.

Next, we aim to independently tune the nanoreactor properties, size and gold loading, using formulation parameters. Nanoreactor assembly depends on the relative time scales of block copolymer micellization, gold nanoparticle clustering, and co-precipitate nucleation and growth. Therefore, the overall nanoreactor size can be affected by the ratio of core material to block copolymer, as well as the total concentration of components in the organic stream [73].

Varying the ratio of block copolymer to core materials has been an effective method for tuning nanostructure size via Flash NanoPrecipitation [72,97]. To vary nanoreactor size, the amount of block copolymer concentration can be increased (Figure 3.3), but the gold loading is also affected. In order to vary the nanoreactor size while holding the gold loading constant, we varied the total solids concentration holding the mass ratio of gold to polystyrene co-precipitate constant. As expected, the nanoreactor size increased with increasing total solids concentration. This effect has been attributed to an increase in the rate of particle core relative to nucleation [72,98]. Using this approach, the nanoreactor size could be tuned between 100 and 200 nm with nominal gold loading of 4 wt % (Figure 3.4a). This level of gold loading is comparable other polymer nanocomposite systems with low volume additions of inorganic nanoparticles that demonstrate enhanced functional performance [93].

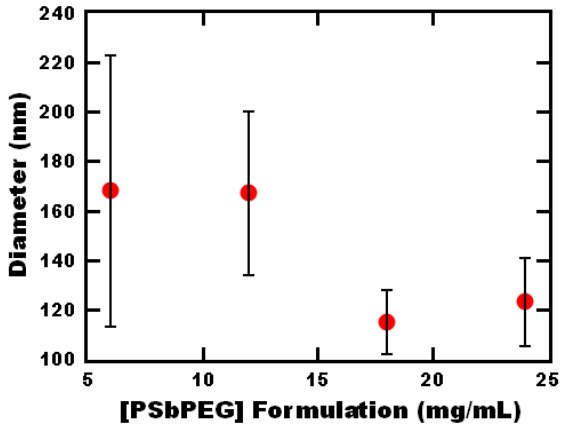

Figure 3.3: Effect of block copolymer concentration on nanoreactor size. Increasing the block copolymer concentration resulted in a decrease in nanoreactor size and gold loading. Diameters reported are an average of four measurements; the error bars represent the standard deviation of four measurements.

Next, we aimed to vary the gold loading independently of nanoparticle size. Holding the total core material mass constant and varying the ratio of gold to polymer resulted in a decrease in nanoparticle size with increasing gold concentration. In contrast, with gold nanoparticles and block copolymer without a co-precipitate, Gindy et al. observed that increasing the gold loading results in an increase in nanocomposite particle size that is attributed to the increase in the amount of gold core relative to the block copolymer [21]. The difference is our use of a co-precipitate. We attribute the trend observed in this case to the increase in the number density of gold nanoparticles that act as nucleating agents that seed particle growth via heterogeneous nucleation [36,98].

To guide nanoreactor formulation, the Smoluchowski diffusion limited aggregation model has previously been used to formulate inorganic nanoparticle-polymer nanocomposite particles via Flash NanoPrecipitation [72]. Based on the model, nanoreactor size can be predicted using:

$$R = \left(K \frac{k_B T c_{core}^{5/3}}{\pi \mu \rho c_{BCP}} \right)^{1/3} \tag{3.3}$$

where R is the aggregate radius, K is a constant of proportionality for formation time, k_B is Boltzmann's constant, T is the absolute temperature, c_{core} is the concentration of core material, c_{BCP} is the concentration of block copolymer, μ is the solvent viscosity, and ρ is the core material density. This model suggests that the nanoreactor size is affected by the volume more than the mass of the core. Thus, as an alternative to holding the mass of the core constant, we held the volume of the core constant, according to:

$$V_{cm} = \frac{m_{AuNP}}{\rho_{AuNP}} + \frac{m_{PS}}{\rho_{PS}} \tag{3.4}$$

where V_{cm} is the total volume of the core materials, m_{AuNP} and m_{PS} are the masses of the gold nanoparticles and polystyrene core materials, respectively, finally ρ_{AuNP} and ρ_{PS} are the densities of the gold nanoparticles and polystyrene core materials, respectively. The core volume was selected from the standard formulation, a nominal gold loading of 4% and nanoreactor concentration of 2.4 mg/mL. Using the density of bulk gold and polystyrene, which are 19.32 g/mL and 1.04 g/mL, respectively, the core material volume was found to be 5.33 μL. Using the approach of constant volume, the gold loading was tuned between 4 and 50 nominal wt % at a nanoreactor size of ~130 nm (Figure 3.4b).

Overall, nanoreactors were assembled in a rapid, scalable, single-step method using Flash NanoPrecipitation. Nanoreactor size could be tuned independently of gold loading by varying the total solids concentration at a constant ratio of gold to polystyrene. Interestingly, the gold loading was tuned independently of nanoreactor size by varying the ratio of gold to polystyrene at constant total core volume. The constant core volume approach may be useful for formulations of multiple components with disparate densities *e.g.,* inorganic particle-polymer nanocomposite particles.

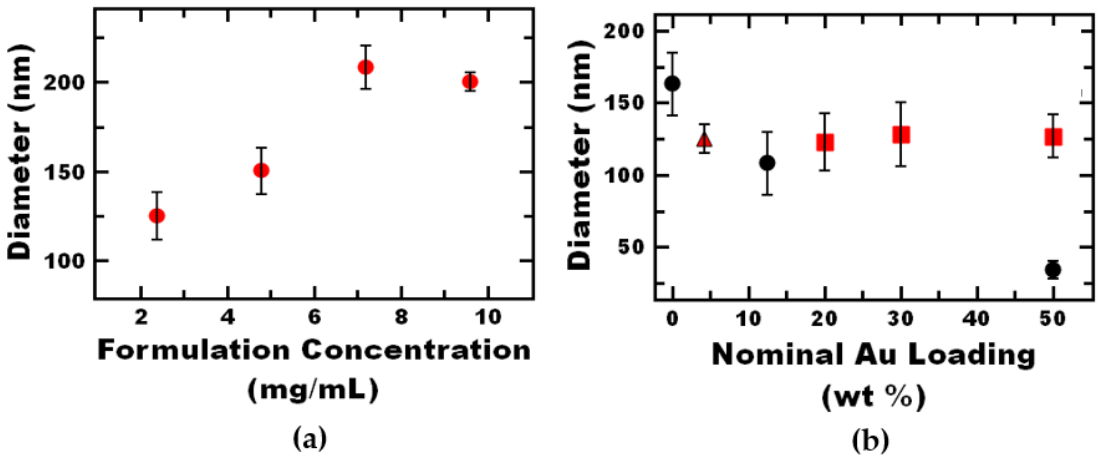

Figure 3.4: Hydrodynamic diameter of polystyrene nanoreactors measured by DLS with varying total nanoreactor material concentration in the formulation. (a) By varying the total material concentration with constant ratio of components tunable nanoreactor size between 100 – 200 nm. (b) By varying the gold to polystyrene co-precipitate ratio at a constant nanoreactor core volume (red squares), as opposed to constant mass ratio (black circles), the nominal gold loading of polystyrene nanoreactors can be tuned at constant nanoreactor size (~130 nm). The standard formulation (4 wt % nominal gold loading, 2.4 mg/mL) is shown by the red triangle. Diameters reported are an average of four measurements; the error bars indicated the standard deviation of the four measurements.

3.3.2 Initial Characterization of Nanoreactor Performance

To evaluate the catalytic performance of the nanoreactor, the reduction of 4-nitrophenol by sodium borohydride was used as a model reaction [99]. First, we confirmed the nanoreactors remained intact following the reaction; no significant change in size or polydispersity was observed by DLS (Figure 3.2a). Further, no macroscopic precipitation of gold nanoparticles was observed following the reaction.

In these initial studies, we assume all of the gold nanoparticles included in the formulation are associated with the nanoreactor and contribute to the observed catalytic activity. From TEM (Figure 3.2c), the gold nanoparticles may be associated with the hydrophobic core or hydrophilic shell or may be

unencapsulated. Unencapsulated gold was not observed precipitating from the nanoreactors and would not contribute to the observed activity (Table 3.1, DDT supported AuNP). This is likely due to the lack of solubility as other hydrophobic inorganic nanoparticles have shown activity in water:solvent reaction mixtures [49]. If the dispersions contained trace amounts of unencapsulated gold, the reported values for k_1 would be slightly underestimated. The conversion of 4-nitrophenol confirmed the gold nanoparticles associated with the nanoreactors were catalytically active (Figure 3.5a). The apparent reaction rate constant per surface area of gold, k_1, for the nanoreactors was 0.414 ± 0.095 L $m^{-2}s^{-1}$, which is comparable to the citrate-stabilized, 5 nm gold particles.

Table 3.1: Rate constants and induction times for various gold nanoparticles. (n=3)

Support	Diameter (nm)	k_1 (L m^{-2} s^{-1})	Induction Time (s)	Reference
PS	5	0.414 ± 0.095	229 ± 21	This Paper
DDT	5	Undetected	N/A	This Paper
Citrate	5	0.173 ± 0.026	5 ± 1	This Paper
Ligand-Free	7	0.17	N/A	[47]

Comparing the performance of the nanoreactors with other metal nanoparticle-polymer systems using the reaction rate considering the amount of gold catalyst (e.g., k_1 in Table 3.2), the nanoreactors demonstrate over 110-fold better catalytic activity than gold within poly(N-isopropylacrylamide)-block-poly-4-vinyl-pyridene (PNIPAm-b-P4VP) micelles, despite a larger overall nanoreactor size. This difference may be attributed to P4VP-gold interactions that affect availability of active sites. Thus, the use of non-interacting co-precipitates and Flash NanoPrecipitation may provide an advantage to other polymer micelle systems that rely on gold-polymer interactions for self-assembly.

Further, the induction time and kinetics are similar to immobilized gold nanoparticles within polyelectrolyte brush shell on polystyrene core particle systems [54]. Specifically, the kinetics of the nanoreactors we report with 5 nm gold are comparable to polyelectrolyte brushes with 2.2 nm gold nanoparticles at the surface of the core-shell nanostructures, which are expected to have similar activities [43]. This result suggests that association of the catalyst with the nanoreactor does not sacrifice reactivity.

Table 3.2: Rate constants for various metal/polymer nanocomposite nanoreactors. (n=3)

Support	AuNP Diameter (nm)	k_1 (L m^{-2} s^{-1})	Reference
Polystyrene nanoreactors	5	$(4.14 \pm 0.95) \times 10^{-1}$	This Paper
PNIPAM-b-P4VP Micelles	3.3	3.70×10^{-3}	[100]
Polyelectrolyte brush	2.2	2.70×10^{-1}	[55]

Leaching studies were also carried out to evaluate the effectiveness of catalyst incorporation within the polymer nanoreactor. Polymer nanoreactors prepared via FNP were compared to polystyrene nanoparticles with hydrophobic gold nanoparticles added to the mixture. In this way the effect of gold nanoparticle incorporation via FNP could be addressed. In both cases, there was an observed decrease in K_{app} after reuse. The gold nanoparticles added to the polymer nanoparticles lost all activity after the first recycling step (Figure 3.5a). For the gold nanoparticles added to polymer nanoparticles, no catalytic activity was observed after the first recycle whereas the nanoreactors retain activity after three recycles (Figure 3.5a), indicating that the retained activity can be attributed to the nanoreactors.

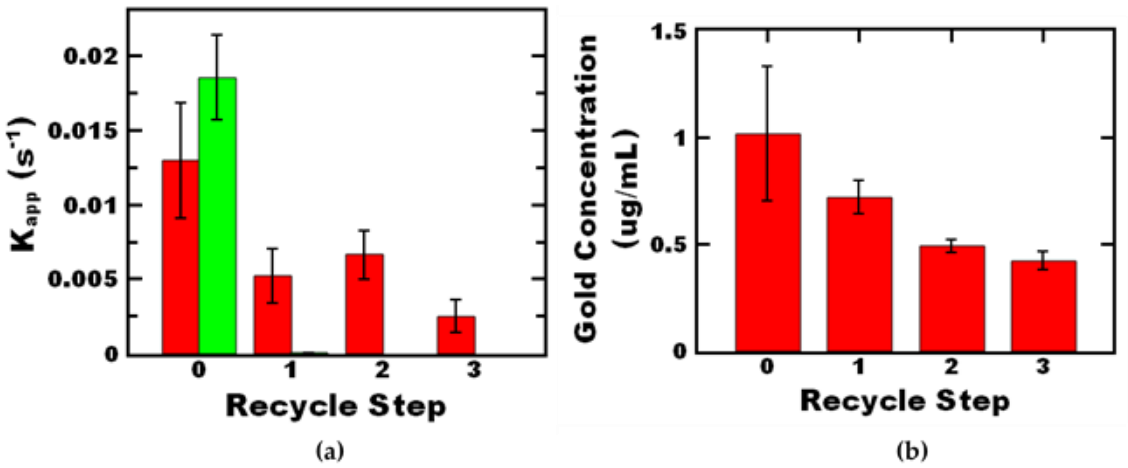

Figure 3.5: Leaching studies of polymer nanoreactors and polystyrene nanoparticles with gold nanoparticles added to solution. (a) The apparent rate constants of polymer nanoreactors (red bars) and polystyrene nanoparticles with added gold nanoparticles (green bars) after subsequent recycling steps. Reported rate constants are an average of three trials; the error bars represent the standard deviation of three trials. (b) The gold concentration of the reaction solution at each recycling step for polymer nanoreactors. The gold concentration reported is an average of three trials; the error bars represent the standard deviation of three trials. No activity is seen from the polystyrene nanoparticles with added gold nanoparticles after 1 recycling step.

The decrease in k_1 after three recycles (Table 3.3) suggests leaching from the gold nanoreactor does occur with multiple reuses. ICP-OES analysis on the filtrate determined there was ~30% reduction in gold content with each recycle step (Figure 3.5b); thus, the loss in activity corresponds to loss of gold. Since 70% retention of nanoparticles has been reported using centrifugal based separations [101], the loss of gold can be attributed, in part, to the loss of nanoreactors.

Table 3.3: Reaction rate constant per catalyst surface area after nanoreactor recycling. (n=3)

Recycle Step	k_1 (L m^{-2} s^{-1})
0	0.4139 ± 0.0952
1	0.2246 ± 0.0901
2	0.4419 ± 0.1266
3	0.1984 ± 0.0632

3.3.3 Probing Potential Mass Transfer Limitations

3.3.3.1. Induction Time

Notably, the induction time of the encapsulated gold nanoparticles is ~50-fold longer than citrate-stabilized nanoparticles (Table 3.1). This relatively long induction time has been previously observed with gold-nanoparticle-polymer nanoreactor systems. It may be attributed, in part, to slow surface restructuring upon encapsulation within the hydrophobic polystyrene microenvironment [55]. Additional factors that may increase induction time include: poisoning of the active sites when encapsulated within the nanoreactor core, reduction of the dissolved oxygen present in the reaction dispersion, and/or diffusion limitations [102,103].

To further understand the nature of the induction time in the nanoreactor system, we investigated both the sequence of addition and the time between adding the reactants (Figure 3.6). Under standard model reaction conditions, 4-nitrophenol was added first and allowed to equilibrate for 1 minute, followed by the addition of the sodium borohydride. To probe potential diffusion limitations, we increased the time between adding the 4-nitrophenol and sodium borohydride 10-fold, and no significant change in induction time was observed. This result suggests that the induction time is not related to diffusion of 4-nitrophenol.

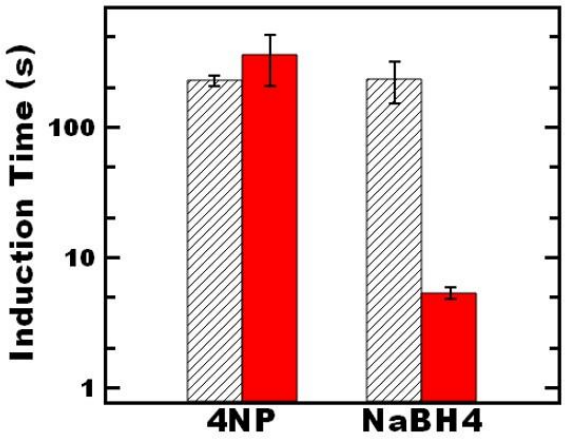

Figure 3.6: The effect of the sequence of reagent addition on the induction time of the 4-nitrophenol reaction. In all experiments, the 4-nitrophenol and sodium borohydride concentration followed standard conditions of 0.01 mM and 0.01 M, respectively. The indicated reagent was the first to be added, after which the reagent was allowed to equilibrate in the solution for either 1 minute (black striped bars) or 10 minutes (red solid bars). The end of the equilibration period was the addition of the second reagent, at which point the reaction could progress. Each reported induction time is an average of three trials; the error bars represent the standard deviation of three trials.

Moreover, switching the sequence to adding sodium borohydride first, followed by 4-nitrophenol after 1 minute of equilibration did not significantly affect the induction time (Figure 2.7). Interestingly, when the equilibration time was increased in this case, the induction time was reduced by two orders of magnitude. This ~5 second induction time is comparable to the value measured for citrate-capped gold nanoparticles. This result indicates that long induction times relative to citrate stabilized gold nanoparticles may be attributed to diffusion of sodium borohydride. Further examining the effect of equilibration time, the induction time decreased from ~100 to 5 seconds when increasing the equilibration time from 1 to 3 minutes (Figure 3.7). Further increasing the equilibration time beyond 3 minutes did not significantly impact the induction time. Thus, it appears that it takes ~3 minutes for sufficient sodium borohydride to partition into the nanoreactor for the reaction to progress. This required equilibration time can be reduced

by increasing the concentration of the borohydride (constant ratio of borohydride to 4-nitrophenol, Figure 3.8) which further indicates the relatively long induction time of the nanoreactors relative to citrate stabilized gold nanoparticles can be attributed to diffusion of the borohydride.

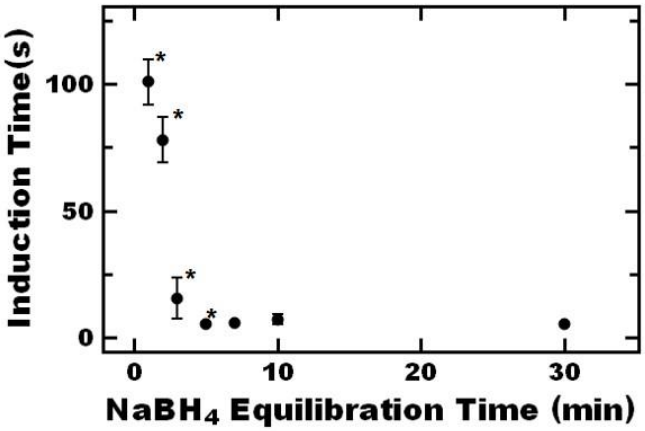

Figure 3.7: The effect of sodium borohydride equilibration on the induction time of the 4-nitrophenol reaction. Standard reagent concentrations of 0.01 mM and 0.01 M were used for 4-nitrophenol and sodium borohydride, respectively. Data points marked with an asterisk (*) are significantly different than each other ($p < 0.1$). Reported induction times are an average of three trials; the error bars represent the standard deviation of three trials.

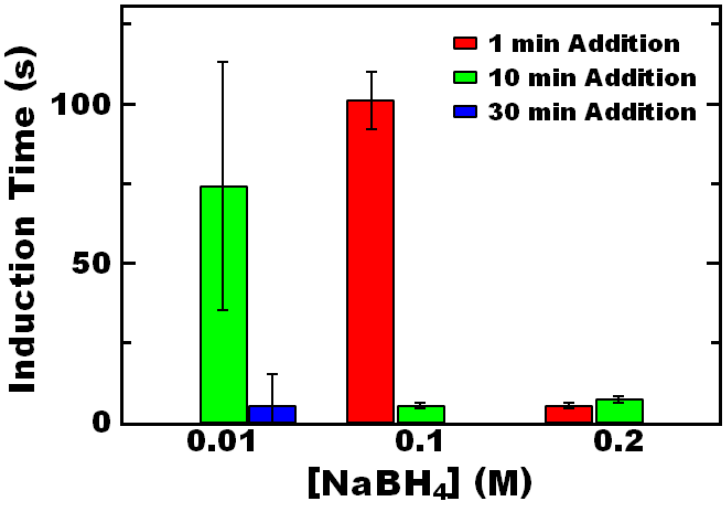

Figure 3.8: The effect of 4-nitrophenol interval of addition (reverse addition sequence) on the induction time present in the reduction of the 4-nitrophenol at varying concentration of reagent. As reagent

concentration increases, the length of addition interval necessary to achieve the minimum induction time of roughly 5 seconds decreases. Reported induction times are an average of three trials; the error bars represent the standard deviation of three trials.

3.3.3.2. Reaction Rate

Next, we further investigated potential mass transfer limitations on the observed reaction rate following the induction time. A useful tool for determination of diffusion limitations is the second Damköhler number (DaII), which is a ratio of the reaction rate to the diffusion rate given by:

$$DaII = \frac{k_{app} C^{n-1}}{\beta a} \tag{3.5}$$

where n is the reaction order, β is the mass transport coefficient (which is a quotient of the diffusion coefficient and the characteristic length of the system), and a is the interfacial area. To calculate *DaII* for a 130 nm diameter particle, the interfacial area (nanoreactor area per unit volume of nanoreactor dispersion) was estimated to be 2×10^4 m^{-1} based on the number of nanoreactors estimated using the aggregation number of the block copolymer previously reported [104,105]. The diffusion coefficient for 4-nitrophenol in the nanoreactor system was experimentally determined by NMR. Using PFG-NMR in conjunction with the STD spectroscopy, the effective diffusion coefficient of the 4-nitrophenol within the nanoreactors was determined to be $1.91 \pm 0.01 \times 10^{-8}$ m^2/s (Figure 3.9). Using this experimentally determined effective diffusion coefficient, the *DaII* is on the order of 10^{-6} indicating the reaction is significantly slower than diffusion; therefore, the apparent kinetics are reaction limited.

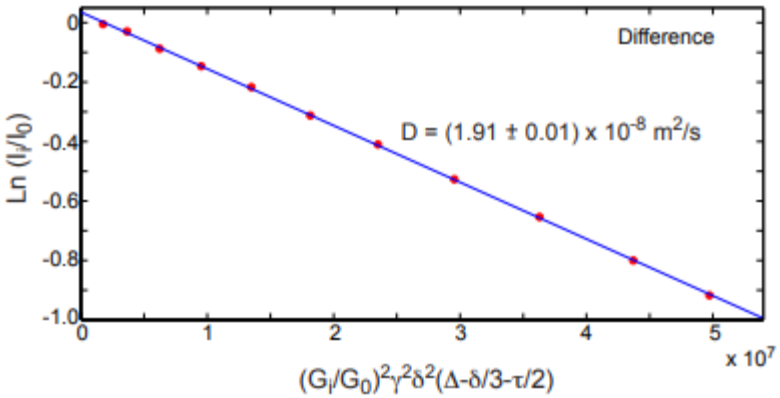

Figure 3.9: Results of saturation transfer differentiated PFG-NMR of 4-nitrophenol in a solution of polystyrene nanoreactors. The blue line corresponds to the curve fit. The difference spectra correspond to the signal from the 4-nitrophenol in closest proximity to polystyrene (within the nanoreactors), which we interpret as an effective diffusion coefficient of 4-nitrophenol within the nanoreactors of 1.9 x 10^{-8} m^2/s.

A complementary approach was to consider the theoretical bimolecular reaction between 4-nitrophenol and nanoparticle catalyst using the Smoluchowski diffusion limited reaction model [106]. For a surface catalyzed bimolecular reaction, in the limit of slow diffusion (compared to electron transfer), the bimolecular rate constant per gold nanoparticle, $k_{bm,}$ can be approximated as

$$k_{bm} = 4\pi r D \tag{3.6}$$

where r is the radius per nanoreactor and D is the diffusion coefficient. The estimated value of the k_{bm} can be compared, after multiplication with Avogadro's constant, to the experimentally observed rate constant k as an indication of mass transfer limitations. Specifically, the experimentally observed rate kinetics are described as:

$$\frac{d[4NP]}{dt} = k[4NP][Au] = k_{app}[4NP] \tag{3.7}$$

where [4NP] and [Au] are 4-nitrophenol concentration and gold nanoparticle catalyst concentration respectively, k is the 2nd order rate constant and k_{app} is the pseudo-first-order rate constant and

$$k_{app} = k[Au] \tag{3.8}$$

Therefore, the 2nd order rate constant, k, can be determined from measuring the k_{app} as a function of gold catalyst concentration [105,106]. An experimentally determined k value approaching (or greater than) k_{bm} would suggest a diffusion limitation.

We therefore varied the gold concentration by (1) varying the nanoreactor concentration to probe potential external diffusion limitations, and (2) varying the gold loading at constant nanoreactor concentration to examine potential internal diffusion limitations (Figure 3.10). When the nanoreactor concentration or the gold loading was increased, k_{app} increased; the 2nd order rate constant was on the order of 10^6 $M^{-1}s^{-1}$. These values are much lower than the k_{bm} ~ 10^8 $M^{-1}s^{-1}$, indicating that neither internal nor external diffusion from the bulk solution to the nanoreactor limited the apparent reaction kinetics.

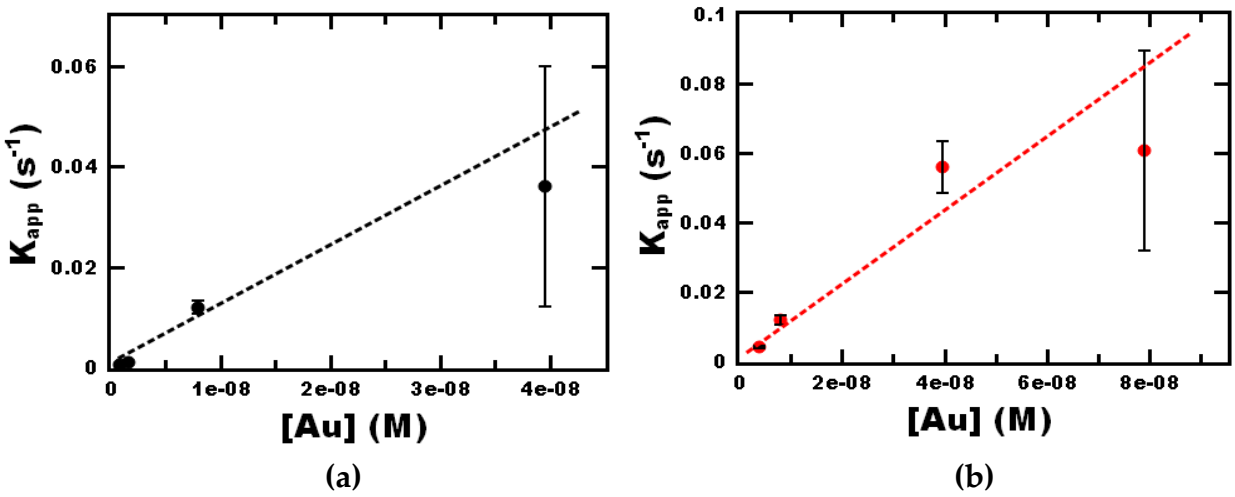

Figure 3.10: The effect of gold concentration on the reaction rate kinetics of 4-nitrophenol reduction by varying (a) the nanoreactor concentration to probe external mass transfer and (b) varying the nanoreactor loading to probe internal mass transfer. Reported rate constants are an average of three trials; the error bars represent the standard deviation of three trials.

Since there were no indications of diffusion limitations associated with the reaction following the induction time, we further characterized the reaction kinetics using Langmuir-Hinshelwood kinetics. Based on the previously established two-step reaction model [54], and fitting the measured concentration of 4-

nitrophenol as a function of time (normalized after the induction time for conversions up to 30%) [54], the kinetics were comparable to other gold nanoparticle-polymer nanoreactor systems (Table 3.4). Interestingly, k_a and k_b observed for the gold encapsulated within the nanoreactors are comparable to ligand-free gold nanoparticles. This result suggests that the reactivity of the gold nanoparticle surface is not significantly affected by self-assembly and their incorporation into the nanoreactors.

Table 3.4: Langmuir-Hinshelwood rate constants obtained from fits to experimental data. (n=3)

Reactor	k_a (10^4 mol/m^2 s)	k_b (10^5 mol/m^2 s)	Reference
Polystyrene Nanoreactors	4.32 ± 0.14	4.3 ± 0.5	This Study
Ligand-Free	5.8 ± 3.1	5.4 ± 2.0	[49]
Brush Shell	9.7 ± 2.9	7.8 ± 1.7	[54]

The model and experimental data are plotted in Figure 3.11 with good agreement. The full fit parameters are provided in Table 3.5.

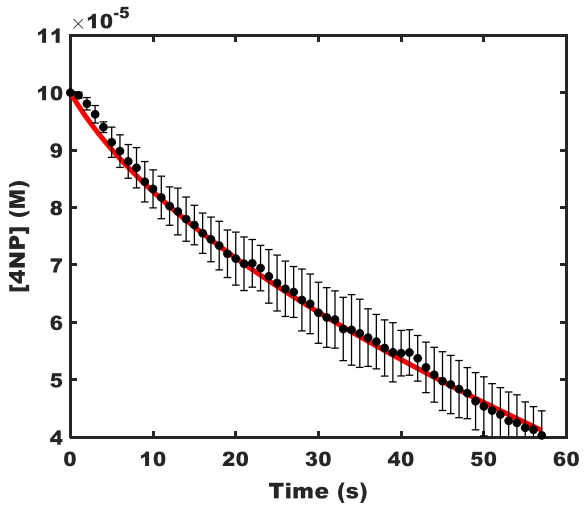

Figure 3.11: Langmuir-Hinshelwood model fit of experimental data for polystyrene nanoreactors. The black circles correspond to experimental data points and the red line represents the fitted curve. Reported

4-nitrophenol concentrations are an average of three trials; the error bars represent the standard deviation of three trials.

Table 3.5: Langmuir-Hinshelwood Fitting Parameters [54].

K_{nip} (L/mol)	K_{bh} (L/mol)	K_{hx} (L/mol)	S (m^2/L)	C_{bh} (mol/L)	C_{nip} (mol/L)	n
4600	62	175000	0.084	0.1	0.0001	0.5

Since the data is well described by the model, the assumptions of first-order rate kinetics, without mass transfer limitations, appear valid within the polymer microenvironment. For fitting, we assume the initial concentrations of the reagents are the same as the bulk. Given the high solubility of borohydride in water compared to organic solvents, the concentration of sodium borohydride of local microenvironment may be lower than the bulk, which may lead to underestimation of the rate constants.

Overall, diffusion and partitioning of sodium borohydride into the polymer nanoreactor affect the induction time for the reaction. Sufficient equilibration time between adding the sodium borohydride and the 4-nitrophenol (~3 minutes) for the borohydride to partition and diffuse minimizes induction time. Notably, mass transfer effects are not observed after the induction time and the intrinsic kinetics are comparable to ligand-free gold nanoparticles.

3.4 Conclusions

Overall, we have presented rapid, scalable self-assembly of hybrid metal nanoparticle catalyst-polymer composite nanoreactors. The size and gold loading of the nanoreactors can be tuned independently, with sizes and nominal loadings ranging from 100-200 nm and 4-50 wt% respectively. Using the 4-nitrophenol reduction as a model reaction, the induction time is affected by sequence or reagent addition, time between addition, and reagent concentration. Combined, our experiments indicate that the

induction time is most influenced by diffusion of sodium borohydride. Scaling analysis and effective diffusivity measured using NMR, the observed reaction rate after the induction time are reaction- rather than diffusion-limited. Finally, the intrinsic reaction kinetics of gold associated with the polymer was comparable to ligand-free particles indicating the self-assembly process and resulting polymer microenvironment does not de-activate or block the catalyst active sites. Building on this foundational study, practical considerations such as nanoreactor recycling will be considered in future work.

Chapter 4 : Self-Assembled Polymer Nanoreactors with Tunable Hydrophobic Microenvironments: Effect on 4-Nitrophenol Reduction Rate Kinetics

Portions of this work published in *Polymers* **2020**, *12*(8), 1774; https://doi.org/10.3390/polym12081774

Abstract

Confining reactions to hydrophobic microenvironments using self-assembled amphiphilic small molecules and macromolecules can facilitate organic phase reactions in a bulk aqueous phase to formulate self-assembled filled polymer micelle nanoreactors (NR) encapsulating gold nanoparticle catalysts (AuNP) within various hydrophobic microenvironments with comparable hydrodynamic nanoreactor size and gold concentration in the nanoreactor dispersion. We systematically vary the properties of the hydrophobic microenvironment and determine that core materials that interact with gold are beneficial for improving incorporation efficiency of the gold nanoparticles into the nanocomposite nanoreactor during self-assembly but decrease catalytic performance. For the non-interacting core materials, the catalytic performance is strongly affected by the hydrophobic microenvironment. Specifically, the apparent reaction rate per surface area using castor oil (CO) is over 8-fold greater than polystyrene (750 g/mol, PS 750). The increase in apparent catalytic performance can be attributed to differences in reactant solubility rather than differences in mass transfer or intrinsic kinetics; higher reactant solubility enhances apparent reaction rates. While we note a trade-off between stability and apparent kinetics as the PS 750 NRs had the lowest apparent reaction rate per surface area with the best stability, full conversion of 4-nitrophenol was achieved within 3 minutes for at least 10 sequential reactions demonstrating that the nanoreactors can be used for multiple reactions.

4.1 Introduction

Confining reactions to hydrophobic microenvironments through the use of self-assembled amphiphilic molecules allows traditionally organic phase reactions to be carried out in a bulk aqueous phase. Replacing the organic solvent with these "nanoreactors" may reduce solvent waste. Furthermore,

confining the reactions such small volumes has shown added benefits of improved efficiency and selectivity over bulk phase reactions [5,8,107].

Small molecule amphiphiles have been used to facilitate a wide range of reactions. For example, Lipshutz and co-workers have developed a series of "designer surfactants" for aqueous micellar catalysis. Using several generations of PEG based amphiphilic surfactants they have demonstrated nanoreactor applicability to a wide range of organic reactions such as cross-couplings [16–18], oxidations [19], reductions [20], and peptide synthesis [21] all in bulk aqueous solutions with high yield. By designing a surfactant molecule with longer PEG portion and a shorter carbon linker between vitamin E and PEG, the micelles were larger and faster reactions were observed [23] in various transition metal-catalyzed reactions (e.g. Suzuki-Miyaura, cross metathesis, amination, C-H activation, borylation, silylation, etc.). Changing the hydrophobic portion of the surfactant from vitamin E to β-sitosterol improved conversion of cross metathesis reactions [23,24]. Surfactants with polar sulfone components within the nonpolar, hydrophobic cores used to facilitate peptide synthesis has recently been reported [21]. It is important to note design of these systems has generally involved syntheses of libraries of new amphiphilic molecules and screening their reactivity [21].

Macromolecular amphiphilic nanoreactor systems have also been considered, with improved stability compared to self-assembled small molecule amphiphilic systems [26,27]. For example, O'Reilly and co-workers incorporated 4-(N,N-dimethylamino)pyridine, a nucleophilic catalyst for a number of reactions including esterifications, into the hydrophobic block of an amphiphilic block copolymer using reversible-addition fragmentation chain (RAFT) polymerization which self-assembled into kinetically frozen micelles. The stable, micellar nanoreactors catalyzed the competitive esterification between multiple anhydrides. More hydrophobic substrates resulted in higher conversions. Further, the hydrophobicity of the substrate could also be used to modify selectivity [26,27]. In other work, L-proline, a chiral organocatalyst for the aldol reaction, was incorporated into the hydrophobic block of an amphiphilic block copolymer via

reversible-addition fragmentation chain (RAFT) polymerization. Upon self-assembly in water, core-shell micellar nanoreactors with catalytic hydrophobic cores were achieved that were significantly more efficient than the unsupported catalyst [31] which was attributed to the hydrophobic microenvironment of the micelle core. The catalyst loading and core hydrophobicity affected the turnover number but the effects could not be decoupled from micelle swelling.

Studies of the effect of nanoreactor composition on nanoreactor performance are limited. With micellar (small molecule and macromolecular) nanoreactors, such a study necessitates synthesis of a new amphiphilic stabilizer for each nanoreactor. Micellar nanoreactors of gold nanoparticles stabilized by water soluble 1, 2, 3-triazlyl dendronized polymers have also been reported by Liu et al. who observed that the catalytic performance is affected by the length and architecture (i.e. linear or branched), as well as the composition of the polymer stabilizer. These results demonstrate that properties of the polymer microenvironment influence the catalytic performance. The dendronized polymer-gold nanoparticle composite formed self-assembled micelles in water and was used to catalyze the reduction of 4-nitrophenol to 4-aminophenol. Turnover frequencies (TOF) were reported as high as 7350 h^{-1}. Varying the properties in this case requires synthesis of different types of 1, 2, 3-triazlyl ligands as well as click-compatible polymer tails [108]. As an alternative, Flash Nanoprecipitation offers a simple approach to produce filled polymer micellar nanoreactors with comparable hydrodynamic size and catalyst concentration in the nanoreactor dispersion but different core materials in order to study the effects of composition of reactor performance. Systematic investigations to understand the effect of the hydrophobic microenvironment core material on the nanoreactor performance with respect to catalyst performance have yet to be established.

Therefore, our focus in this work is to investigate the effect of hydrophobic microenvironment core material on catalytic performance of self-assembled polymer nanoreactors fabricated via Flash NanoPrecipitation. Specifically, in this work, we formulate self-assembled filled polymer micelle nanoreactors encapsulating gold nanoparticle catalysts with various hydrophobic microenvironments.

Formation of the nanoreactors is indicated by DLS and TEM. Since our focus is evaluating the catalytic performance of nanoreactors with various hydrophobic materials, we have selected the reduction of 4-nitrophenol (4NP) with sodium borohydride as a model reaction. Because this reaction proceeds at room temperature without side products and byproducts, it is a well-established model reaction for kinetic studies using gold nanoparticles [51,52,54,76,77,109,110]. We also note that reduction of 4-nitrophenol is important in waste water treatment [111,112] and the product resulting from the model reaction, 4-aminophenol, has several applications e.g. a corrosion inhibitor as well as an intermediate in the pharmaceutical industry [113]. We evaluate the effect of hydrophobic microenvironment on differences in effective diffusion coefficient, localized reagent concentrations through experimentally determined 4-nitrophenol nanoreactor core:water partition coefficients, as well as inherent rate kinetics using the Langmuir Hinshelwood model. The effect of core material on nanoreactor stability when performing sequential reactions is also discussed.

4.2 Materials and Methods

4.2.1 Materials

Polystyrene (PS, M_w 750 g/mol) was purchased from Polymer Source Inc. Sodium borohydride, 4-nitrophenol, dodecane, dodecanethiol, and potassium chloride were purchased from Sigma Aldrich (St. Louis, MO, USA). Castor oil was purchased from Alfa Aesar (Haverhill, MA, USA). Dodecylamine was purchased from Beantown Chemical Corporation (Hudson, NH, USA). Dodecanethiol (DDT) stabilized 5 nm nanoparticles, tetrahydrofuran (tetrahydrofuran (THF), HPLC grade), ethanol (ACS reagent grade), and diethyl ether (ACS reagent grade) were purchased from Fisher Scientific (Fairmont, NJ, USA). Environmental Grade Hydrochloric Acid 30-38% and Environmental Grade Nitric Acid 70% were purchased from GFS Chemicals (Columbus, OH, USA). The ^{1}H-NMR solvent D_2O with 4,4-dimethyl-4-silapentane-1-sulfonic acid DSS as an internal standard was purchased from Cambridge Isotope Lab, Inc

(Andover, MA, USA). These chemicals and materials were used as received. Polystyrene-b-polyethylene glycol (PS-b-PEG, PS_m-b-PEG_n where m = 1600 g/mol and n = 5000 g/mol) was obtained from Polymer Source (Product No. P13141-SEO). Prior to use, PS-b-PEG was dissolved in THF (500 mg/mL) and precipitated in ether (~1:20 v/v THF:ether). The PS-b-PEG was recovered by centrifuging, decanting, and drying under vacuum at room temperature for 2 days as previously described [110].

4.2.2 Nanoreactor Assembly

Initially, the as-received dodecanethiol stabilized gold nanoparticles in toluene (1 mL) were precipitated into ethanol (45 mL) and filtered using a Buchner funnel. The filtered nanoparticles were resuspended in THF and concentrated via evaporation at room temperature overnight to achieve a nominal concentration of around 20 mg/mL for nanoreactor self-assembly. The final concentration was confirmed by inductively coupled plasma optical emission spectroscopy using an Agilent 5110 (ICP-OES, Santa Clara, CA, USA). UV spectra collected on an Ocean Optics FLAME-S-UV-VIS with a HL-2000-FHSA light source (Largo, FL, USA) were compared before and after the solvent switch to confirm processing did not significantly affect gold nanoparticle size.

Nanoreactors were produced via Flash NanoPrecipitation similar to previous reports [110]. Briefly, PS-b-PEG (12 mg), dodecanethiol stabilized 5 nm gold nanoparticles (1 mg), and PS homopolymer, M_W 750 g/mol, abbreviated PS 750 (co-precipitate, 11 mg) were added to 1 mL of tetrahydrofuran (THF) and sonicated at 55 °C for 30 minutes. Using a manually operated confined impinging jet mixer with dilution (CIJ-D) [23,24] and achievable Reynolds' numbers > 1,300, the resulting THF mixture was rapidly mixed against 1 mL of water into a stirring vial of water (8 mL). The resulting dispersion (10 mL total) of nanoreactors was stored at room temperature for further characterization and analysis without purification.

In this work, we formulated nanoreactors encapsulating gold nanoparticle catalysts with various hydrophobic microenvironments. To create nanoreactors with various microenvironments, the PS homopolymer co-precipitate was switched for a different co-precipitate to tune the hydrophobic microenvironment. The various microenvironments used in this study were dodecane, dedecylamine, dodecanethiol, and castor oil.

For comparison to nanoreactors prepared via FNP, we added gold nanoparticles to pre-formed polymer nanoparticles (NP w AuNP). Polymer nanoparticles (NP) filled only with PS 750 or CO were prepared via FNP. Following FNP, gold nanoparticles suspended in THF (500 μL, 2 mg/mL) was added dropwise to a stirring a 5 mL dispersion of pre-formed polymer nanoparticles over 5 minutes.

4.2.3 Nanoreactor Characterization

Nanoreactor size (i.e. hydrodynamic diameter) was measured after mixing using a Malvern Zetasizer Nano ZS (Westborough, MA, USA) with a backscatter detection angle of 173°. Intensity weighted size distributions are reported using the average of four measurements of the intensity weight distributed with normal resolution. The reported size is the peak 1 mean intensity. The polydispersity index (PDI) is defined from the moment of the cumulant fit of the autocorrelation function calculated by the instrument software (appropriate for samples with PDI < 0.3) and is reported as a measure of particle size distribution [71]. For stability analysis, reaction solutions were allowed to sit for at least 24 hours prior to analysis to reduce the formation of bubbles within the solution.

UV absorbance spectra (300 to 1200 nm) of the nanoparticle dispersions were measured at room temperature with an Ocean Optics FLAME-S-UV-VIS with a HL-2000-FHSA light source (Largo, FL, USA) after formulation.

For visualization by TEM, samples were prepared by submerging a grid in a diluted nanoreactor solution (1:10) for 1 hour. After submersion, the grids were removed from the solution and dried at ambient

conditions overnight. Samples were imaged using a Zeiss Libra 120 TEM (Oberkochen, Germany) using an accelerating voltage of 120 kV.

To determine the gold concentration in the nanoreactor dispersions, the nanoreactor dispersions were dissolved in THF and digested in aqua regia (1:3 nitric acid:hydrochloric acid by volume) for at least 24 hours. The samples were then diluted to 5% v/v aqua regia. Gold concentration of the digested sample was measured using inductively coupled plasma optical emission spectroscopy measurements with an Agilent 5110 (Santa Clara, CA, USA). A matrix modifier, potassium chloride (2 mg/mL) in 5% v/v aqua regia, was used to increase the ion concentration which proved beneficial for peak resolution. The reported concentrations are the average of three trials.

To determine the incorporation efficiency of the catalytic gold nanoparticles into the nanocomposite nanoreactor structure during self-assembly, the nanoreactor dispersions were extracted with an equal volume of diethyl ether thrice to remove gold nanoparticles that were unassociated with the nanoreactors. The gold content in the aqueous phases following extraction were analyzed by ICP-OES. Incorporation efficiency was calculated according to:

$$IE = \frac{[Au_{aq}]}{[Au_i]} \tag{4.1}$$

where IE is the incorporation efficiency, $[Au_i]$ is the gold concentration of the original, unextracted solution (total gold in the nanoreactor dispersion), and $[Au_{aq}]$ is the gold concentration of the aqueous fraction after extraction (gold associated with the nanoreactor after extracted with ether which removes gold nanoparticles that are unassociated with the nanoreactors).

4.2.4 Kinetic Analysis

The catalytic performance of the nanoreactors was evaluated using the reduction of 4-nitrophenol with sodium borohydride as a model reaction using well established procedures [54,77]. Generally, gold

nanoreactors (NR) (120 uL, 0.0079 mol% AuNP) produced using FNP were diluted with water (1.527mL) in a quartz cuvette with a stir bar. The nanoreactor solution and sodium borohydride addition solution volumes were adjusted such that the final reaction volume was 2 mL and the sodium borohydride solution had an initial concentration of 6 M. The reaction was monitored under stirring with an Ocean Optics FLAME-S-VIS-NIR-ES (Largo, FL, USA) using an HL-2000-FHSA light source (300-1200 nm), with a CUV-UV cuvette holder (Ocean Optics) placed on a stir plate. The spectrometer was blanked to the reaction mixture. Typically, 4-nitrophenol (20 uL of 0.01M solution) was added to the reaction mixture, and data collection began. After 1 minute, sodium borohydride (333 uL of a 6 M solution) was added to the stirring reaction mixture. Scans were taken every millisecond and averaged over 10 scans with data recorded every 50 milliseconds. The reaction was tracked by monitoring the change in intensity of 4-nitrophenol peak at 425 nm. Absorbance at 425 nm was background corrected be subtracting out the time dependent 600 nm absorbance intensity from the corresponding data point. The induction period was fit to a line, and the data set was normalized to the maximum data point amongst the first witnessed domain of, at least, five consecutive points to fall 1% below the fitted line. The final reaction mixture contained less than 0.01 vol% THF that would have been residual from the self-assembly process. The values of K_{app} and induction time are the averages (± standard deviations) of at least 3 trials of each experiment.

4.2.4.1. Induction Time Determination

Initially, the spectra of the polymer nanoreactor dispersion was recorded as a reference to be subtracted from subsequent spectra as background. The 4-nitrophenol was added resulting in an increase in absorbance at 425 nm. The increase in absorbance due to the addition of 4-nitrophenol occurs within 30 seconds. After 1 minute, the sodium borohydride is added, which results in a further increase in absorbance at 425 nm due to formation of the 4-nitrophenolate ion. The initiation of reaction conditions corresponding to the start of the induction period was defined as the time at which the absorbance at 425 nm increased to

at least 10% of the absorbance at 45 seconds. The induction time itself is characterized by a slow decrease (0.002 Abs/s) in absorbance that is followed by a sharp (> 0.01 Abs/s) decline in absorbance indicating beginning of the reduction reaction, which signifies the end of the induction period. Changes in the slope of the absorbance vs. time was used to quantitatively determine the induction time. Specifically, the absorbance vs. time during the induction time was presumed to be adequately described by a line calculated from fitting the initial region of the induction period (no less than 10% of the total approximate induction time domain). For example, if the induction period lasted roughly 300 seconds based upon visual inspection, the linear fit of the induction time was based on the first 60 seconds of the induction time. Next, the maximum value within the first five, or more, consecutive data points which were at least 1% less than the fitted line was used to normalize the data set. Importantly, these consecutive data points must occur after the start of the induction time period. The time point designating the end of the induction time was then defined as the last occurrence of the normalized data point with a value of 1.

4.2.4.2. Apparent Reaction Rate Constant

For analysis of the reaction rate, the natural log of the normalized absorbance was plotted with respect to time and regions of two distinct slopes were observed. The first region has been attributed to formation of an intermediate [54]. In order to avoid analysis of the intermediate reaction, the apparent reaction rate was calculated from the second region corresponding to when the normalized absorbance fell below 0.67. Data corresponding to a 15% conversion was analyzed when determining apparent reaction rate. If the 15% conversion domain contained less than 4 data points, one data point above the determined region and below the region were included such that no analysis included less than three data points. The induction time and apparent reaction rate are reported as the average ± standard deviation of three experimental trials.

With a sufficiently large excess of sodium borohydride compared to 4-nitrophenol, the reaction kinetics can be described by pseudo-first-order kinetics. For heterogeneous catalysts, the apparent rate constant is assumed to be proportional to the surface of the catalyst described by [54]:

$$-\frac{dc}{dt} = k_{app}c = k_1 Sc \tag{4.2}$$

where c is the concentration of 4-nitrophenol at time (t), k_{app} is the apparent rate constant, k_1 is the rate constant normalized to surface area of gold nanoparticles per unit volume of the reaction (S). Experimentally, k_1 is determined by the change in 4-nitrophenol concentration after the induction period and the mass of gold measured by ICP (surface area calculated assuming 5 nm spherical particles). Pseudo-first order rate kinetics are characteristically described by a linear fit when the natural log of the reagent concentration is plotted with time.

4.2.5 *Partition Coefficient Determination*

To better understand the reactant concentration in the hydrophobic microenvironments, our goal was to determine the partition coefficient of the 4-nitrophenol between water and the hydrophobic microenvironment used as the nanoreactor core which is a ratio of the concentration in the hydrophobic microenvironment to the bulk aqueous phase. To estimate this partition coefficient, an aqueous solution of 4-nitrophenol (0.1 mM) was placed in equilibrium with an immiscible organic solvent representing the polymer nanoreactor core material. Toluene was used as a proxy for polystyrene, while castor oil was used directly. After vigorous shaking for 10 minutes, the emulsion was allowed to rest for 1 week prior to analysis. After 1 week, UV-Vis analysis was used to analyze the absorbance of 4-nitrophenol in the original solution and the aqueous phase of two phase equilibrium. According to Beer's law (concentration is proportional to absorbance), the partition coefficient was calculated using the absorbance at 425 nm:

$$P_{4NP} = \frac{[4NP]_{hydrophobic}}{[4NP]_{aq}} = \frac{1-\frac{Abs_{4NP_{aq}}}{Abs_{4NP_i}}}{Abs_{4NP_{aq}}} \tag{4.3}$$

where P_{4NP} is the partition coefficient is the ratio of the of 4-nitrophenol in the hydrophobic microenvironment of the nanoreactor core and water, $Abs_{4NP_{aq}}$ is the absorbance of 4NP in the aqueous phase of the equilibrium and Abs_{4NP_i} is the absorbance of 4NP in the initial solution of water prior to being placed into equilibrium with the organic phase. The absorbances were averages of three measurements.

4.2.6 NMR Measurements

To evaluate effective transport of the 4-nitrophenol, ^{1}H-NMR spectroscopy and pulsed field gradient (PFG) NMR, combined with saturated transfer difference (STD) spectroscopy, using a Bruker 800 MHz cryo-probe (Billerica, MA, USA) was performed in accordance with the methods described previously (our paper). Briefly, 4-nitrophenol molecules in close proximity to the nanoreactor core were analyzed based on spin diffusion of selectively saturated core material (polystyrene or castor oil), in conjunction with an applied magnetic field gradient. Relevant peak intensities were analyzed as a function of gradient strength to determine the diffusion coefficient of 4-nitrophenol molecules of interest. Since nanoreactors diffuse in free solution at least 3 orders of magnitude slower than molecules, the measured diffusion coefficient was considered the effective diffusion coefficient of the solute within the nanoreactor [88,89]. A detailed method explanation has been published previously [110].

4.2.7 Langmuir-Hinshelwood Kinetics

For more detailed kinetic analysis, we performed full kinetic analysis considering the two-step reaction mechanism previously established [54]. Importantly, to consider the effect of localized reagent concentrations, the partition coefficient for 4-nitrophenol was incorporated and the referenced Langmuir-Hinshelwood mechanistic equations were adapted as follows:

$$-\left(\frac{dc_{nip}}{dt}\right) = k_a S \frac{\left(K_{nip}P_{nip}c_{nip}\right)^n \left(K_{BH_4}c_{BH_4}\right)}{\left[1+\left(K_{nip}P_{nip}c_{nip}\right)^n + K_{Hx}c_{Hx} + K_{BH_4}c_{BH_4}\right]^2} \quad (4.4)$$

$$\left(\frac{dc_{Hx}}{dt}\right) = k_a S \frac{(K_{nip}P_{nip}c_{nip})^n (K_{BH_4}c_{BH_4})}{\left[1+(K_{nip}P_{nip}c_{nip})^n + K_{Hx}c_{Hx} + K_{BH_4}c_{BH_4}\right]^2}$$

$$- k_b S \frac{K_{Hx}c_{Hx}K_{BH_4}c_{BH_4}}{\left[1+(K_{nip}P_{nip}c_{nip})^n + K_{Hx}c_{Hx} + K_{BH_4}c_{BH_4}\right]^2} \quad (4.5)$$

where P_{nip} is the partition coefficient of 4-nitrophenol. Full kinetic analysis is described by the reaction rate of each step and the Langmuir adsorption constants of 4-nitrophenol, borohydride, and the stable intermediate. We determined the rate constants for both steps by solving the coupled rate equations using the numerical method previously described and fitting the experimental data (average of three experimental trials) [54].

4.2.8 Sequential Reactions

As a measure of nanoreactor stability [58,114], we tested the ability to perform multiple, sequential reactions. Following the standard reaction conditions, sequential additions of 4-nitrophenol (20 μL, 0.01 M) were carried out after the initial addition of 4-nitrophenol and sodium borohydride (333 μL, 6 M) with 3 minutes between each subsequent addition. No additional sodium borohydride was added. UV-Vis absorbance was analyzed continuously over the 35 minute time period in accordance with the previously described method.

Bubbles were manually popped prior to each addition of 4-nitrophenol while carefully avoiding contact with the reaction mixture. Due to the presence of bubbles in bubbles in subsequent reactions, the start of subsequent reactions was determined by taking an average of 5-consecutive data points after the maximum post-4NP addition absorbance. The last time point with a value equal to, or greater than, this average was defined as the beginning of the reaction. After determining the start of the reaction, the rest of the kinetic analysis follows the procedure described in the Supporting Information. The apparent rate constant of each sequential reaction was determined from the average of three trials.

4.3 Results

4.3.1 Nanoreactor Formulation and Characterization

To fabricate filled polymer micelle nanoreactors encapsulating gold nanoparticle catalysts with various hydrophobic microenvironment, we performed Flash NanoPrecipitation (FNP) with varying co-precipitates and hydrophobic gold nanoparticles. FNP is a rapid, scalable platform for polymer-directed self-assembly of colloidal nanoparticles with versatile materials selection [73,78,110]. To incorporate gold nanoparticles, hydrophobic gold nanoparticles are dispersed with a dissolved amphiphilic block copolymer and hydrophobic core material in a water miscible organic solvent and rapidly mixed against water using a confined impinging jet mixer. Upon mixing, the rapid decrease in solvent quality causes the nanoparticles to aggregate, hydrophobic core material to precipitate and the block copolymer to micellize directing formation of the overall nanocomposite particle. This nanocomposite particle assembly ends when the hydrophobic block of the block copolymer adsorbs on the nanoparticle clusters with precipitating core material preventing further growth and colloidal aggregation, while the hydrophilic block sterically stabilizes the nanoparticle. Given the molecular weight of the block copolymer, dynamic exchange of the block copolymer does not occur [8,28,29], and the resulting structure is kinetically-trapped. Successful polymer nanoreactor assembly results in uniform dispersions with no macroscopic precipitation of the hydrophobic components, including the gold nanoparticles. Further evidence of successful self-assembly of dispersed polymer systems is evident by dynamic light scattering (DLS). Specifically, DLS results confirm that the composite nanoparticles are uniform with a single peak in the size intensity distribution measured by DLS indicating the hydrodynamic diameter is ~100 nm; representative data for the PS750 nanoreactors is shown in blue in Figure 4.1A.

We also examined the structure of the nanoreactors using TEM. Self-assembled nanoreactors show incorporation of the gold nanoparticles throughout the nanoreactor (Figure 4.1B). Gold nanoparticles

appear to be incorporated within the core of the polymer nanoreactor. The gold also appears to be associated with the PEG layer. Thus, the gold in the core of the polymer nanoreactor appears dark, the hydrophobic microenvironment appears light, and the PEG layer with gold associated has a medium contrast due to the electron density. The nanoreactors appear spherical and the size seen in the images is comparable to the DLS reported hydrodynamic diameters and generally on the order of 100 nm (Table 4.1) with some aggregation of the nanoreactor structures apparent upon drying. The TEM images suggest there are multiple gold nanoparticles per nanoreactor structure, which is possible based on the gold nominal loading (4 wt. % (wt. gold/total solids) and the estimated number of polymer nanoreactors formed during FNP (calculated based on the aggregation number) [103,104].

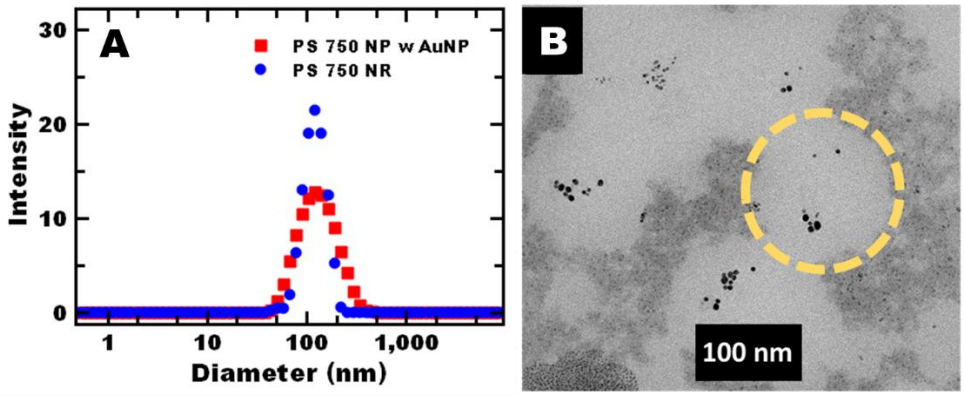

Figure 4.1: A) Representative DLS spectra for PS 750 NR (●) and pre-formed PS 750 NP with AuNP (■, PS 750 NP w AuNP). A single intensity peak is seen for both PS NR and pre-formed PS 750 NP with post-formulation added AuNP. Reported intensities are a Malvern reported average of four measurements. B) Representative TEM image of self-assembled polymer nanoreactors (PS 750 NR). A dotted line is used to indicate the nanoreactor core to guide the eye. In the nanoreactors prepared by FNP shown in (B), gold nanoparticles appear to be incorporated within the nanoreactor core as well as associated with the PEG layer. Thus, the gold in the core of the polymer nanoreactor appears dark the hydrophobic PS750 microenvironment appears light, and the PEG layer with gold associated has a medium contrast due to the electron density.

To evaluate the effect of incorporating the gold nanoparticles into the nanoreactors during FNP, we formulated polymer nanoparticles and added gold nanoparticles after formulation. Specifically, polymer nanoparticles of PS 750 and castor oil of comparable hydrodynamic size were formulated (Table 4.1). Following FNP, hydrophobic gold nanoparticles dispersed in THF were added to the dispersed polymer nanoparticles. No macroscopic aggregation of the gold nanoparticles in the aqueous phase was observed; and were thus loosely associated with the polymer nanoparticle via nonspecific adsorption. TEM confirms that gold is associated with the surface of the pre-formed polymer particles (Figure 4.2). Some agglomeration of the gold is evident and further supported by the peak shift witnessed in UV-Vis spectra for pre-formed polymer nanoparticles, especially PS 750, with added gold nanoparticles (Figure 4.3A, Table 4.2).

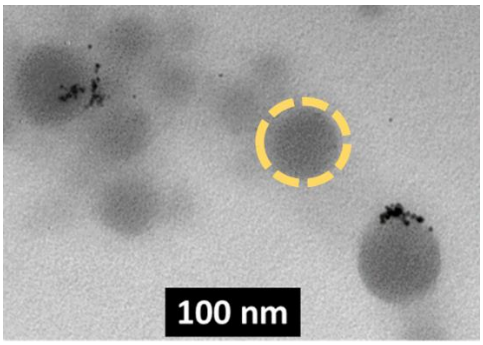

Figure 4.2: TEM image of pre-formed PS 750 NP with AuNP. A dotted line is used to indicate the nanoreactor core to guide the eye. Gold nanoparticles appear to be incorporated along the surface of the nanoreactor with some agglomeration of gold nanoparticles. In this case, the relatively large pre-formed particle-core has medium contrast, the aggregated gold particles adsorbed to the surface appear dark, and the PEG-layer has light contrast (and is not visible), thus the structures appear smaller than their hydrodynamic size measured by DLS and smaller than PS 750 NRs. These results are consistent with previous studies [98,115–117].

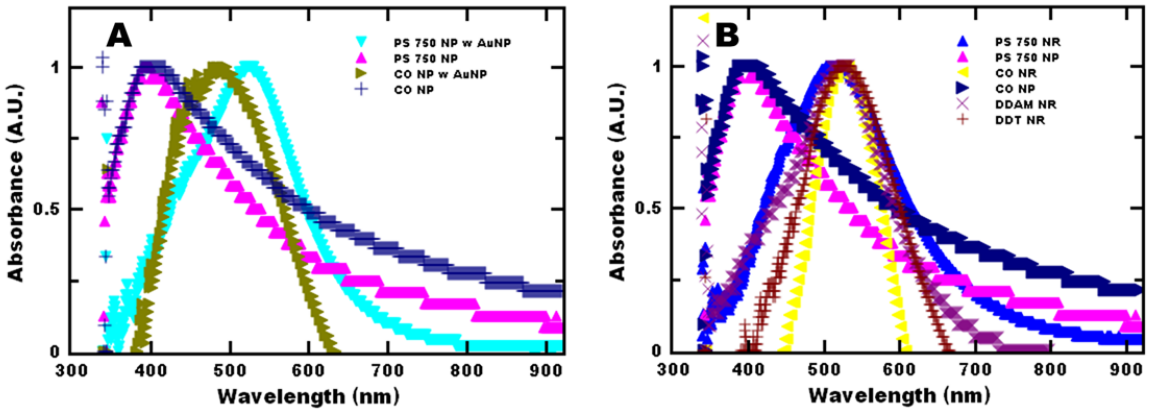

Figure 4.3: UV-Vis spectra from 300 to 900 nm of all A) pre-formed polymer nanoparticles with gold nanoparticles compared to polymer nanoparticles (without gold nanoparticles) and B) nanoreactors compared to polymer nanoparticles (without gold nanoparticles). The spectra for polymer nanoparticles (without gold nanoparticles) were used as background spectra in order to account for scattering due to the polymer structures. Shoulders witnessed in nanoreactor and pre-formed polymer nanoparticles with gold nanoparticles around 400-450 nm can be attributed to polymer nanoparticle scattering and slight mismatch in nanoparticle concentrations between the sample used for the background spectra and the sample. In A) the peak shift compared to 5-nm gold in toluene (peak at 495 nm) for the gold NPs added to pre-formed PS 750 nanoparticles could be attributable to gold nanoparticle agglomeration observed in TEM images. In B), the peak shift to ~520 nm is consistent with gold nanoparticles incorporated into polymer nanoreactors. In this case, the peak shift compared to 5-nm gold in toluene (peak at 495 nm) may be attributed to the hydrophobicity of the nanoreactor or plasmonic coupling due to close proximity of the incorporated gold nanoparticles within the nanoreactors. Reported absorbances are an average of ten measurements.

Comparing the TEM images of the self-assembled nanoreactors (Figure 4.1B) to the gold nanoparticles added to pre-formed polymer nanoparticles (Figure 4.2) suggests that there are spatial differences in the gold nanoparticle distribution. Specifically, when gold nanoparticles are added to pre-formed polymer

particles the gold is associated with the surface of the polymer particle. With FNP, the gold nanoparticles are incorporated throughout the nanoreactor structure, i.e. there are gold nanoparticles in the hydrophobic microenvironment as well as associated with the PEG layer. In this study, we are interested in comparing the catalytic performance of these systems to determine the effect of the hydrophobic microenvironment.

Thus, our next goal was to achieve nanoreactors of comparable hydrodynamic size and gold concentration in the nanoreactor dispersion with various co-precipitates to tune the hydrophobic microenvironment surrounding the catalyst. To study the effect of catalyst co-precipitate interactions, we examined dodecane, dodecylamine, and dodecanethiol. We also compared co-precipitates that did not interact with gold with different solubility parameters, such as castor oil and a low molecular weight polystyrene (PS, MW 750 g/mol). The constant core volume approach previously established was used to affect the nanoreactor hydrodynamic size and gold concentration in the dispersion while changing the core-material [110]. Since the densities of the core materials are comparable, using the same co-precipitate concentration in the organic stream during FNP (11 mg/mL co-precipitate with 1 mg/mL gold nanoparticles and 12 mg/mL block copolymer stabilizer), the hydrodynamic size of the nanoreactors were comparable [110]. As shown in Table 4.1, all systems formed nanoreactors around 130 nm with low polydispersity (< 0.3 PDI) as measured by DLS. A representative size intensity distribution measured by DLS for the nanoreactors and nanoparticles with gold nanoparticles after formulations are shown compared in Figure 4.1A. All nanoreactors except for dodecane remained stable, in regards to size and polydispersity, over a period of at least 1 week at room temperature; they did not undergo a size change from the initial DLS measurement of more than 30% and their PDI remained under 0.3 (Table 4.1). In contrast, after one week, dodecane nanoreactors analyzed by DLS were found to have an average size of 195 ± 41 nm and a PDI of 0.361. Unlike the initial analysis, after a week multiple size distribution peaks were present in the DLS analysis as thus were not considered stable.

Table 4.1: Size and stability of various nanoreactor formulations. (n=4)

System	Size (nm)	PDI	Stability*
PS 750 NR	124 ± 6	0.131 ± 0.012	Yes
PS 750 NP w AuNP	150 ± 27	0.144 ± 0.013	Yes
CO NR	113 ± 10	0.184 ± 0.011	Yes
CO NP w AuNP	136 ± 7	0.147 ± 0.006	Yes
Dodecane NR	168 ± 6	0.108 ± 0.003	No
Dodecylamine NR	143 ± 23	0.263 ± 0.019	Yes
Dodecanethiol NR	101 ± 6	0.087 ± 0.028	Yes

*Stability defined as change in diameter < 30% and a PDI < 0.3 after 1 week of storage at room temperature as measured by DLS

Following FNP, we aimed to determine the amount of gold successfully incorporated into the nanoreactor during self-assembly, which we quantify with the incorporation efficiency (IE). To remove any hydrophobic gold nanoparticles in the dispersion that were not incorporated into the nanoreactors, we performed an ether extraction to selectively remove unincorporated gold nanoparticles while preventing disruption of the nanoreactors (as PEG is insoluble). To demonstrate that the ether extraction would remove unincorporated gold nanoparticles, dodecanethiol-capped gold nanoparticles in water were processed and the calculated incorporation efficiency was 5 ± 1% indicating that 95 ± 1% of the gold

nanoparticles were recovered (Table 4.2). This result demonstrates that ether extraction is effective for selectively removing unincorporated gold nanoparticles from the nanoreactor dispersions.

Next, we performed an ether extraction with the nanoreactor dispersions prepared using the various co-precipitants to examine the incorporation efficiency for the various co-precipitates. The incorporation efficiency for gold nanoparticles via FNP was greater than 77 ± 5 % for all systems (Table 4.2). Co-precipitates that interact with gold had the highest incorporation efficiencies. Both dodecanethiol and dodecylamine had incorporation efficiencies greater than 95% (Table 4.2). Performing DLS analysis after extraction, we confirmed that the nanoreactors remain intact through the extraction process which we attribute to the insolubility of the amphiphilic polymer, PS-b-PEG, in diethyl ether.

We compared the incorporation efficiencies of the nanoreactor systems prepared via FNP to adding gold nanoparticles to polymer nanoparticles after formulation. Interestingly, PS 750 NP w AuNP and CO NP w AuNP systems had 89 ± 7% and 94 ± 2% incorporation efficiencies, respectively, which are comparable to the formulated nanoreactors (Table 4.2). This result could be due to affinity of the hydrophobic gold nanoparticle and the core-shell interface of the formulated polymer nanoparticle. Once associated with the polymer nanostructure, there is a sufficient barrier to prevent partitioning of the gold nanoparticles during extraction.

Table 4.2: Characterization of gold concentration in the nanoreactor dispersion and incorporation efficiency (IE) of the gold nanoparticles into the nanocomposite particles. (n=3)

System	[Au] (μg/mL)	IE (%)	Absorbance (nm)
PS 750 NR	137 ± 1	85 ± 2	514 ± 16
PS 750 NP w AuNP	119 ± 6	89 ± 7	525 ± 8

System	[Au] (μg/mL)	IE (%)	Absorbance (nm)
CO NR	106 ± 1	84 ± 3	526 ± 11
CO NP w AuNP	118 ± 11	94 ± 2	490 ± 9
Dodecylamine NR	85 ± 1	98 ± 3	522 ± 17
Dodecanethiol NR	101 ± 3	97 ± 1	528 ± 13
Hydrophobic AuNP in Water	71 ± 1	5 ± 1	N/A

Since the absorbance of gold nanoparticles due to the plasmon resonance is well known to be both size and environment dependent [94,95] we compared the effect of incorporating the gold nanoparticles into the nanoreactors during FNP to adding gold nanoparticles to pre-formed polymer nanoparticles using UV-vis analysis (Figure 4.3). We have previously reported that the dodecanethiol-stabilized nanoparticles dispersed in toluene show a peak absorbance at 495 nm (as received and after switching solvents) [110]. The peak absorbance of CO NP w AuNP was similar with a peak absorbance at 490 nm. Interestingly, a slight peak shift to 525 nm was observed for gold nanoparticles added to pre-formed PS750 particles. The shift in peak absorbance could also indicate agglomeration of the gold nanoparticles supporting the TEM observations (Figure 4.2) [118]. The peak absorbance for the self-assembled nanoreactors were ~520 nm, consistent with previous reports [110] Such shifts in peak absorbance to higher wavelengths have been previously observed and may be due to the local environment of polymer nanostructure as the peak absorbance is sensitive to the refractive index of the solvent medium (compared to toluene) [94,96,119,120].

The peak shift could also be attributed to plasmonic coupling due to close proximity of the incorporated gold nanoparticles [95,110].

4.3.2 Kinetic Analysis

To assess the catalytic performance of the nanoreactor systems prepared by FNP compared to gold nanoparticles added to pre-formed polymer nanoparticles, the reduction of 4-nitrophenol by sodium borohydride was used as a model reaction [54,77]. For all the nanoreactor systems, we confirmed that the nanoreactor size is stable following reaction (Table 4.3). Given the high incorporation efficiency of gold, extractions were not performed on samples prior to further analysis. We note that we have previously established that dodecanethiol-capped gold nanoparticles aggregate in water and thus do not catalyze the reduction of 4-nitrophenol in water without the presence of a polymer nanoreactor [110]. Therefore, observed catalytic activity can be attributed to gold nanoparticles associated with nanoreactor in the case of the self-assembled systems or the pre-formed polymer nanoparticles rather than unincorporated dodecanethiol-capped gold nanoparticles. Since the dodecanethiol and dodecylamine reactors did not show significant catalytic activity (Table 4.4), we focus on characterization of the other nanoreactor systems, namely the PS750 and CO systems, in this report. We note the structures of the castor oil and PS 750 nanoreactors were comparable (Figure 4.2).

Table 4.3: Nanoreactor Reaction Stability (*Stability defined as change in diameter < 30% and a PDI < 0.3 as measured by DLS after reaction at 1 M $NaBH_4$, 0.1 mM 4-nitrophenol). (n=4)

System	Size (nm)		PDI	
	Before Rxn	**After Rxn**	**Before Rxn**	**After Rxn**
PS 750 NR	124 ± 6	144 ± 8	0.131 ± 0.012	0.090 ± 0.013
PS 750 NP w AuNP	150 ± 27	109 ± 10	0.144 ± 0.013	0.297 ± 0.024
CO NR	113 ± 10	154 ± 8	0.184 ± 0.011	0.220 ± 0.012
CO NP w AuNP	136 ± 7	113 ± 6	0.147 ± 0.006	0.111 ± 0.004

To facilitate pseudo-first order rate kinetics, this reaction is generally carried out with a large excess of sodium borohydride [54,77]. Thus, we first examined the effect of sodium borohydride concentration on reaction kinetics. For the PS 750 NRs prepared via FNP, we observe the apparent reaction rate per surface area of gold (k_1) increased with sodium borohydride concentration until it plateaus at a sodium borohydride concentration of 1.0 M sodium borohydride (Figure 4.4A). Interestingly, the witnessed plateau in activity occurs at lower sodium borohydride concentrations for CO NR compared to PS 750 NR, with maximum reaction rate constants occurring at 0.8 M sodium borohydride concentration. These results are similar to previous reports for gold nanoparticle-polymer nanoparticle systems [54]. This plateau has been attributed to active site blocking predicted by Langmuir-Hinshelwood kinetics when one reagent predominantly occupies the catalyst surface [54,100,121]. Interestingly, the sodium borohydride

concentration required to achieve a plateau for the nanoreactors was a 10-fold increase from previous reports [54,121] which could suggest differences in localized reagent concentrations compared to other systems i.e. a difference between the bulk sodium borohydride concentration and the concentration at the catalyst surface due to partitioning and diffusion. Thus, the bulk sodium borohydride concentration in the reaction medium was 1.0 M to achieve pseudo-first order rate kinetics.

We also note that increasing the concentration of sodium borohydride decreases the induction time (Figure 4.4B) for both CO and PS 750 NR systems. These results are consistent with the trends in which changes in induction time and reaction kinetics were inversely proportional to one another reported by Ballauff [54]. The change in induction time that we observe in this case appears to be related to an increase in sodium borohydride concentration which has recently been attributed to consumption of oxygen by sodium borohydride [122].

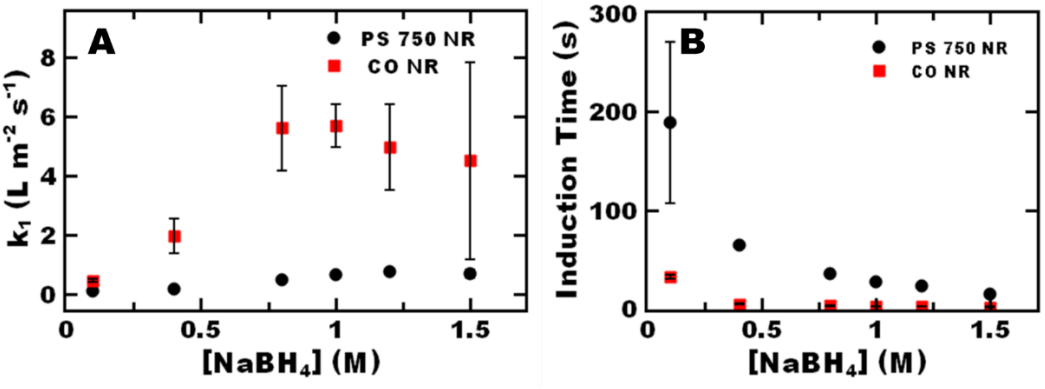

Figure 4.4: The effect of varying concentration of sodium borohydride in the 4-nitrophenol reduction on A) reaction rate constant and B) induction time using PS 750 NR (●) and CO NR (■). The initial concentration of 4-nitrophenol in each reaction was 0.1 mM. A) A plateau in apparent reaction rate constant per surface area of gold (k_1) is observed for PS 750 NR and CO NR above 1 and 0.8 M $NaBH_4$ concentration respectively. CO NR show a maximum k_1 of 5.7 ± 0.7 L m^{-2} s^{-1} compared to 0.7 ± 0.1 L m^{-2} s^{-1}. B) The CO NR system shows a maximum induction time of 32 ± 2 s compared to 189 ± 82 s for PS 750 NR. Both systems show a decrease in the induction time with increasing sodium borohydride concentration. Reported rate

constants and induction times are averages of three trials; the error bars represent the standard deviation of three trials.

Using 1.0 M sodium borohydride concentration and 0.1 mM 4-nitrophenol concentration to achieve pseudo-first order rate kinetics, we next compared to the apparent reaction kinetics of the various nanoreactor systems using PS 750 nanoparticles without gold (less than 1 ppm by ICP-OES) as a negative control (Table 4.4). Interacting core materials such as dodecanethiol and dodecylamine did not catalyze the 4-nitrophenol reduction, likely due to active site blocking. While gold-core material interactions are beneficial for improving incorporation efficiency, there is a trade off with catalytic performance. Therefore, nanoreactors prepared via FNP, which is driven by hydrophobic interactions, may offer advantages over self-assembled systems that rely on gold-polymer interactions [55,100].

For the non-interacting core materials, the apparent reaction rate for CO NRs is over 8-fold greater than PS 750 NRs with apparent reaction rate constant per surface area of gold of 5.7 ± 0.7 L m^{-2} s^{-1} for CO NRs compared to 0.7 ± 0.1 L m^{-2} s^{-1} for PS 750 NRs (Table 4.4). We note, the gold nanoparticles added to pre-formed PS 750 or CO nanoparticles presented apparent reaction rate constants per surface area that were between the nanoreactor systems, with rate constants of 3.5 ± 0.4 and 1.6 ± 0.4 L m^{-2} s^{-1} respectively. This relatively small difference (less than 2-fold for gold added to pre-formed nanoparticles compared to over 8-fold difference between self- assembled systems) may be due to differences in gold nanoparticle agglomeration and distribution which are not homogeneous for gold nanoparticles added to pre-formed polymer nanoparticles based on TEM (Figure 4.2).

Table 4.4: Reaction Kinetics of Different Polymer Nanoreactors at 1.0 M $NaBH_4$, 0.1 mM 4-Nitrophenol. (n=3)

Nanoreactor	k_1 (L m^{-2} s^{-1})
PS 750 NR	0.7 ± 0.1
PS 750 NP w AuNP	3.5 ± 0.4
CO NR	5.7 ± 0.7
CO NP w AuNP	1.6 ± 0.4
Dodecylamine NR	< 0.001 ± 0.001
Dodecanethiol NR	< 0.001 ± 0.001
PS 750 NP without AuNP	0.001 ± 0.001

In addition to comparing the PS 750 and CO nanoreactor systems to each other, comparisons to previously reported nanoparticle-based catalyst systems can also be made. Notably, at these reaction conditions the apparent reaction rate constant per surface area of gold (k_1) for both PS 750 NR and CO NR are at least 2-fold greater than ligand-free gold nanoparticles [49,121] and approximately 10-fold greater than gold nanoparticles functionalized with pH responsive poly(acrylic acid) [51]. The turnover frequency (TOF) is related to apparent reaction rate constant, the initial amount of 4-nitrophenol, and the amount of gold catalyst and is calculated as follows [123]:

$$TOF = \frac{k * n_{o_{4NP}}}{n_{Au}} \quad (4.6)$$

Where k is the apparent reaction rate constant, while n_{Au} and $n_{o_{4NP}}$ are the molar amounts of gold and initial 4-nitrophenol in the reaction solution, respectively.

Based on the observed reaction rate constants, the TOFs for CO and PS 750 NRs were approximately 300,000 and 30,000 min^{-1}, respectively (Table 4.5). These TOFs are higher than typically reported for gold-based catalysts (~1-2 min^{-1}) [124–126]. The TOF of the self-assembled nanoreactors are also higher than gold-polymer systems previous reported such as gold nanoparticles coated with poly(glycidyl methacrylate) TOF ~ 15,000 min^{-1} [127] and dendrimer encapsulated gold nanoparticle catalysts TOF ~2,000 min^{-1} [128] as well as gold nanoparticles on N-containing polymer nanospheres TOF ~17,000 min^{-1} [129]. These results suggest that self-assembled nanoreactors produced via Flash NanoPrecipitation have promising catalytic performance. Furthermore, these results indicate the catalytic performance is highly influenced by the microenvironment of the catalyst.

Table 4.5: Turnover Frequencies of Nanoreactor and Nanoparticle Systems. (n=3)

System	TOF (x 10^{-4} min^{-1})
PS 750 NR	3.3 ± 0.2
CO NR	29.7 ± 3.8

To further understand the effect of the microenvironment on the catalytic performance, we further investigated the difference between the PS 750 and CO nanoreactor systems. Based on the apparent

kinetics, we considered potential mass transfer limitations using scaling analysis and the second Damkohler number (*DaII*), i.e. a ratio of the reaction and diffusion rates given by,

$$DaII = \frac{k_{app} c^{n-1}}{\beta a} \tag{4.7}$$

where $\boldsymbol{n}$ is the reaction order, $\boldsymbol{\beta}$ is the mass transport coefficient (which is a quotient of the diffusion coefficient and the characteristic length of the system), and $\boldsymbol{a}$ is the interfacial area. Using a previously established NMR method [110], the diffusion coefficient for 4-nitrophenol in CO NR was determined to be 1.70 ± 0.02 x 10^{-8} m^2 s^{-1} (Figure 4.5) which is slightly lower than for polystyrene 1.91 ± 0.01 × 10^{-8} m^2/s [110]. Based on these experimentally determined diffusion coefficients, the second Damkohler number was found for all systems to be on the order of 10^{-4} or smaller, signifying there are no diffusion limitations for either the CO NRs or PS 750 NRs.

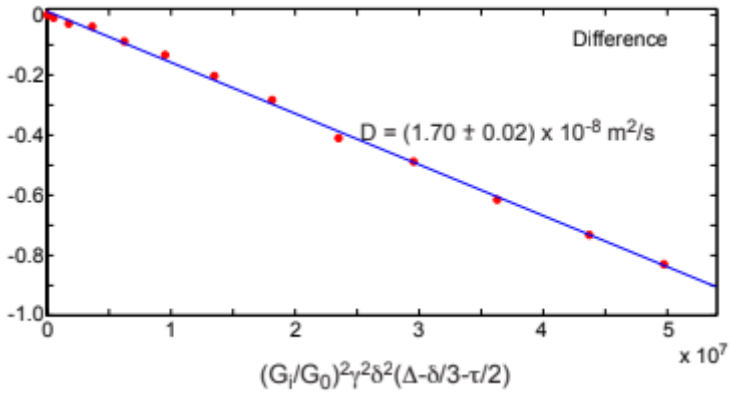

Figure 4.5: Results of saturation transfer differentiated PFG-NMR of 4-nitrophenol in a solution of castor oil nanoreactors. The blue line corresponds to the curve fit. The difference spectra corresponds to signal from the 4-nitrophenol in closest proximity to the hydrophobic phase (within the nanoreactors) which we interpret as an effective diffusion coefficient of 4-nitrophenol within the nanoreactors of 1.7 x 10^{-8} m^2/s.

Table 4.6: Hansen Solubility Parameters of Various Compounds

Compound	δ_d (MPa$^{1/2}$)	δ_p (MPa$^{1/2}$)	δ_h (MPa$^{1/2}$)	4NP RA^2
Polystyrene [130]	18.5	4.5	2.9	244
Toluene [131]	18	1.4	2.0	336
Castor Oil [132]	15.9	4.6	12	170
Ethanol [131]	15.8	9.8	19.4	120
PEO 4000 [131]	21.5	10.9	13.1	13
Methacrylamide [131]	15.8	12.1	12.8	64
PMMA 30 [131]	17.2	7.2	3.5	120
4-nitrophenol [131]	20	14.5	14.2	0

We posited that the difference in apparent catalytic performance may be attributed to differences in local reactant concentration and specifically 4-nitrophenol concentration. Hanson solubility parameters suggest that castor oil is a better solvent for 4-nitrophenol than polystyrene (Table 4.6) and the effective 4-nitrophenol concentration within CO NRs would be higher than PS 750 NRs. This is demonstrated by the HSP Distance, or RA^2, which is a measure of how alike two compounds are. The smaller the RA^2 value, the more likely they are to be compatible with each other. The HSP distance is calculated as follows:

$$RA^2 = 4\left(\delta_{d_1} - \delta_{d_2}\right)^2 + \left(\delta_{p_1} - \delta_p\right)^2 + \left(\delta_{h_1} - \delta_{h_2}\right)^2 \quad (4.8)$$

Of the hydrophobic core materials chosen, castor oil presents the lowest RA^2 value and would likely interact with 4-nitrophenol the most favorably.

In order to confirm this difference in solubility of 4-nitrophenol in different nanoreactor microenvironments, we measured the partition coefficient of 4-nitrophenol between water and castor oil or toluene (to mimic PS). As seen in Table 4.7, the core material:water partition coefficient for castor oil is 7.81 ± 0.16 compared to 0.09 ± 0.01 for toluene. The higher core material:water partition coefficient for castor oil compared to toluene suggests that the effective concentration of 4-nitrophenol in the CO NRs would be over 80-fold higher than in the PS 750 NRs contributing to enhanced apparent catalytic performance.

Practically, improving the apparent catalytic performance (i.e. the reduction of 4-nitrophenol) could be beneficial for waste water treatment [111,112]. Additionally, increasing the production of 4-aminophenol could be useful for applications e.g. a corrosion inhibitor as well as an intermediate in the pharmaceutical industry [113]. Broadly, ability to enhance the apparent catalytic performance through selection of the core material (i.e. choosing a core material that the reactant is highly soluble in) is promising approach for rational design of nanoreactors.

Table 4.7: Core Material:Water Partition Coefficients for 4-nitrophenol (4NP). (n=3)

Core Material Organic Phase	Core material:Water Partition Coefficient of 4NP
Castor Oil	7.81 ± 0.16
Toluene	0.09 ± 0.01

4.3.3 Langmuir-Hinshelwood Kinetics

Next, we examined the intrinsic kinetics of the 4-nitrophenol reduction on the gold nanoparticle catalyst surface based on the Langmuir-Hinshelwood mechanism [54,133]. For nanoreactors, the concentration in 4-nitrophenol was calculated based on the bulk concentration and the experimentally determined core material:water partition coefficient. For gold nanoparticles added to pre-formed polymer nanoparticles, the 4-nitrophenol concentration was taken to be the concentration in the bulk aqueous phase. Initially, we used a two-step reaction model involving reduction of 4-nitrophenol to 4-hydroxylaminophenol and the rate limiting step of 4-hydroxylaminophenol to 4-aminophenol previously used for gold-polymer systems [49,54]. The two-step reaction is evident by a change in reaction rate typically when the conversion of 4-nitrophenol is above 30% [54]. While we observe a change in reaction rate, it generally occurs around 70% conversion of 4-nitrophenol. This difference may be due to partitioning of 4-nitrophenol and the product within the nanoreactor. Fitting data up until 70% conversion resulted in non-real solutions. Therefore, all systems' reaction data were fitted for up to 30% conversion of 4-nitrophenol. The resulting rate constants are reported in Table 4.8. Interestingly, the k_a values found for polymer nanoreactors exceed the reported ligand-free AuNP by two orders of magnitude. Systems of polymer nanoparticles with post-formulation added AuNP were found to have reaction rate constants that were an order of magnitude greater than ligand-free AuNP. These results suggest that incorporation of the gold nanoparticles via FNP does not significantly affect the intrinsic catalytic properties.

Table 4.8: Langmuir-Hinshelwood Fitted Kinetic Parameters. (n=3)

System	k_a (mol m^{-2} s^{-1})	k_b (mol m^{-2} s^{-1})
PS 750 NR	0.0164 ± 0.0034	0.0091 ± 0.2168
PS 750 NP w AuNP	0.0590 ± 0.1489	0.1986 ± 286.6143
CO NR	0.0148 ± 0.0333	0.0196 ± 2.0271
CO NP w AuNP	0.0043 ± 0.0003	0.0052 ± 0.0211
Ligand-Free AuNP [49]	5.8 ± 3.1 x 10^{-4}	5.4 ± 2.0 x 10^{-5}

To reduce the error associated with the fitted parameters, we used an alternative model. Specifically, the data up to 30% conversion was modeled using a single reaction step and no observed change in reaction rate based on previous reports of polymer-gold systems [76], according to:

$$-\left(\frac{dc_{nip}}{dt}\right) = k_0 S \frac{\left(K_{nip}P_{nip}c_{nip}\right)^n \left(K_{BH_4}c_{BH_4}\right)}{\left[1+\left(K_{nip}P_{nip}c_{nip}\right)^n + K_{BH_4}c_{BH_4}\right]^2} \quad (4.9)$$

where c_{nip} is the bulk aqueous phase concentration of 4-nitrophenol, k_0 is the reaction rate constant of the single step reaction, S is the reaction solution specific catalyst surface area concentration, P_{nip} is the core material:water partition coefficient of 4-nitrophenol, n is the reaction order, and K_{nip} and K_{BH_4} are the Langmuir-Hinshelwood adsorption constants of 4-nitrophenol and sodium borohydride, respectively. For

nanoreactors, the 4-nitrophenol concentration was calculated based on the bulk concentration and the experimentally determined core material:water partition coefficient (equation 4.3). For gold nanoparticles added to pre-formed polymer nanoparticles, the 4-nitrophenol concentration was taken to be concentration in the bulk aqueous phase.

Using the adsorption parameters previously reported [54], the calculated rate constants are reported in Table 4.9. Notably, the rate constants for all systems studied were comparable. This result suggests that the intrinsic kinetics of the catalysts for all the systems are comparable once the partition coefficient is used to estimate the 4-nitrophenol concentration for each microenvironment. Thus, incorporating the gold nanoparticles into the nanoreactors via self-assembly does not appear to adversely impact the intrinsic catalytic performance compared to adding gold nanoparticles to pre-formed gold nanoparticles.

Comparing the rate constants from the Langmuir Hinshelwood model to previous literature, we found that the rate constants for the systems prepared by Flash NanoPrecipitation (Table 4.9) are at least 2-magnitudes greater than previously reported gold-polymer systems [76]. Their system and their analysis were comparable to the gold nanoparticles added to pre-formed polymer particles. These results further indicate that Flash NanoPrecipitation is a promising platform for producing nanoreactors while preserving the intrinsic activity of the catalyst. We note these results suggest the apparent catalytic performance of the various nanoreactor systems is affected by solubility of the reactants rather than changes in the intrinsic catalytic properties. Thus, we note Hansen Solubility Parameter Distance (RA^2) may be a useful tool for future nanoreactor design.

Table 4.9: Langmuir-Hinshelwood Single-Step Fitted Kinetic Parameters. (n=3)

System	k_0 (mol m^{-2} s^{-1})
PS 750 NR	0.0166 ± 0.0003
CO NR	0.0103 ± 0.0015
CO NP w AuNP	0.0084 ± 0.0001
SBP*	$2.27 \pm 0.34 \times 10^{-4}$

*spherical brush polymer with AuNP at 25 °C [76]

4.3.4 Sequential Addition

Finally, we consider the ability to use the nanoreactors for multiple reactions as an initial step to understanding the robustness of these nanoreactor systems. When performing sequential reactions, a decrease in activity is seen when sequentially adding 4-nitrophenol into the reaction mixture under 1 M $NaBH_4$ conditions (Figure 3.6). CO NR undergo an immediate 5-fold decrease in activity from the initial 4-nitrophenol reduction to the first sequential reaction. For CO NR, the tenth sequential reaction is 6-fold slower than the first sequential reaction and 30-fold slower than the initial reaction, with a final minimum activity of 0.18 ± 0.01 L m^{-2} s^{-1} (Figure 4.6A). The results for gold nanoparticles added to pre-formed CO nanoparticles were comparable (Figure 4.6A). In contrast, PS 750 NRs were more stable than gold nanoparticles added to preformed PS nanoparticles (Figure 4.6B). PS 750 NR maintain a stable activity through four sequential reactions, after which the activity decreases (Figure 3.7A). The PS 750 NR activity

drops only 3-fold after 10 sequential additions, to a minimum value of 0.12 ± 0.01 L m^{-2} s^{-1}. These results indicate there is a trade-off between stability and apparent kinetics as the PS 750 NRs had the lowest apparent reaction rate per surface area with the best stability.

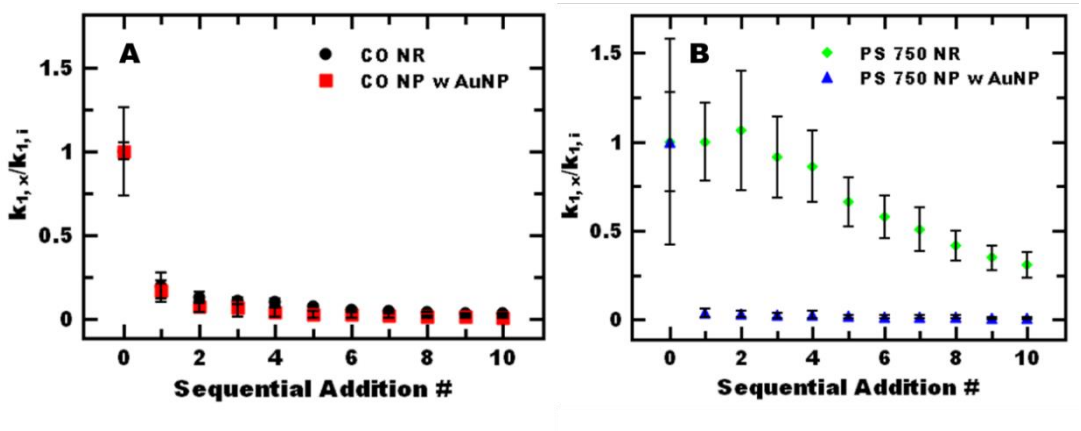

Figure 4.6: Sequential addition of 4-nitrophenol to the reaction mixture of A) CO NR (●) and pre-formed CO NP with AuNP (■) as well as B) PS 750 NR (◆) and pre-formed PS 750 NP with AuNP (▲) under reaction conditions of 1 M $NaBH_4$. The reduction in rate constant is immediate in the case of CO NR but delayed for a period of four additions with PS 750 NR. Both pre-formed CO NP and PS 750 NP with AuNP showed immediate reductions in reaction rate constants. Reported rate constants are averages of three trials; the error bars represent the standard deviation of three trials.

Interestingly, when the sodium borohydride concentration is reduced to 0.1 M the apparent reaction rate increases with sequential additions for both PS 750 and CO NRs (Figures 4.7A and 4.7B, respectively). For the PS 750 NR system, a plateau in apparent reaction rate constant per surface area is reached after four sequential additions; the apparent reaction rate constant is 8-fold greater than the initial reaction rate of 0.045 ± 0.006 L m^{-2} s^{-1}. Similarly, using 0.1 M $NaBH_4$, the apparent reaction rate constant per surface area of the CO NRs increases from 0.325 ± 0.081 L m^{-2} s^{-1} to 1.14 to ± 0.19 L m^{-2} s^{-1}; subsequent reactions reduced the apparent reaction rate. These results indicate that high sodium borohydride concentrations can reduce the activity. Similar results have been previously reported and attributed to competitive adsorption on the

catalyst surface [134]. Thus, these results suggest that catalyst reuse without loss of activity may be possible with proper selection of the reaction conditions, which can be guided by Langmuir-Hinshelwood kinetic models.

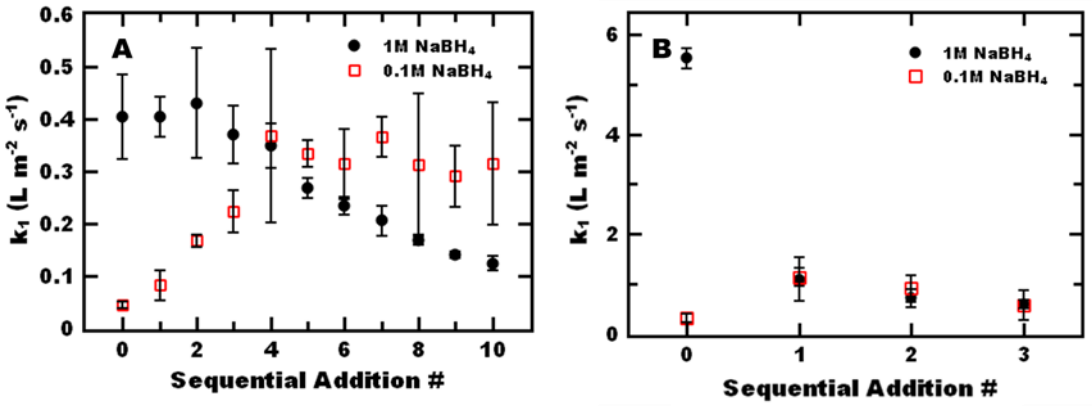

Figure 4.7: Sequential additions of 4-nitrophenol into A) PS 750 NR and B) CO NR reaction solutions with 1 M (●) and 0.1 M (□) $NaBH_4$ respectively. Using 0.1 M $NaBH_4$, we note the time between each addition was extended from 3 minutes to 6 minutes to reach full conversion of 4-nitrophenol before the subsequent reaction was started. At 0.1 M $NaBH_4$ an initial increase in activity is witnessed for both NR systems while at 1 M $NaBH_4$ the activity decreases over repeated sequential additions. Reported rate constants are averages of three trials; the error bars represent the standard deviation of three trials.

Importantly, full conversion of the 4-nitrophenol was achieved for both the CO and PS 750 nanoreactor systems within 6 minutes using 0.1 M $NaBH_4$ and within 3 minutes using 1 M $NaBH_4$ for at least 10 sequential reactions. This indicates that the kinetically trapped polymer nanoreactor systems resist irreversible aggregation of catalyst, leading to complete loss of activity [52], though losses in activity might be attributed to partial catalyst aggregation. Decreases in reaction rate constant with multiple reactions is consistent with previous reports [51,52]. For example, Kitchens and co-workers have reported similar findings of reduced activity after cyclic recovery and subsequent reaction [52]. The loss of activity was attributed to aggregation in the presence of sodium borohydride [51].

Notably, even after 10 sequential reactions, the remaining catalytic activity exceeds that observed in other systems. For example, the apparent reaction rate constant k_1 of CO NR after 10 sequential additions is 3-orders of magnitude greater than previously reported gold nanoparticle-polymer brushes systems [101] and equivalent to roughly equivalent to ligand free gold nanoparticles [49]. Further, after 10 sequential additions (despite the 3-fold decrease in activity), the TOF is 23,000 min^{-1} for the CO nanoreactors and 13,000 min^{-1} for the PS 750 nanoreactors which are higher than typically reported for gold-based catalysts (~1-2 min^{-1}) [124–126] and comparable to previously reported gold-polymer based systems [127,129]. Further studying reusability of the nanoreactors including the retained catalytic activity after additional reactions will be pursued in future work.

4.4 Conclusions

We have demonstrated Flash NanoPrecipitation is a versatile platform for formulating self-assembled filled polymer micelle nanoreactors encapsulating gold nanoparticle catalysts within various hydrophobic microenvironments with comparable hydrodynamic nanoreactor size and gold concentration in the nanoreactor dispersion. Core materials that interact with gold are beneficial for improving incorporation efficiency but decrease catalytic performance. For the non-interacting core materials, the catalytic performance is strongly affected by the hydrophobic microenvironment. For example, the apparent reaction rate per surface area for CO NRs is over 8-fold greater than PS 750 NRs. The difference in apparent catalytic performance can be attributed to differences in reactant solubility; higher reactant solubility enhances apparent reaction rates. While we note a trade-off between stability and apparent kinetics as the PS 750 NRs had the lowest apparent reaction rate per surface area with the best stability, full conversion was achieved within 3 minutes for at least 10 sequential reactions demonstrating that the nanoreactors can be used for multiple reactions. Building on these promising results in terms of catalytic performance, further structural characterization of the nanoreactors will be considered in future work.

Chapter 5 : Aqueous Benzyl Alcohol Oxidation with Self-Assembled Polymer Nanoreactors

Abstract

The oxidation of alcohols to aldehydes and ketones is an important class of chemistry used throughout industrial chemical syntheses, especially in the pharmaceutical industry. While these oxidations are traditionally performed in organic solvents at high temperature, aqueous phase catalysis offers a promising route to more efficiently perform these reactions with less waste. Incorporation of metal nanoparticles catalysts in block-copolymer nanoparticles to form nanoreactors has shown great promise for performing traditionally organic phase reactions in a bulk aqueous solution. Metal nanoparticle/polymer composite nanoreactors have been self-assembled through Flash Nanoprecipitation and analyzed for their ability to oxidize benzyl alcohol in water at room temperature. Sodium hypochlorite was found to be the most efficient oxidant in this system. Limited reaction solution stability suggests the need for greater stabilization of the polymer nanoreactors (e.g. crosslinking).

5.1. Introduction

Carbonyl compounds, which can be achieved via selective oxidation of alcohols, are important molecules in society and their formation is imperative for producing pharmaceuticals, dyes, and agrochemicals [135–137]. For example, benzaldehyde is commonly found in food additives and perfumes, with annual production exceeding 7000 tons [138]. While mainly synthesized from the oxidation of toluene at elevated temperature, alternative routes involving the catalytic oxidation of benzyl alcohol have been studied [139,140]. Gold nanoparticles have been shown to be an effective catalyst for the oxidation of benzyl alcohol, often reporting increased selectivity preventing over-oxidation products using molecular oxygen in solvent free, or aqueous conditions [137,139,141].

Tsukada et al. first demonstrated the size-specific activity of gold nanoparticles stabilized by the hydrophilic polymer hydrophilic polymer, poly(N-vinyl-2-pyrrolidone) for the aqueous, aerobic oxidation of benzyl alcohol at room temperature in the presence of excess potassium carbonate. Gold nanoparticles

around 1 nm in diameter showed greater activity, by 4-orders of magnitude, than 9 nm particles in that study. Greater than 80% conversion of the benzyl alcohol was witnessed. However, the yield was primarily the over-oxidated benzoic acid product [142]. While using a water-soluble polymer stabilizer for the gold nanoparticle catalyst eliminated the need for a co-solvent, selective oxidation to benzaldehyde was not achieved.

Buonerbo et al. incarcerated gold nanoparticles within crosslinked polystyrene microcapsules in which the gold nanoarpticles are stabilized by the π electrons of benzene rings of the polystyrene moiety to perform aqueous aromatic alcohol oxidation with an oxygen atmosphere with base, water, and co-solvent [143]. The roughly 6 nm gold nanoparticle catalysts were active towards oxidation of 1-phenylethanol, facilitating a 30% yield in 24 hours at room temperature. However, the yield increased to over 80% when 9 nm gold nanoparticles were used. Under a 1:1 mixture of H_2O:$CHCl_3$, the 9 nm gold nanoparticle catalysts were able to fully oxidize benzyl alcohol to benzaldehyde in 6 hours, at a temperature of 35°C.

In this work, we examine the use of gold stabilized by amphiphilic block copolymers for oxidation of benzyl alcohol. Aqueous dispersions of polymer nanoreactors that incorporate pre-synthesized nanoparticle catalysts using polystyrene-b-polyethylene oxide were fabricated by polymer-directed self-assembly through Flash Nanoprecipitation. Building on our previous work demonstrating that the incorporated gold nanoparticles are catalytically active using the reduction of 4-nitrophenol as a model reaction catalysts, we look to expand to oxidation of benzyl alcohol. The effect of the oxidant on conversion and selectivity for the production of benzaldehyde was analyzed. The effect of the reaction on nanoreactor stability was also assessed.

5.2. Materials and Methods

5.2.1. Materials

Polystyrene (PS, 7500 g/mol) was purchased from Polymer Source Inc. Potassium chloride, sodium hypochlorite 10-15%, benzyl alcohol, and benzaldehyde were purchased from Sigma Aldrich (St. Louis, MO, USA). Dodecanethiol (DDT) stabilized 5 nm nanoparticles, tetrahydrofuran (tetrahydrofuran (THF), HPLC grade), ethanol (ACS reagent grade), and diethyl ether (ACS reagent grade) were purchased from Fisher Scientific (Fairmont, NJ, USA). Environmental Grade Hydrochloric Acid 30-38% and Environmental Grade Nitric Acid 70% were purchased from GFS Chemicals (Columbus, OH, USA). Potassium carbonate was purchased from Acros Organics (NJ, USA). Hydrogen peroxide 30% was purchased from Bio Basic (NY, USA). (Diacetoxyiodo)benzene was purchased from AmBeed (IL, USA). These chemicals and materials were used as received. Polystyrene-b-polyethylene glycol (PS-b-PEG, PS_m-b-PEG_n where m = 1600 g/mol and n = 5000 g/mol) was obtained from Polymer Source (Product No. P13141-SEO). Prior to use, PS-b-PEG was dissolved in THF (500 mg/mL) and precipitated in ether (~1:20 v/v THF:ether). The PS-b-PEG was recovered by centrifuging, decanting, and drying under vacuum at room temperature for 2 days as previously described [110].

5.2.2. Nanoreactor Assembly

Initially, the as-received dodecanethiol stabilized gold nanoparticles in toluene (1 mL) were precipitated into ethanol (45 mL) and filtered using a Buchner funnel. The filtered nanoparticles were resuspended in THF and concentrated via evaporation at room temperature overnight to achieve a nominal concentration of around 20 mg/mL for nanoreactor self-assembly. The final concentration was confirmed by inductively coupled plasma optical emission spectroscopy using an Agilent 5110 (ICP-OES, Santa Clara, CA, USA) using potassium chloride as an external matrix modifier. UV spectra collected on an Ocean

Optics FLAME-S-UV-VIS with a HL-2000-FHSA light source (Largo, FL, USA) were compared before and after the solvent switch to confirm processing did not significantly affect gold nanoparticle size.

Nanoreactors were produced via Flash NanoPrecipitation similar to previous reports [110]. Briefly, PS-b-PEG (12 mg), dodecanethiol stabilized 5 nm gold nanoparticles (1 mg), and PS homopolymer, M_W 7500 g/mol, abbreviated PS 7500 (co-precipitate, 11 mg) were added to 1 mL of tetrahydrofuran (THF) and sonicated at 55 °C for 30 minutes. Using a manually operated confined impinging jet mixer with dilution (CIJ-D) [23,24] and achievable Reynolds' numbers > 1,300, the resulting THF mixture was rapidly mixed against 1 mL of water into a stirring vial of water (8 mL). The resulting dispersion (10 mL total) of nanoreactors was stored at room temperature for further characterization and analysis without purification.

5.2.3. Nanoreactor Characterization

Nanoreactor size (i.e. hydrodynamic diameter) was measured after mixing using a Malvern Zetasizer Nano ZS (Westborough, MA, USA) with a backscatter detection angle of 173°. Intensity weighted size distributions are reported using the average of four measurements of the intensity weight distributed with normal resolution. The reported size is the peak 1 mean intensity. The polydispersity index (PDI) is defined from the moment of the cumulant fit of the autocorrelation function calculated by the instrument software (appropriate for samples with PDI < 0.3) and is reported as a measure of particle size distribution [71]. For stability analysis, reaction solutions were allowed to sit for at least 24 hours prior to analysis to mimic reaction conditions.

UV absorbance spectra (300 to 1200 nm) of the nanoparticle dispersions were measured at room temperature with an Ocean Optics FLAME-S-UV-VIS with a HL-2000-FHSA light source (Largo, FL, USA) after formulation.

For visualization by TEM, samples were prepared by submerging a grid in a diluted nanoreactor solution (1:10) for 1 hour. After submersion, the grids were removed from the solution and dried at ambient conditions overnight. Samples were imaged using a Zeiss Libra 120 TEM (Oberkochen, Germany) using an accelerating voltage of 120 kV.

To determine the gold concentration in the nanoreactor dispersions, the nanoreactor dispersions were dissolved in THF and digested in aqua regia (1:3 nitric acid:hydrochloric acid by volume) for at least 24 hours. The samples were then diluted to 5% v/v aqua regia. Gold concentration of the digested sample was measured using inductively coupled plasma optical emission spectroscopy measurements with an Agilent 5110 (Santa Clara, CA, USA). A matrix modifier, potassium chloride (2 mg/mL) in 5% v/v aqua regia, was used to increase the ion concentration which proved beneficial for peak resolution. The reported concentrations are the average of three trials.

5.2.4. Benzyl Alcohol Oxidation

To a 2 mL centrifuge tube equipped with a magnetic stir bar was added 60 μL of the nanoreactor solution, 500 μL of an aqueous K_2CO_3 solution (0.36 M), and 20 μL of benzyl alcohol (0.19 M). Potassium carbonate was chosen based on previous reports of benzyl alcohol oxidation using gold nanoparticles [144]. The oxidant of choice (H_2O_2 or bleach) was then added to the reaction solution in the appropriate specified amount (1 equivalent). Water was then added to the reaction solution to attain a total volume of 1 mL and the reaction solution was allowed to stir overnight at room temperature. In the case of atmospheric oxygen being the oxidant of study, the centrifuge tube was left uncapped during stirring. Prior to analysis, 20 uL of diglyme was added to the reaction solution as an internal standard.

5.2.5. GCMS Analysis

The reaction solution (1 μL) was analyzed on an HP 6890 GC system equipped with an HP-5MS column flowing 1 mL/min Helium. The inlet operated with a split ratio of 50:1 with a Helium flow of 50

mL/min. From the reaction mechanism, the moles of benzaldehyde produced from the reaction is equivalent to the moles of benzyl alcohol consumed during the reaction, therefore the conversion of benzyl alcohol was calculated according to:

$$\varepsilon_{BA} = \frac{mol_{BA_i} - mol_{BA_f}}{mol_{BA_i}} * 100\% = 1 - \frac{mol_{BA_f}}{mol_{BA_i}} * 100\% = \left(1 - \frac{\frac{A_{BA_f} * A_{d_f}}{F * mol_d}}{\frac{A_{BA_i} * A_{d_i}}{F * mol_d}}\right) * 100\% \quad (5.1)$$

where ε_{BA} is the conversion of benzyl alcohol as a percentage, mol_{BA_i}, mol_{BA_f}, and $\mathrm{mol_d}$ are the initial and final moles of benzyl alcohol and the moles of diglyme, respectively. A_{BA_i}, A_{BA_f}, $\mathrm{A_{d_i}}$, and $\mathrm{A_{d_f}}$ are the chromatograph peak areas of benzyl alcohol initially and after the reaction has completed as well as the internal standard diglyme, respectively. Finally, F is the response factor of benzyl alcohol to the internal standard diglyme. The initial concentration of benzyl alcohol was measured from a sample prepared in a similar manner to reaction solutions but without the presence of nanoreactors or base. The initial and final peak areas of both benzyl alcohol as well as diglyme were the averages of three trials.

Additionally, yield of benzaldehyde was calculated according to:

$$\gamma_{ALD} = \frac{mol_{ALD_a}}{mol_{ALD_t}} * 100\% = \frac{A_{ALD} * A_d}{F * mol_d * mol_{ALD_t}} * 100\% \quad (5.2)$$

where γ_{ALD} is the yield of benzaldehyde, $\mathrm{mol_{ALD_a}}$ and $\mathrm{mol_{ALD_t}}$ are the actual and theoretical moles of benzaldehyde respectively, $\mathrm{mol_{DG}}$ is the moles of diglyme, A_{ALD} and $\mathrm{A_d}$ are the chromatograph peak areas of benzaldehyde and diglyme respectively, and finally F is the response factor of benzaldehyde to the internal standard diglyme.

5.3. Results and Discussion

5.3.1. Formulation

Polymer nanoreactors containing gold nanoparticle catalysts were prepared through Flash Nanoprecipitation. Briefly, dodecanethiol stabilized 5 nm gold nanoparticles were dispersed in THF with

the molecularly dissolved, PS and PS-b-PEG, and rapidly mixed with water using a hand-operated confined impinging jet mixer. The resulting nanoreactor dispersion was analyzed by DLS for size and polydispersity. The average diameter of the nanoreactor was 125 ± 10 nm with a PDI well below 0.2 (Figure 5.1A and Table 5.1), similar to previous studies [110]. UV-vis analysis showed a prominent absorbance at 520 nm, indicative of the 5 nm gold nanoparticles. The concentration of gold in the nanoreactor dispersion was 95 ± 8 μg/mL by ICP-OES (Table 5.1). TEM imaging confirms the presence of multiple gold nanoparticles incorporated in the polymer nanoreactor structure (Figure 5.1B). The catalytic ability of the gold nanoparticles incorporated in the polymer nanoreactors has been previously confirmed [110].

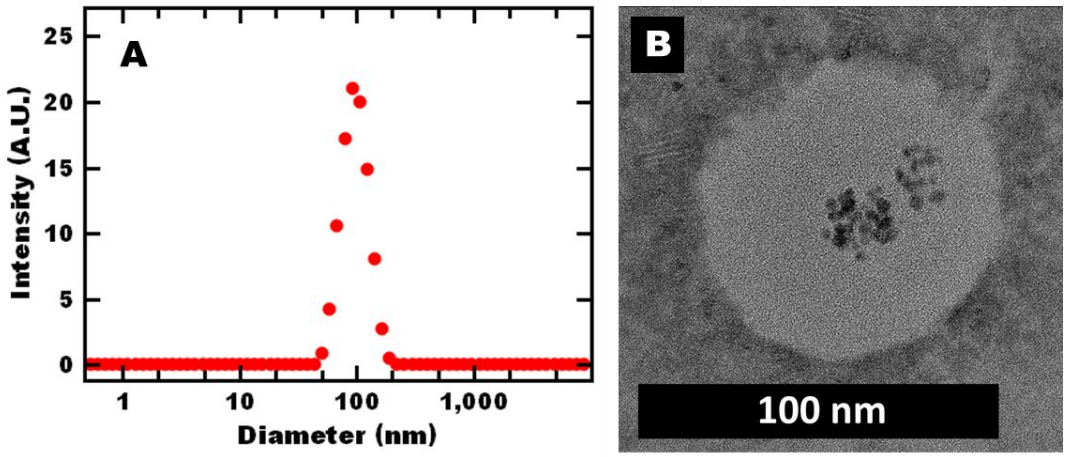

Figure 5.1: Representative A) DLS analysis and B) TEM image of PS 7500 NR. A single peak around 100 nm is seen by DLS. Gold nanoparticles (dark circles) can be seen incorporated in the polystyrene core (lighter circle) of the polymer nanoreactors. Reported intensities are a Malvern reported average of four measurements.

Table 5.1: Nanoreactor Characterization. (n=3)

Nanoreactor	Diameter (nm)	PDI	[Au] (ug/mL)
Polystyrene 7500 NR	99 ± 2	0.112 ± 0.015	95 ± 8

5.3.2. Benzyl Alcohol Oxidation

Reports suggest that gold nanoparticles are capable of benzyl alcohol oxidation at room temperature using atmospheric oxygen as an oxidant [67]. Both Kobayashi and Rossi demonstrate that potassium carbonate is the ideal base to use for this reaction, which has been attributed to the multiple oxidation states and buffering abilities [144]. Under these conditions we found that PS nanoreactors with incorporated gold nanoparticle catalysts did not facilitate the oxidation (Table 5.2). No conversion of benzyl alcohol was observed after 5 days by GCMS.

Table 5.2: Benzyl Alcohol Oxidation with PS 7500 NR. (n=3)

Oxidant	Benzyl Alcohol (M)	Oxidant (M)	Yield (%)		Conversion (%)	
			no NR	NR	no NR	NR
Air	0.19	-	-	0.2 ± 0.1	-	-7.4 ± 9.8
H_2O_2	0.19	0.20	6.1 ± 2.0	3.6 ± 0.6	30.7 ± 8.1	11.6 ± 13.1
Bleach	0.19	0.07	0.3 ± 0.5	10.7 ± 1.9	-2.3 ± 6.6	10.8 ± 4.9
Bleach	0.19	0.20	5.5 ± 2.1	19.1 ± 7.3	18.3 ± 8.1	69.5 ± 9.4

Previous reports have found that without oxygen (or an oxidant) the reaction cannot progress [144]. Therefore, we elected to study a variety of oxidants with greater strength than molecular oxygen. Specifically, we studied H_2O_2 and sodium hypochlorite (bleach), which are established oxidants [139,145]. Using H_2O_2 as the oxidant, the conversion was not higher than the auto-oxidation observed under these conditions without nanoreactors (no NR, Table 5.2). As shown in Table 5.2, the only oxidant that resulted in significant conversion of benzyl alcohol was NaClO. Using 1 equivalent, the conversion of benzyl

alcohol was 70 ± 9% with a yield to benzaldehyde of 19 ± 7% due to over-oxidation of benzaldehyde to benzyl benzoate. The conversion in the presence of bleach was significantly higher than the auto-oxidation observed under these conditions without nanoreactors (no NR) (Table 5.2). Under these conditions the nanoreactors were not stable (Table 5.3), so a reduced amount of bleach was also tested. Using a 1/3 equivalent of bleach resulted in significantly less conversion (10.8 ± 4.9%) while still destabilizing the nanoreactors (Table 5.3).

Unfortunately, the nanoreactors were not stable when performing the reaction with an oxidant other than air; after reaction the PDI's > 0.3 as analyzed by DLS in all cases (Table 5.3). Interestingly, the nanoreactor stability appears to be related to the reaction as the nanoreactors remained intact with comparable size and PDI's < 0.3 and polydispersity in the presence of individual reactants and products (Table 5.4) over the same time period (24 hours). Notably, the PDI of the nanoreactor dispersion did increase at high concentrations of benzaldehyde (corresponding to 100% conversion of benzyl alcohol to benzaldehyde). This result could be due to increased partitioning of the benzaldehyde into the nanoreactor core due to its relatively high hydrophobicity (logPow = 1.5 Sigma Aldrich MSDS) (Table 5.4). Thus, the combination of reactants (oxidant and reactants and/or products destabilizes the nanoreactors. Since the nanoreactors were not stable, and the conversions were relatively low, no further oxidation reactions were pursued.

Table 5.3: PS 7500 Nanoreactor Stability during Benzyl Alcohol Oxidation. (n=4)

Oxidant	Diameter (nm)	PDI
Air	158 ± 3	0.105 ± 0.009
H_2O_2	900 ± 379	0.682 ± 0.194

Oxidant	Diameter (nm)	PDI
Bleach (0.07 M)	1969 ± 1311	0.576 ± 0.315
Bleach (0.2 M)	1400 ± 1449	0.380 ± 0.110

Table 5.4: PS 7500 Nanoreactor Stability in Presence of Reagents. (n=4)

Reagent	Diameter (nm)	PDI
None	99 ± 2	0.112 ± 0.015
K_2CO_3	98 ± 3	0.111 ± 0.016
Bleach	120 ± 3	0.130 ± 0.009
H_2O_2	105 ± 7	0.107 ± 0.010
Benzyl Alcohol	109 ± 6	0.132 ± 0.014
Diglyme	112 ± 7	0.119 ± 0.006
Benzaldehyde (0.1% v/v)	108 ± 6	0.121 ± 0.009
Benzaldehyde (2% v/v)	119 ± 28	0.163 ± 0.007

5.4. Conclusions

Polymer nanoreactors were self-assembled using Flash Nanoprecipitation with incorporation of gold nanoparticle catalysts and studied for their ability to oxidize benzyl alcohol. Up to 70% conversion of benzyl alcohol was seen through the use of bleach as the oxidant, though over-oxidation of the benzaldehyde product to benzyl benzoate was witnessed. Despite nanoreactor stability in all of the reagents individually, the reactors were not stable under the reaction conditions. Future work should investigate nanoreactor stability in solutions with combinations of reagents. Co-precipitate hydrophobicity should also be examined for its effect on nanoreactor stability, with the goal of tailoring the product solubility in the core to prevent destabilization.

Chapter 6 : Self-Assembled Gold Nanoparticle/Polymer Nanocomposites for a One-Pot Reaction

Abstract

Gold nanoparticle/polymer nanocomposites were self-assembled through Flash Nanoprecipitation. The polymer nanoreactor were applied to the one-pot condensation of benzaldehyde with 4-nitrophenol performed in water at ambient conditions. The desired 4-benzylideneaminophenol product spontaneously precipitated from the reaction mixture. The nanoreactors were stable in dispersion whereas citrate-stabilized gold and PEG-coated gold precipitated with the product. After the product was extracted from the precipitate, the result analytically pure by NMR and a 66% isolated yield was achieved. The E-factor for the reaction performed in water was around 25, comparable to previous reports.

6.1. Introduction

Imines are an important class of molecules that are commonly used for the preparation of heterocycles [146], anti-inflammatory agents [147], and anti-cancer agents [148]. Traditionally, imines are synthesized by reaction of an aldehyde or ketone with aldehyde under reflux and separating the water the water as it is formed [149,150]. Thus, elevated temperatures are required to remove the water using distillation [151,152]. Imines can also be prepared using homogeneous catalysts. These reactions also generally require high temperatures and tedious work up procedures [149]. Practically, recovery of homogenous catalysts can be challenging. Developing new approaches that facilitate synthesis of imines under mild conditions with ease of product isolation and catalyst reuse would be desirable.

To achieve synthesis of imines at mild conditions, use of nitroarenes, which are inexpensive and readily available, as starting materials has been considered with various heterogeneous catalysts. For example, palladium nanoparticles supported on magnetic Fe_3O_4 core-carbon shell composite nanoparticles have been used for one pot reductive amination reactions. The magnetic support eased catalyst recovery and reuse. Specifically, direct reductive amination of nitrobenzene with benzaldehyde could be performed

in water under hydrogen atmosphere. Elevated temperatures (60-80°C) were required to improve yields [153].

One-pot amination reactions involving reduction of the nitro group to an amine followed by condensation with the aldehyde has also been performed with a Ni/SiO_2 based catalyst. High conversion and selectivity were achieved from nitrobenzene and a variety of aldehydes using ethanol as the solvent. The resulting catalysts were magnetic which facilitated recovery and reuse. Reaction conditions typically involved elevated temperature (105°C) and pressurized H_2 (1.4 MPa). Alternatively, gold-based catalysts have been applied. Small gold nanoparticles supported on titania have been used for selected reduction of nitroarenes. Reactions were carried out under atmospheric CO at room temperature using ethanol as the solvent. Ultimately, the product was isolated by chromatography [149].

Performing multiple reaction steps in "one-pot " is promising for reducing solvent waste associated with liquid phase chemical processing because isolation of intermediates becomes unnecessary, thereby reducing waste by orders of magnitude [1,32]. Overall, these results are promising and demonstrate that the reaction can be performed in water or at room temperature. However, these approaches have not enabled a "one pot" reaction in water at room temperature. Ease of product isolation and catalyst recovery and reuse are also important considerations.

In this work, we investigate the potential of kinetically-trapped polymer nanoreactors to facilitate imide synthesis via one-pot condensation in water at ambient conditions with product isolation via spontaneous phase separation. We use reaction of benzaldehyde with 4-nitrophenol as a model reaction. As a catalyst, we incorporate gold nanoparticles into polystyrene nanoreactors. The effect of reducing agent is discussed. The amphiphilic polymer nanoreactors are compared to gold nanoparticles stabilized by hydrophilic stabilizers such as citrate and PEG.

6.2. Materials and Methods

6.2.1. Materials

Polystyrene (PS, M_w 7500 g/mol) was purchased from Polymer Source Inc. Sodium borohydride, 4-nitrophenol, benzaldehyde, formic acid, trisodium citrate, sodium hydroxide, deuterated water, and potassium chloride were purchased from Sigma Aldrich (St. Louis, MO, USA). Dodecanethiol (DDT) stabilized 5 nm nanoparticles, tetrahydrofuran (tetrahydrofuran (THF), HPLC grade), ethanol (ACS reagent grade), diethyl ether (ACS reagent grade), and PEGylated 5 nm gold nanoparticles were purchased from Fisher Scientific (Fairmont, NJ, USA). 4-aminophenol was purchased from Tokyo Chemical Industry Co. (Portland, OR, USA). Environmental Grade Hydrochloric Acid 30-38% and Environmental Grade Nitric Acid 70% were purchased from GFS Chemicals (Columbus, OH, USA). The ^{1}H-NMR solvent Acetone-D6 with 4,4-dimethyl-4-silapentane-1-sulfonic acid (DSS) as an internal standard was purchased from Cambridge Isotope Lab, Inc (Andover, MA, USA). Phenylsilane, triethylsilane, and sodium cyanoborohydride were acquired from Chem-Impex (Wood Dale, IL, USA). Citrate stabilized 5 nm gold nanoparticles were purchased from Ted Pella (Redding, CA, USA). These chemicals and materials were used as received. Polystyrene-b-polyethylene glycol (PS-b-PEG, PS_m-b-PEG_n where m = 1600 g/mol and n = 5000 g/mol) was obtained from Polymer Source (Product No. P13141-SEO). Prior to use, PS-b-PEG was dissolved in THF (500 mg/mL) and precipitated in ether (~1:20 v/v THF:ether). The PS-b-PEG was recovered by centrifuging, decanting, and drying under vacuum at room temperature for 2 days as previously described [110].

6.2.2. Nanoreactor Assembly

Initially, the as-received dodecanethiol stabilized gold nanoparticles in toluene (1 mL) were precipitated into ethanol (45 mL) and filtered using a Buchner funnel. The filtered nanoparticles were resuspended in THF and concentrated via evaporation at room temperature overnight to achieve a nominal

concentration of around 20 mg/mL for nanoreactor self-assembly. The final concentration was confirmed by inductively coupled plasma optical emission spectroscopy using an Agilent 5110 (ICP-OES, Santa Clara, CA, USA). UV-vis spectra collected on an Ocean Optics FLAME-S-UV-VIS with a HL-2000-FHSA light source (Largo, FL, USA) were compared before and after the solvent switch to confirm processing did not significantly affect gold nanoparticle size.

Nanoreactors were produced via Flash NanoPrecipitation similar to previous reports [110]. Briefly, PS-b-PEG (12 mg), dodecanethiol stabilized 5 nm gold nanoparticles (1 mg), and PS homopolymer, M_W 7500 g/mol, abbreviated PS 7500 (co-precipitate, 11 mg) were added to 1 mL of tetrahydrofuran (THF) and sonicated at 55 °C for 30 minutes. Using a manually operated confined impinging jet mixer with dilution (CIJ-D) [23,24] and achievable Reynolds' numbers > 1,300, the resulting THF mixture was rapidly mixed against 1 mL of water into a stirring vial of water (8 mL). The resulting dispersion (10 mL total) of nanoreactors was centrifuged at 14000 rpm for 20 minutes, the supernatant separated from the pellet and reconstituted to the original volume with DI water. The supernatant solutions were stored at room temperature for further characterization and analysis.

For comparison to nanoreactors prepared via FNP, we analyzed as-received 5 nm PEGylated gold nanoparticles and 5 nm citrate stabilized gold nanoparticles for kinetic ability in similar manner to the nanoreactors.

6.2.3. Nanoreactor Characterization

Nanoreactor size (i.e. hydrodynamic diameter) was measured using a Malvern Zetasizer Nano ZS (Westborough, MA, USA) with a backscatter detection angle of 173°. Intensity weighted size distributions are reported using the average of four measurements of the intensity weight distributed with normal resolution. Unless otherwise noted, the reported size is the peak 1 mean intensity. The polydispersity index (PDI) is defined from the moment of the cumulant fit of the autocorrelation function calculated by the

instrument software (appropriate for samples with PDI < 0.3) and is reported as a measure of particle size distribution [71]. For stability analysis following the 4-nitrophenol reduction, reaction solutions were allowed to sit for at least 24 hours prior to analysis to reduce the formation of bubbles within the solution.

UV absorbance spectra (300 to 1200 nm) of the nanoparticle dispersions were measured at room temperature in a quartz cuvette with an Ocean Optics FLAME-S-UV-VIS with a HL-2000-FHSA light source (Largo, FL, USA) after formulation.

To determine the gold concentration in the nanoreactor dispersions, the nanoreactor dispersions were dissolved in THF and digested in aqua regia (1:3 nitric acid:hydrochloric acid by volume) for at least 24 hours. The samples were then diluted to 5% v/v aqua regia. Gold concentration of the digested sample was measured using inductively coupled plasma optical emission spectroscopy measurements with an Agilent 5110 (Santa Clara, CA, USA). A matrix modifier, potassium chloride (2 mg/mL) in 5% v/v aqua regia, was used to increase the ion concentration which proved beneficial for peak resolution.

Polymer nanoreactor concentration was measured with thermogravimetric analysis (TGA) using a Perkin Elmer Pyris 1 TGA (Waltham, MA, USA). First, the polymer nanoreactor solution was concentrated using Amicon Ultra 2 mL Ultracel 50k centrifugal filters (50,000 NMWL Burlington, MA, USA) and spinning 1 mL of solution at 4000 rpm for 20 minutes; 20 uL of retentate was used for the TGA measurement. The sample was held for 5 minutes at 28 °C, then the temperature was ramped up to 110 °C at 10 °C/min. Finally, the sample was held at 110 °C for 30 minutes. The final weight of the sample was calculated from an average of 10 data points taken immediately after 40 minutes from the beginning of the TGA method [154].

The actual gold loading of the polymer nanoreactors was determined through ICP-OES and TGA according to:

$$Au_{load} = \frac{[Au]}{[PSbPEG]+[PS]+[Au]} = \frac{[Au]}{[tot_{sol}]} \quad (6.1)$$

where Au_{load} is the actual gold loading of the nanoreactors, $[Au]$, $[PSbPEG]$, and $[PS]$ are the concentrations of gold, PS-b-PEG, and PS 7500 respectively, and $[tot_{sol}]$ is the total solids concentration. The gold and total solids concentrations were determined from ICP-OES and TGA respectively.

6.2.4. 4-Nitrophenol Reduction with Sodium Borohydride Analysis

The ability of the nanoreactors to reduce 4-nitrophenol was evaluated using sodium borohydride following well established procedures [54,77]. Unless otherwise noted, to the nanoreactors (0.0079 mol% AuNP) were added 4-nitrophenol (20 μL, 0.01 M, abbreviated 4NP) followed by aqueous sodium borohydride (within 5 minutes of preparation, abbreviated $NaBH_4$) to form a 2 mL reaction solution. The nanoreactor solution and sodium borohydride solution (initially 6 M)volumes added to the nanoreactor dispersion were adjusted such that the final reaction volume was 2 mL. The reduction of 4-nitrophenol was monitored using UV spectroscopy (Ocean Optics FLAME-S-VIS-NIR-ES, Largo, FL, USA, with a HL-2000-FHSA light source (300-1200 nm) with a CUV-UV cuvette holder placed on a stir plate. The final reaction mixture contained less than 0.01 vol% THF that would have been residual from the self-assembly process. The induction time and apparent reaction rate (K_{app}) were determined from tracking the absorbance at 425 nm as a function of time. The values of K_{app} and induction time are the averages (± standard deviations) of at least 3 trials of each experiment. The catalyst surface area normalized reaction rate constant (k_1) was then determined according to equation 4.2.

6.2.5. 4-Nitrophenol Reduction with Alternative Reducing Agents

The ability of the nanoreactors to reduce 4-nitrophenol was evaluated using either phenyl silane, triethylsilane, or trisodium citrate. Unless otherwise noted, to the nanoreactors (0.0079 mol% AuNP) were added 4-nitrophenol (20 μL, 0.01 M) followed by the chosen reducing agent (0.1 M) to form a 2 mL reaction solution. Phenylsilane and triethylsilane reactions were carried out using deuterated water instead of deionized water. For trisodium citrate, the reduction of 4-nitrophenol was monitored using UV

spectroscopy (Ocean Optics FLAME-S-VIS-NIR-ES, Largo, FL, USA, with a HL-2000-FHSA light source (300-1200 nm) with a CUV-UV cuvette holder placed on a stir plate. The phenylsilane and triethylsilane reducing agent reactions were analyzed after 24 hours by NMR for the presence of 4-aminophenol. The final reaction mixture contained less than 0.01 vol% THF that would have been residual from the self-assembly process. For the trisodium citrate reaction, the induction time and apparent reaction rate (K_{app}) were determined from tracking the absorbance at 425 nm as a function of time. The values of K_{app} and induction time are the averages (± standard deviations) of at least 3 trials of each experiment.

6.2.6. Condensation of Benzaldehyde with 4-Aminophenol

For the condensation reaction benzaldehyde (20 μmol) and 4-aminophenol (18 μmol) were placed in 2 mL of water. The reaction solution was allowed to sit overnight and the solution was analyzed by GCMS (HP 6890 GC with HP 5973 MSD) with a 5% Phenyl Methyl Siloxane column. If a precipitate was present, the solution was then filtered through a syringe filter to remove the precipitate. The filter was washed with acetone d-6 (1 ml) and the solution analyzed by NMR to confirm the presence of the desired reaction product. The pH was adjusted using the appropriate amounts of formic acid and NaOH (10 M).

6.2.7. Cascade Reaction

The cascade reaction was carried out in a 10 mL conical tube. Unless otherwise noted, polymer nanoreactors (500 μL) were added to 960 μL of water followed by the addition of 4-nitrophenol (500 μL, 4 mg/mL). A fresh solution of sodium borohydride (40 μL, 3.78 mg/mL) was then added to the reaction solution. Once the solution turned colorless, formic acid (20 μL) was added in order to degrade the remaining sodium borohydride. After bubbling in the reaction solution had subsided, benzaldehyde (20 μmol) was added followed by sodium hydroxide solution (10 M, 30 μL). The reaction solution was allowed to sit overnight, after which the solution was centrifuged at 4000 rpm for 20 minutes and the supernatant separated from the pellet. The pellet was dried at room temperature overnight. Then, the pellet was

dissolved in acetone d-6 and analyzed by GCMS (HP 6890 GC with HP 5973 MSD) and NMR (Bruker 400 MHz). The GCMS was equipped with a 5% Phenyl Methyl Siloxane column. After analysis, the acetone was evaporated and the resulting solid was weighed to determine an isolated yield of desired product as calculated from:

$$\gamma_{BAP} = \frac{mol_{BAP_a}}{mol_{BAP_t}} * 100\% = \frac{m_{BAP_a}}{m_{BAP_t}} * 100\% \quad (6.2)$$

Where γ_{BAP} is the isolated yield of 4-benzylideneaminophenol, mol_{BAP_a} and mol_{BAP_t} are the actual and theoretical (based on 100% conversion of 4-nitrophenol) moles of 4-benzylideneaminophenol, and finally m_{BAP_a} and m_{BAP_t} are actual and theoretical isolated masses of 4-benzylideneaminophenol. The isolated yield of the product was an average of three trials. Any solid that was insoluble in the acetone-d6 extraction was also weighed. The other solid precipitate mass was reported as an average of three trials. Finally, the pellet was digested with 667 μL of aqua regia for 24 hours, diluted to 5% v/v aqua regia, and analyzed by ICP-OES for gold content. A matrix modifier, potassium chloride (2 mg/mL) in 5% v/v aqua regia, was used to increase the ion concentration which proved beneficial for peak resolution.

6.3. Results

6.3.1. Nanoreactor Characterization

In similar manner to previously reported methods [110,155] polymer nanoreactors were self-assembled through Flash Nanoprecipitation. This method of kinetically-trapped self-assembly relies upon rapid mixing of an organic solvent, containing at least a hydrophobic core material and an amphiphilic polymer, against a miscible anti-solvent, such as water, which precipitates those components from the solution. To fabricate the nanoreactors, PS-b-PEG and PS 7500 were dissolved in THF and sonicated for 30 minutes at 55°C. After cooling, dodecanethiol-stabilized gold nanoparticles were dispersed in the THF solution, thereby comprising the organic stream. This organic stream was rapidly mixed against water,

which decreases the solvent quality of the mixture resulting in the precipitation of the hydrophobic materials in the organic stream. The precipitates grow until sufficient block copolymer adsorbs via hydrophobic interactions between precipitate core and the hydrophobic block of the PS-b-PEG amphiphiles. The nanoreactor is sterically stabilized in the aqueous dispersion by the PEG block of the block copolymer. After formulation, the polymer nanoreactors exhibited an average diameter of 91 ± 5 nm and PDI of 0.163 ± 0.018 by DLS.

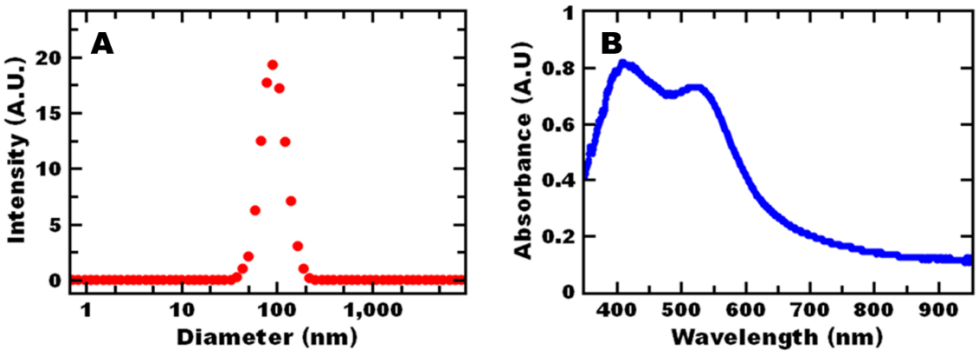

Figure 6.1: Representative A) DLS and B) UV-Vis of PS 7500 nanoreactors. Scattering by the polymer nanoreactors is seen around 400 nm while the absorbance around 520 nm is characteristic of gold nanoparticles. Reported intensities and absorbances are averages of four and ten measurements respectively.

UV-Vis analysis (Figure 6.1B) shows absorbance peaks around 400 nm and 520 nm. The absorbance peak around 520 nm is indicative of gold nanoparticles [47,96]. The plasmon resonance absorbance wavelength can be impacted by environment, size, and proximity to other gold nanoparticles. 5 nm gold nanoparticles dispersed in water typically show an absorbance around 520 nm [110]. The absorbance peak witnessed at 400 nm can be attributed to scattering from the nanoparticles.

ICP-OES analysis confirms the presence of gold in the polymer nanoreactor dispersion with a measured gold concentration of 21.6 ± 0.3 μg/mL. The gold concentration in the dispersion was much lower than the expected value of 100 μg/mL based on the formulation. Loss of gold may have occurred during

the solvent switch from toluene to THF, the nanoreactor formation step, as well as during the centrifuging of the nanoreactors.

Next, we examined the gold loading in the resulting nanoreactors (wt. gold/wt. nanoreactors). Thermogravimetric analysis (TGA) was used to determine the total solids concentration. The total solid mass in the nanoreactor dispersion was 1.95 ± 0.01 mg/mL, compared to a nominal concentration of 2.4 mg/mL. The differences between the two values is mainly attributed to losses in the centrifugal filtration [156]. Actual gold loading of the nanoreactors was determined from the experimentally confirmed gold and polymer concentrations in the nanoreactor solutions to be 1.1 ± 0.01% while the nominal gold loading was 4.3%. The lower than expected gold loading can be attributed to the lower than expected amount of gold in the dispersion.

6.3.2. Confirmation of Catalyst System Activity

Initially, we confirmed the gold nanoparticles incorporated in the nanoreactors were catalytically active and compared their activity to citrate-stabilized gold nanoparticles and PEG-coated gold nanoparticles using the reduction of 4-nitrophenol with sodium borohydride. The 4-nitrophenol reduction is a well known model reaction for studying the activity of gold nanoparticle catalysts [34,49–52,54]. We have previously demonstrated that kinetically-trapped polymer nanoreactors are active catalysts for the reduction of 4-nitrophenol [110,155]. The polymer nanoreactors used in this study were also subjected to the same reaction to demonstrate activity. The catalyst surface area normalized reaction rate constants (k_1) compared to PEG AuNP, and citrate AuNP at the same conditions are reported in Table 6.1. At a sodium borohydride concentration of 0.1 M the polymer nanoreactors demonstrated 2-fold greater activity than citrate AuNP and statistically equivalent activity with PEG AuNP. This demonstrates the effectiveness of incorporating gold nanoparticle catalysts in a kinetically trapped filled polymer micelle. These results also demonstrate that polymer stabilizers can enhance apparent catalytic

activity. The difference in reaction kinetics between the systems could be attributed to reagent solubility differences in the localized reaction environments [32], which might suggest that the gold nanoparticle catalysts are dispersed throughout the core and shell of the polymer nanoreactors, given the similarity in activity to the PEG AuNP catalyst.

Table 6.1: 4-Nitrophenol Reduction Rate Constants of Polymer Nanoreactors and Gold Colloids at Various Reagent Concentrations. (n=3)

Catalyst	[4NP] (mM)	[$NaBH_4$] (M)	k_1 (L m^{-2} s^{-1})
No Catalyst	0.1	0.1	N/A
	7.2	0.2	N/A
PS 7500 NR	0.1	0.1	0.41 ± 0.03
	7.2	0.2	0.07 ± 0.01
PEG AuNP	0.1	0.1	0.41 ± 0.03
	7.2	0.2	0.10 ± 0.01
Citrate AuNP	0.1	0.1	0.20 ± 0.04
	7.2	0.2	0.03 ± 0.01

After demonstrating that the nanoreactors could reduce 4-nitrophenol to 4-aminophenol and that gold was required for the reaction to proceed, increased reagent concentrations were examined. For these reactions, the 4-nitrophenol reagent concentration was increased by 70 fold compared to the 4-nitrophenol reduction conditions, giving a reaction solution concentration of 7 mM, in order to make

analysis possible by NMR. As the 4-nitrophenol reduction has previously been shown to follow Langmuir-Hinshelwood kinetics [49,54,110,155], there is a danger in saturating the surface of the gold nanoparticles with 4-nitrophenol effectively blocking hydride from active sites and stalling the reaction. Therefore, the nanoreactor concentration was increased 4-fold in order to increase the availability of catalyst surface area and the sodium borohyride concentration was increased 2-fold. Under these conditions the PS 7500 NR outperformed the citrate AuNP by 2-fold (Table 6.1). However, the PEG AuNP demonstrated a slightly greater activity for the high concentration reduction than the PS 7500 NR, with a catalyst surface area normalized reaction rate constants of 0.10 ± 0.01 and 0.07 ± 0.01 L m^{-2} s^{-1} respectively.

When we attempted a one-pot cascade reaction adding all the reactants (4-nitrophenol, sodium borohydride, and benzaldehyde) at the same time, the desired cascade reaction of reduction of 4-nitrophenol to 4-aminophenol followed by reaction with benzaldehyde was not achieved. Instead, analysis by GCMS showed that under these circumstances the benzaldehyde is reduced to benzyl alcohol by the sodium borohydride. This is consistent with previous studies involving the reductive amination of benzaldehyde with sodium borohydride [157].

Alternative reducing agents were therefore investigated for the ability to selectively reduce 4-nitrophenol without reducing the benzaldehyde. Because the ability to reduce the 4-nitrophenol is paramount to the success of the cascade, that reaction was further investigated with the use of either sodium cyanoborohydride ($CNBH_4$), triethylsilane (TES), phenyl silane (PhSi), or trisodium citrate as the reducing agent (Table 6.2). For cyanoborohydride and trisodium citrate reactions, no color change was observed after 24 hours, therefore it was concluded that no reaction took place. The reactions with triethylsilane and phenylsilane were performed in D_2O and were analyzed by ^{1}H-NMR after 24 hours because of the lack of ability to track the 4-nitrophenolate ion via UV-Vis [55]. After 24 hours, no

evidence of 4-aminophenol was evident by ^{1}H-NMR. None of the alternative reducing agents studied were able to facilitate the reduction of 4-nitrophenol, either with or without a catalyst, and in the case of TES and PhSi a second phase was present. Notably, the only reducing agent that produced a color change indicative of the 4-nitrophenol reduction, was sodium borohydride, (Table 6.2).

Table 6.2: Application of Various Reducing Agents to the Reduction of 4-Nitrophenol

Reducing Agent	**Reducing Agent Conc. (M)**	**Conversion of 4NP after 24 hrs* (%)**
$NaBH_4$	0.1	100
$CNBH_4$	0.1	< 5
TES	0.1	< 5
PhSi	0.1	< 5
Citrate	0.1	< 5

*Conversion of 4-nitrophenol identified by UV-Vis analysis.

From these results we determined that sodium borohydride was necessary for the reduction of 4-nitrophenol, but caused an unwanted side reaction in the presence of benzaldehyde. Therefore, it was necessary to neutralize the sodium borohydride prior to the addition of benzaldehyde. Thus, our approach to performing these reactions in "one pot" was to neutralize the sodium borohydride with formic acid following reducing of 4-nitrophenol indicated by the color change from yellow to colorless and then titrate the pH of the reaction as necessary (Figure 6.2).

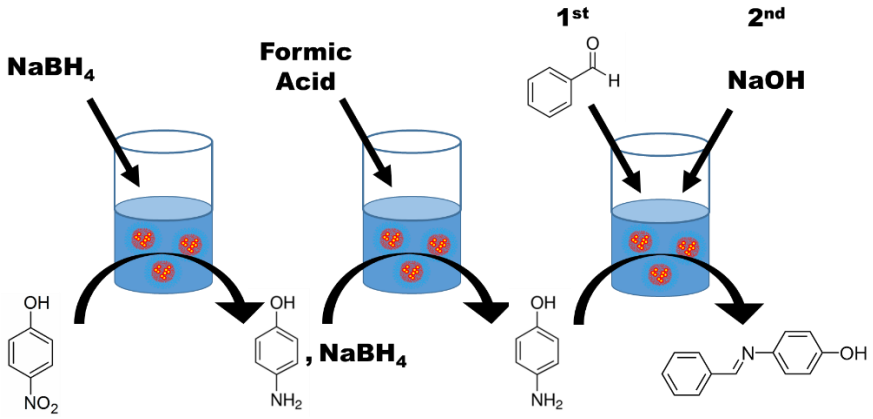

Figure 6.2: Schematic of the one-pot condensation of benzaldehyde with 4-nitrophenol. 4-nitrophenol is reduced in an aqueous dispersion of polymer nanoreactors upon addition of sodium borohydride. After reduction, addition of formic acid degrades the remaining sodium borohydride. Finally, addition of benzaldehyde followed by sodium hydroxide allows the condensation of benzaldehyde to occur.

To determine the appropriate titration steps, we examined the effect of pH on the desired reaction between 4-aminophenol and benzaldehyde. Experiments in the condensation of benzaldehyde with 4-aminophenol without nanoreactors showed that the pH of the reaction solution strongly influences the reaction outcome (Figure 6.3). At pH 4, no desired reaction product is witnessed and the reaction solution remains colorless with no precipitate formed. In contrast, at neutral or basic pH's either precipitates are formed or the solution color changes respectively.

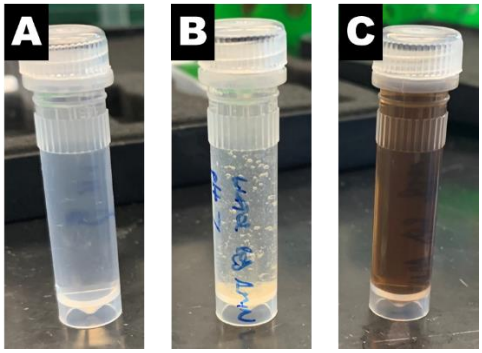

Figure 6.3: The effect of pH on the aqueous condensation of benzaldehyde with 4-aminophenol. A) Reaction solution pH of 4 with no color change or precipitate observed. B) Reaction solution pH of 7 with a precipitate observed. C) Reaction solution pH of 10 with a brown color changed observed and no precipitate.

Specifically, at neutral pH, there is a color change to a light brown and a precipitate forms. Representative NMR of the precipitate in acetone d-6 is shown in Figure 6.4. The aromatic region shows two sets of doublets 6.9 and 7.2 ppm, consistent with the aromatic protons on the phenol group. A doublet of doublets is seen further downfield consistent with the aromatic protons in the benzyl group. Lastly, the singlet located at 8 ppm which integrates for 1 proton compared to the doublet peaks at 6.9 ppm is consistent with the benzylidene proton. The precipitate formed at neutral pH is consistent by NMR to the desired product 4-benzylideneaminophenol.

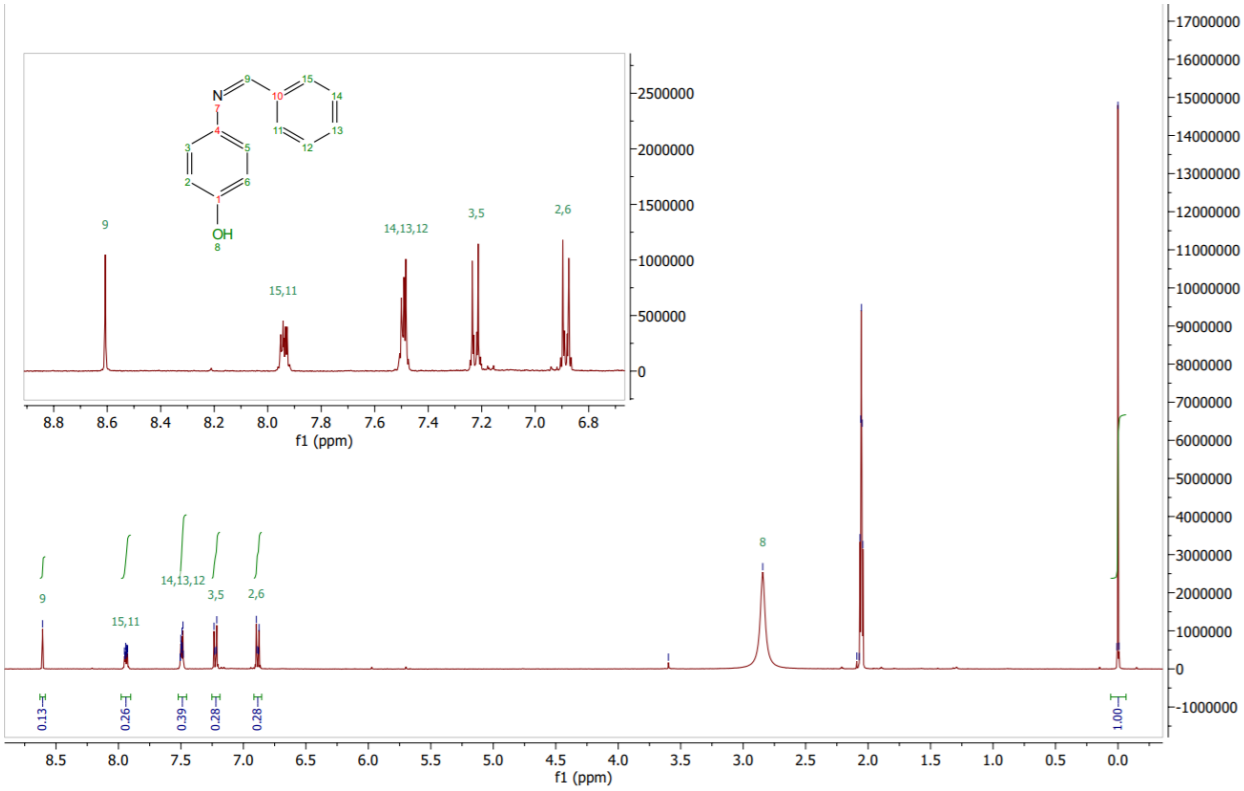

Figure 6.4: Representative image of ^{1}H-NMR spectra for the imine formation product 4-benzylideneaminophenol. The singlet peak at 8.6 ppm integrates for 1 proton relative to the doublet peaks at 6.9 ppm confirming the presence of 4-benzylideneaminophenol.

At basic pH, the solution turns a dark brown (Figure 6.3). However, the desired product is not seen by either GCMS or NMR. The unknown compound may be attributed to oxidation induced polymerization of 4-aminophenol [158].

Given these results, it is clear that after sodium borohydride neutralization the reaction solution must be adjusted to at least pH of 7. Two approaches to adjust the pH following the 4-nitrophenol reduction reaction were investigated: (1) dropwise addition of sodium hydroxide and (2) rapid addition of sodium hydroxide.

With the dropwise addition of sodium hydroxide, more precise control of the pH was expected. However, the titration of the solution to pH 7 was a time consuming endeavor. In the time that it took to

achieve a pH 7 with high precision, we observed the unwanted color change to dark brown associated with the unknown product happening shortly after neutral pH conditions were reached.

Based on the titration, approximately 20 uL of 10 M NaOH was required to achieve a pH 7 or greater. Therefore, we switched to a rapid addition of sodium hydroxide following formic acid to reduce the amount of time the 4-aminophenol is sitting in the solution and possibility of polymerization. Benzaldehyde was added to the acidic reaction solution followed by the addition of a standard 20 uL of 10 M NaOH (Figure 6.2). In this case, there was a color change to light brown associated with the desired reaction as well as a precipitate. The precipitate was characteristic of the condensation of benzaldehyde with 4-aminophenol at neutral pH. The result of solution color change and formation of precipitate was similar to the slow titration results, but the characteristics were more consistent, likely due to the more repeatable method. Due the importance of the pH, consistent time between addition of sodium borohydride and neutralization steps is an important factor.

After the reaction solution was allowed to sit overnight, the solution was centrifuged to pellet the precipitate and the supernatant was subsequently removed, dried and weighed. The desired product was extracted from the dried pellet to separate it from an insoluble solid. NMR analysis of the acetone showed analytically pure 4-benzylideneaminophenol. After drying the acetone, the mass of product was measured and the yield (based on the molar amounts of 4-nitrophenol and benzaldehyde), the isolated yield was 65%. Importantly, these results demonstrate that multiple reactions could be achieved in "one pot" using water as the bulk solvent at ambient temperature and pressure. Since the desired product is hydrophobic, it spontaneously phase separated from the reaction mixture.

After analysis by NMR and yield calculations, the precipitate pellet was treated with 667 uL of aqua regia for 24 hrs, diluted to 10 mL and analyzed by ICP-OES for the presence of gold. No gold was indicated

in the precipitate by ICP-OES indicating that the gold nanoparticles did not precipitate during the reaction, suggesting that the nanoreactors were stable during the reaction.

Table 6.3: DLS Measurements of Nanoreactor Reaction Solution During Cascade Reaction. (n=4)

Cascade Step	Peak 1 (nm)	Peak 2 (nm)	PDI
Before Rxn	91 ± 5		0.163 ± 0.018
After 4NP Reduction	98 ± 6		0.133 ± 0.014
After Neutralization	114 ± 25		0.177 ± 0.001
After Imine Formation	461 ± 198	47 ± 8	0.660 ± 0.235
After Centrifuge	104 ± 6		0.139 ± 0.012

We further analyzed the effect of the cascade reaction steps on the stability of the polymer nanoreactors. Stability was defined as maintaining a hydrodynamic diameter and PDI within 25% of the initial DLS measurement, as long as the PDI remained below a maximum value of 0.400. As can be seen in Table 6.3, the nanoreactors were stable until after the imine formation step which showed an increase in the PDI and multiple peaks by DLS. This increase in PDI may occur due to precipitation of the reaction product. After centrifugation of the solution however, there is only one peak by DLS with corresponds to a diameter around the initial size of the nanoreactors and the PDI again falls below 0.400. This indicates that the precipitate in the solution was leading to the polydispersity of the DLS measurement and that the nanoreactors are stable throughout the reaction. Since the product spontaneously phase separates from the nanoreactors, this is a promising approach to ease reuse of the catalyst.

Table 6.4: Cascade Reaction Yields. (n=3)

Catalyst*	Isolated Product (mg)	Other Solid (mg)	Gold in Precipitate (mg)	NR Stability** (y/n)
none	0 ± 0.0	0 ± 0.0	N/A	NA
PS 7500 NR	1.8 ± 0.1	2.4 ± 1.0	0.2 ± 0.7	Y
PEG AuNP	1.5 ± 0.5	4.9 ± 1.7	3.6 ± 0.2	N
Citrate AuNP	1.4 ± 0.3	5.3 ± 1.9	4.3 ± 0.4	N

*Approximately 10 μg of Au in each catalyzed reaction

**Catalyst stability was determined by DLS and ICP-OES. Catalyst stability was defined as changes in hydrodynamic diameter less than 25% of the original size and a PDI below 0.400 without the precipitation of the gold catalyst.

Finally, we compared the results using the nanoreactors to the PEG-coated gold nanoparticles and the citrate-stabilized gold nanoparticles. Throughout the cascade reaction, no significant changes in the size or polydispersity of the dispersions were observed although both polydisperse initially and maintained that polydispersity throughout the reaction sequence; no precipitation of gold was observed. Both PEG AuNP and citrate AuNP yielded ~1.5 mg of product which is comparable to the polymer nanoreactors (Table 6.4). However, both yielded more of the undesired product than the polymer nanoreactors with 4.9 ± 1.7 mg and 5.3 ± 1.9 mg for the PEG AuNP and the citrate AuNP respectively (statistically significant with 90% confidence). Also, ICP-OES analysis of the precipitate pellets of PEG AuNP and citrate AuNP reactions found gold content of 3.6 ± 0.2 and 4.3 ± 0.4 ug/mL respectively (Table 6.4). This suggests that the ligand-stabilized gold nanoparticles were less stable than the polymer nanoreactors which did not have any measurable gold content in the precipitate pellets. This could be due to removal of the stabilizing ligands by sodium borohydride [50] which resulted in colloidal instability. However, it is possible that the

kinetic barrier present in the kinetically-trapped polymer nanoreactor system prevents loss of the gold nanoparticle catalyst due to ligand loss. While PEG AuNP and citrate AuNP yielded comparable amounts of product as the nanoreactor, there was significant gold in the precipitate as measured by ICP-OES indicated that these systems are not stable during the cascade reaction and precipitate with the product. This would complicate both isolation of the product as well as reuse of the catalyst. Since the product spontaneously phase separates from the nanoreactors without contamination by the catalyst, the block copolymer stabilized structures are a promising approach to ease reuse of the catalyst.

Evaluating Green Chemistry metrics, we examined the E-factor. Since we use water as the bulk solvent the E-factor for the reaction itself is relatively low ~25 and comparable to previous studies (Table 6.5). Since the amount of product using all three gold nanoparticle systems were comparable, the E-factors were also similar. However, since the product is extracted with acetone isolate it from the other precipitated side products, the E-factor is ~400. As evident by this calculation, isolation of the desired reaction product with solvent contributes significantly to the E-factor. Therefore, performing multiple reaction steps in "one-pot" to avoid product isolation of intermediate steps would be beneficial for reducing waste associated with liquid phase chemical processing. The use of an alternative reducing agent that facilitates the reduction of 4-nitrophenol without spontaneously reducing benzyl alcohol could improve the E-factor by 5 to 10-fold. If, by using a non-basic reducing agent, the unwanted side-reaction is also diminished, the need for extraction of the product with acetone becomes unnecessary and the overall E-factor could be reduced by two orders of magnitude. Similarly, a much smaller amount of acetone could be used for purification of the product which would reduce the E-factor by around 10-fold.

Table 6.5: E-Factors of Condensation and Reductive-Amination Reactions with Product Purification

System	Reaction Medium	Temp. (°C)	E-factor	Ref
PS 7500 NR (reaction)	Water	rt	25	This Work
PS 7500 NR (w/ extraction)	Water	rt	400	This Work
Pd NP Zeolite	Water	rt	40	[159]
Supported AuPd NP	Water	50	54	[160]
Supported AuNP	Toluene	120	27*	[161]
Fe/citric acid/K10	Water	rt	52**	[162]
Pd/Fe_3O_4 on carbon	Water	60	41	[153]

*Purification of product was not specified. It was assumed that during the separation of the catalyst equivalent reaction volumes were used during the washing procedure.

**Purification of product was not specified. A theoretical extraction procedure utilizing twice the reaction volume of organic solvent was used for the estimation of the E-factor.

6.4. Conclusions

We used gold-loaded polymer nanoreactors to perform the one-pot imine formation involving reduction of the nitro group to an amine followed by condensation with the aldehyde using the reaction of benzaldehyde with 4-nitrophenol as a model reaction. The polymer nanoreactors first facilitated the

reduction of 4-nitrophenol to 4-aminophenol with sodium borohydride. After the reduction was completed, the sodium borohydride was neutralized with formic acid. Control of the reaction solution pH during the imine formation was also found to be critical, otherwise unwanted side reaction occurred. Specifically, the reaction solution was adjusted to slightly alkaline to promote the amination of benzaldehyde. The resulting precipitate was dried and weighed, then extracted with to determine the amount of product. We determined there was a 66% isolated yield of that was analytically pure by NMR. While PEG AuNP and citrate AuNP yielded comparable amounts of product as the nanoreactor, there was significant gold in the precipitate as measured by ICP-OES indicated that these systems are not stable during the cascade reaction and precipitate with the product. This would complicated both isolation of the product as well as reuse of the catalyst. Since the product spontaneously phase separates from the nanoreactors, the block copolymer stabilized structures are a promising approach to ease reuse of the catalyst. Evaluating Green Chemistry metrics, we examined the E-factor. Since we use water as the bulk solvent the E-factor for the reaction itself is relatively low ~25 and comparable to previous studies. However, since the product is extracted with acetone isolate it from the other precipitated side products, the E-factor is ~400. As evident by this calculation, isolation of the desired reaction product with solvent contributes significantly to the E-factor. Therefore, performing multiple reaction steps in "one-pot" to avoid product isolation of intermediate steps would be beneficial for reducing waste associated with liquid phase chemical processing.

Chapter 7 : Conclusions and Future Work

Summary and Conclusions

The overall goal of this work was to reduce solvent waste associated with liquid phase chemical processing. Our approach was to use polymer nanoreactors that incorporate metal nanoparticle catalysts in an amphiphilic polymer microenvironment. The rationale for this approach was that performing reactions in the presence of self-assembled amphiphilic macromolecules can accelerate reactions while using water as the bulk solvent due to the hydrophobic effect. Systematic investigations to understand the effect of the hydrophobic microenvironment, determined by the hydrophobic portion of the core material, on the nanoreactor performance with respect to catalyst performance have yet to be established. Such studies would require synthesis of a new amphiphilic stabilizer for each nanoreactor. As an alternative to systems that require unique synthesis of amphiphilic molecules to vary the properties of the hydrophobic compartment, Flash Nanoprecipitation offers a simple approach to produce filled polymer micellar nanoreactors with different core materials.

Therefore, the aims of this work were to formulate nanoreactors with comparable size and metal nanoparticle catalyst loading while varying the hydrophobic core material in order to in order to study the effects of composition of reactor performance. We also sought to fundamentally understand the interplay between mass transfer and reaction kinetics within the nanoreactor by combining experiment with scaling analysis and the Langmuir-Hinshelwood kinetic model to study intrinsic kinetics. Finally, we studied the use of these nanoreactors (dispersed in water) in oxidation reactions as well as a two-step imine formation performed in one-pot.

Using polystyrene as a model system, we demonstrated that Flash NanoPrecipitation is a rapid, scalable self-assembly method useful for production of hybrid metal nanoparticle catalyst-polymer composite nanoreactors. The size and gold loading of the nanoreactors can be tuned independently, with sizes and nominal loadings ranging from 100-200 nm and 4-50 wt% respectively. Nanoreactor size could

be tuned independently of gold loading by varying the total solids concentration at a constant ratio of gold to polystyrene. To vary the gold loading independently of nanoparticle size, we developed a constant core volume approach guided by the Smoluchowski diffusion limited aggregation model. Thus, the gold loading was tuned independently of nanoreactor size by varying the ratio of gold to polystyrene at constant total core volume. The constant core volume approach may be useful for formulations of multiple components with disparate densities *e.g.,* inorganic particle-polymer nanocomposite particles.

Since Flash NanoPrecipitation is a versatile platform in terms of materials selection, we prepared a number of other nanoreactor systems with various hydrophobic co-precipitants. We examined dodecane, dodecylamine, and dodecanethiol. In the cases of dodecylamine and dodecanethiol, gold-core material interactions may affect both nanoreactor self-assembly as well as catalytic performance. For self-assembling systems that only involved non-covalent, hydrophobic interactions, we studied dodecane and polystyrene (MW 750 g/mol PS 750) in addition to castor oil. Using these various hydrophobic co-precipitants, nanoreactors with comparable hydrodynamic size and gold loading were achieved using the constant core volume approach.

To fundamentally understand the interplay between mass transfer and reaction kinetics within the polystyrene nanoreactor system, we first examined reduction of 4-nitrophenol with sodium borohydride as a model reaction. We observed that the induction time is affected by sequence of reagent addition, time between reagent addition, and reagent concentration. Combined, our experiments indicate that the induction time is most influenced by diffusion of sodium borohydride. Scaling analysis and effective diffusivity measured using NMR, the observed reaction rate after the induction time are reaction- rather than diffusion-limited. Finally, the intrinsic reaction kinetics of gold associated with the polymer was comparable to ligand-free particles indicating the self-assembly process and resulting polymer microenvironment does not de-activate or block the catalyst active sites.

Next, we examined the effect of co-precipitant on self-assembly and catalytic performance. We determined that core materials that interact with gold are beneficial for improving incorporation efficiency of the gold nanoparticles into the nanocomposite nanoreactor during self-assembly but decreased catalytic performance. Non-interacting core materials could enhance catalytic performance. For example, we observed that the reaction rate normalized per surface area per gold (k_1) for the gold nanoparticles added to the pre-formed castor oil nanoparticles were comparable to the PEG-coated gold nanoparticles and citrate-stabilized gold nanoparticles. Notably, the k_1 of the castor oil nanoreactors was over 2.7-fold faster than these other systems. These results suggest that the hierarchical, amphiphilic structure of the nanoreactors achieved by self-assembly with the amphiphilic polymer, castor oil and gold nanoparticles is beneficial for catalytic performance compared to gold nanoparticles with hydrophilic stabilizers.

Rate acceleration in self-assembled amphiphilic systems has been attributed to increased local concentrations of the reactants. To quantify this difference in concentration, we measured the partition coefficient of 4-nitrophenol between water and castor oil to be 7.81 ± 0.16 indicating an increased local concentration within the nanoreactor was possible. We used this information to examine the intrinsic kinetics of the 4-nitrophenol reduction on the gold nanoparticle catalyst surface based on the Langmuir-Hinshelwood mechanism. Notably, the rate constants for castor oil nanoreactors and castor oil added to preformed castor oil nanoparticles were comparable. Further, the measured intrinsic kinetic parameters were comparable to PEG-coated gold nanoparticles and citrate-stabilized gold nanoparticles. These results suggest that the intrinsic kinetics of the catalysts for all the systems are comparable once the partition coefficient has been used to estimate the 4-nitrophenol concentration for each microenvironment. Thus, incorporating the gold nanoparticles into the nanoreactors via self-assembly does not adversely impact the intrinsic catalytic performance compared to adding gold nanoparticles to pre-formed gold nanoparticles. Therefore, the difference in apparent catalytic performance can be attributed to an increase in local reactant concentration. Notably, the castor oil nanoreactors demonstrated high catalytic activity compared to

previously reported nanoparticle-based catalyst systems as quantified by the turnover frequency. Based on the observed reaction rate constants, the TOFs for castor oil nanoreactors were approximately 300,000 min^{-1}. These TOFs were higher than typically reported for gold-based catalysts (~1-2 min^{-1}) and gold-polymer based systems ~15,000 min^{-1}.

Catalytic performance was strongly affected by the co-precipitant that formed the hydrophobic microenvironment for reaction. For example, the apparent reaction rate per surface area using castor oil (CO) was over 8-fold greater than polystyrene (750 g/mol, PS 750). We further investigated the difference between the PS 750 and CO nanoreactor systems. Diffusion coefficients for 4-nitrophenol within the polymer nanoreactor structures was determined by PFG-NMR for nanoreactors with both polystyrene and castor oil cores to evaluate potential differences in diffusion limitations. Based on the apparent kinetics, the second Damkohler number (*DaII*), i.e. a ratio of the reaction and diffusion rates was found for all systems to be on the order of 10^{-4} or smaller, signifying there were no diffusion limitations for either the CO NRs or PS 750 NRs. Based on our results, we posited that the difference in apparent catalytic performance may be attributed to differences in local reactant concentration and specifically 4-nitrophenol concentration. Hanson solubility parameters suggest that castor oil is a better solvent for 4-nitrophenol than polystyrene and the effective 4-nitrophenol concentration within CO NRs would be higher than PS 750 NRs. In order to confirm this difference in solubility of 4-nitrophenol in different nanoreactor microenvironments, we measured the partition coefficient of 4-nitrophenol between water and castor oil or toluene (to mimic PS). The core material:water partition coefficient for castor oil was 7.81 ± 0.16 compared to 0.09 ± 0.01 for toluene which suggests that the effective concentration of 4-nitrophenol in the CO NRs would be higher than a PS NR contributing to enhanced apparent catalytic performance. Overall, the increase in apparent catalytic performance could be attributed to differences in reactant solubility rather than differences in mass transfer or intrinsic kinetics. Overall, higher reactant solubility enhances apparent reaction rates and may be a useful design parameter for material selection in future nanoreactor studies.

Next, our goal was to examine the applicability of the nanoreactor dispersions in various reactions. First, we examined the possibility of using the gold-loaded polystyrene nanoreactors to perform aqueous, aerobic oxidations of benzyl alcohol at ambient conditions. Various oxidants were studied. No conversion (greater than auto-oxidation) was observed using air or hydrogen peroxide as the oxidant. Using a stronger oxidant, such as NaClO, increased the conversion of benzyl alcohol. Up to 70% conversion of benzyl alcohol was achieved with a benzaldehyde yield of 32 ± 15% due to over-oxidation of benzaldehyde to benzyl benzoate. Under these conditions the nanoreactors were not stable (Table 3), so a reduced amount of bleach was also tested. Using a 1/3 equivalent of bleach resulted in significantly less conversion (10.8 ± 4.9%) while still destabilizing the nanoreactors (Table 3). Unfortunately, the nanoreactors were not stable when performing the reaction with any oxidant other than air; after reaction the PDI's > 0.3 as analyzed by DLS in all cases. Interestingly, the nanoreactor stability appears to be related to the reaction as the nanoreactors remained intact, with comparable size and polydispersity, in the presence of individual reactants and products over the same time period (24 hours). Notably, the PDI of the nanoreactor dispersion did increase at high concentrations of benzaldehyde (corresponding to 100% conversion of benzyl alcohol to benzyaldehdyde). This result could be due to increased partitioning of the benzaldehyde into the nanoreactor core due to its relatively high hydrophobicity ($\log P_{ow}$ = 1.5 Sigma Aldrich MSDS). Thus, the combination of reactants, oxidant, and/or products destabilizes the nanoreactors. Future work should investigate nanoreactor stability in solutions with combinations of reagents. Co-precipitate hydrophobicity should also be examined for its effect on nanoreactor stability, with the goal of tailoring the product solubility in the core to prevent destabilization.

Finally, we attempted a one-pot cascade reaction with the gold-loaded polystyrene nanoreactors. Building on our initial work with the reduction of 4-nitrophenol to 4-aminophenol, we were interested in performing the one-pot imine formation involving reduction of the nitro group to an amine followed by condensation with an aldehyde using the reaction of benzaldehyde with 4-nitrophenol as a model reaction.

To perform two reactions in one pot, the polymer nanoreactors first facilitated the reduction of 4-nitrophenol to 4-aminophenol with sodium borohydride. After the reduction was completed, the sodium borohydride was neutralized with formic acid. Control of the reaction solution pH during the imine formation was also found to be critical, otherwise an unwanted side reaction occurred. Specifically, the reaction solution was adjusted to slightly alkaline to promote the amination of benzaldehyde. We determined there was a 66% isolated yield of 4-benzylideneaminophenol was analytically pure by NMR. The polymer nanoreactors were stable in dispersion and did not precipitate with the desired product. While PEG AuNP and citrate AuNP yielded comparable amounts of product as the nanoreactor, there was significant gold in the precipitate as measured by ICP-OES which indicated that these systems are not stable during the cascade reaction and precipitate with the product. This precipitation with the product would complicate both isolation of the product as well as reuse of the catalyst. Since the product spontaneously phase separates from the nanoreactors, the block copolymer stabilized structures are a promising approach to ease reuse of the catalyst. Evaluating Green Chemistry metrics, we examined the E-factor. Since we use water as the bulk solvent the E-factor for the reaction itself is relatively low ~25 and comparable to previous studies. However, since the product is extracted with acetone in order to isolate it from the other precipitated side products, the E-factor is ~400. As evident by this calculation, isolation of the desired reaction product with solvent contributes significantly to the E-factor. Therefore, performing multiple reaction steps in "one-pot" to avoid product isolation of intermediate steps would be beneficial for reducing waste associated with liquid phase chemical processing.

Overall, we have demonstrated that Flash NanoPrecipitation is a versatile platform for scalable production of polymer nanoreactor with tunable properties (size, catalyst loading) and modular materials selection. Incorporating the metal nanoparticle catalyst does not adversely affect the intrinsic kinetics or introduce mass transfer limitations. Apparent rate enhancement is possible and can be attributed to increased local concentration of the reactants. Thus, solubility parameters may be a useful design

parameter for material selection in future nanoreactor studies. Finally, we demonstrate the nanoreactors can be used for a two-step reaction performed in one-pot (in water at ambient conditions). Performing the reactions in water reduces solvent waste. Furthermore, performing multiple reactions in one pot eliminates the need to isolate the product at intermediate steps which could significantly reduce solvent waste associated with liquid phase chemical processing.

Future Work

In this work, the focus was proof-of-principle demonstrating that multiple reactions in "one-pot" was possible and that the product spontaneously phase separately from the nanoreactor dispersion. Building upon this work, improvements in the one-pot imine formation may be possible using an alternative reducing agent to sodium borohydride that would be capable of selectively reducing 4-nitrophenol without reacting with benzaldehyde. Such a reducing agent would eliminate the need to neutralize the reaction solution with formic acid and potentially reduce the formation of undesirable side products by allowing the 4-aminophenol intermediate to directly react with benzaldehyde. This selective reduction of 4-nitrophenol may be achieved with an alternative reagent such as hydrazine. The reducing agents screened could also be evaluated at additional concentrations, and reaction conditions. Another approach would be to investigate additional derivatives of 4-nitrophenol whose amino- analog is not expected to undergo spontaneous degradation in solution, as was noted with 4-aminophenol. Performing the reactions on larger scales may also improve the E-factor as well as demonstrate scalability.

Furthermore, we have demonstrated that Flash NanoPrecipitation is a versatile platform for scalable production of polymer nanoreactor with tunable properties (size, catalyst loading) and modular materials selection. Ability to tune nanoreactor size and catalyst loading independently is unique to the self-assembled structures achieved via Flash NanoPrecipitation. Therefore, studying the effect of these variables on reaction kinetics using the reduction of 4-nitrophenol as a model reaction would be valuable. Such a study may provide further fundamental understanding of how the polymer microenvironment

affects catalyst and nanoreactor performance. Additional structural characterization of the nanoreactors would be useful for understanding the distribution of gold throughout the nanoreactor structure (i.e. the hydrophobic and hydrophilic compartments) as well as potential aggregation of the catalysts before and after self-assembly, reaction, and/or reuse. For example, small angle x-ray scattering may prove to be a promising technique to determine if the metal nanoparticles are located within either the hydrophobic core or the hydrophilic PEG shell of the nanoreactors or if aggregation of the gold nanoparticles within the nanoreactors has occurred.

To broaden the impact of this work, it would be possible to leverage the modular materials selection of Flash NanoPrecipitation. A future direction of research could involve nanoreactor design for specific reactions though selection of the core material. Specifically, the designing the nanoreactor around product solubility within the nanoreactor core would be an interesting approach based on further understanding on the effect of the nanoreactor microenvironment on reaction kinetics. Given that incorporating gold nanoparticles within the nanoreactors enhances apparent reaction kinetics, use of alternative metal nanoparticle catalysts could be investigated. The application of additional catalysts could facilitate additional classes of reactions as well as improve performance of the nanoreactors in oxidation reactions.

Chapter 8 : Vita

Andrew S. Harrison

601 West Main St., Richmond, VA, 23284

harrisona3@vcu.edu

Education

Virginia Commonwealth University, Richmond, VA, Graduating Dec. 2020
PhD Candidate in the Chemical and Life Sciences Engineering Doctorate Program, GPA: 3.92
Thesis: Self-Assembled Metal Nanoparticle/Polymer Nanocomposites as Nanoreactors for One-Pot Reactions

University of Richmond, Richmond, VA, May 2014
Bachelor of Science Double Major in Biochemistry and Interdisciplinary Physics, GPA: 3.43
Biochemistry Honors Graduate
Dean's List: Fall 2010, Spring and Fall 2011
Sigma Pi Pi National Chemistry Honor Society: Spring 2013 – present
Sigma Pi Sigma National Physics Honor Society: Spring 2013 – present

Skills Summary

Laboratory Skills

Colloid Synthesis
- Flash Nanoprecipitation, Turkevich Method of Gold Nanoparticle Synthesis

Colloid Characterization
- TEM and SEM imaging, DLS and Zeta Potential, TGA

Chemical Characterization and Analysis
- GC-MS, NMR, FT-IR, UV-Vis, Flash Chromatography

General
- Electrospinning, ICP-OES and MS

Computer Skills
- Microsoft Office/Visual Basic, MatLab and Python Experience, SciDaVis

Research Experience

Graduate Research, Virginia Commonwealth University Spring 2016 – Present
- Design and formation of kinetically-trapped metal/polymer nanocomposite colloids
  - Self-directed assembly approach relying on non-covalent interaction of surfactants (amphiphile) and hydrophobic compounds
  - Colloidal design influenced by solubility theory of desired reagents within composite materials
  - Incorporate metal heterogenous catalysts within a polymer colloid using non-covalent interactions
  - Able to formulate micelles as well as filled-micellar structures with tunable properties
- Characterized formulated colloids and micelles using interfacial analysis (Dynamic Light Scattering, Zeta-Potential)
- Utilized the catalyst-polymer "nanoreactors" to perform "one-pot" organic reactions in aqueous solutions
  - Investigate structure-activity relationship of the nanoreactors
  - Quantitative modeling of Langmuir-Hinshelwood reaction kinetics within catalyst-polymer nanoreactor

- Collaborated with chemistry colleagues in Florida to determine nanoscale diffusion parameters for kinetic analysis through innovative analytical techniques
- Incorporated metal nanoparticles within electrospun polymer nanofibers
- Synthesized gold nanoparticles through reduction of gold salts
- Managed undergraduate research student projects to achieve completion within designated periods of time
- Effectively presented project results at local/regional/national scientific conferences through oral and poster presentations

Undergraduate Research, University of Richmond Fall 2012 – Summer 2015

- Developed novel synthetic pathways for marine natural products utilizing Suzuki Cross-Coupling
- Trained junior research members in wet lab protocols
- Presented project results at regional scientific conferences

Publications

- **A. Harrison**, M. Zeevi, C. Vasey, M. Nguyen, C. Tang. "Accelerated Reaction Rates within Self-Assembled Polymer Nanoreactors with Tunable Hydrophobic Microenvironments." *Polymers, Pre-Publication* (2020).
- **A. Harrison**, T. Vuong, M. Zeevi, B. Hittel, S. Wi, C. Tang. "Rapid Self-Assembly of Metal/Polymer Nanocomposite Particles as Nanoreactors and Their Kinetic Characterization." *Nanomaterials, 3*, 318 (2019). doi.org/10.3390/nano9030318
- B. Thornton, **A. Harrison**, A. Pham, C. Castano, C. Tang. "Polyaniline-Functionalized Nanofibers for Colorimetric Detection of HCl Vapor." *ACS Omega*, *3*, 3587–3591 (2018). doi:10.1021/acsomega.8b00054.
- J. Gupton, S. Yeudall, N. Telang, M. Hoerrner, E. Huff, E. Crawford, K. Lounsbury, M. Kimmel, W. Curry, **A. Harrison**, W. Juekun, A. Shimozono, J. Ortolani, K. Lescalleet, J. Patteson, V. Moore-Stoll, C. Rohena, S. L. Mooberry, A. J. Obaidullah, G. E. Kellogg, J.A. Sikorski. "Ortho group activation of a bromopyrrole ester in Suzuki-Miyaura cross-coupling reactions: Application to the synthesis of new microtubule depolymerizing agents with potent cytotoxic activities", *Bioorganic & medicinal chemistry*, *25*, 3206-3214 (2017). doi: 10.1016/j.bmc.2017.04.012
- J. Gupton, N. Telang, J. Patteson, K. Lescalleet, S. Yeudall, J. Sobieski, **A. Harrison**, W. Curry, "The application of formyl group activation of bromopyrrole esters to formal syntheses of lycogarubin C, permethyl storniamide A and lamellarin G trimethyl ether." *Tetrahedron*, 70, 9759–9767 (2014). doi: 10.1016/j.tet.2014.11.035
- J. Gupton, N. Telang, M. Wormald*, K. Lescalleet*, J. Patteson*, W. Curry*, **A. Harrison***, M. Hoerrner*, J. Sobieski*, M. Kimmel*, E. Kluball* and T. Perry*, "Formal Group Activation of a Bromopyrrole Ester in Suzuki Cross-Coupling Reactions: Application to a Formal Synthesis of Polycitone A and B and Polycitrin A", *Tetrahedron,*70, 2738-2745 (2014). doi.org/10.1016/j.tet.2014.02.091

Select Presentations

Oral

- **Andrew Harrison**, Tien Vuong, Michael Zeevi and Christina Tang. *"Microenvironment Effect on Reaction Kinetics within Self-Assembled Polymer Nanoreactors", AIChE Annual Meeting (2018).*
- **Andrew Harrison**, Tien Vuong, Michael Zeevi and Christina Tang. *"Self-Assembled Polymer Nanoreactors: Formulation and Effect of Microenvironment", 92nd ACS Colloids and Surface Science Symposium (2018).*

Poster

- **Andrew Harrison**, Matthew Nguyen, and Christina Tang. "Cascade Reaction using Polymer Nanoreactors", *Soft Matter Workshop (2019).*
- **Andrew Harrison**, Matthew Nguyen, and Christina Tang. "Self Assembled Polymer Nanoreactors for Cascade Reactions", *AIChE Annual Meeting (2019).*
- **Andrew Harrison**, Matthew Nguyen, and Christina Tang. "Benzyl Alcohol Oxidation using Polymer Nanoreactors", *92nd ACS Colloids and Surface Science Symposium (2018).*
- **Andrew Harrison**, Matthew Nguyen, and Christina Tang. "Benzyl Alcohol Oxidation using Polymer Nanoreactors", *AIChE Annual Meeting (2018).*
- **Andrew Harrison**, Tien Vuong, Michael Zeevi, Matthew Nguyen, and Christina Tang. "The Effect of Microenvironment on the Catalytic Ability of Multifunctional Nanoreactors", *AIChE Annual Meeting (2017).*
- **Andrew Harrison**, Tien Vuong, Michael Zeevi, Matthew Nguyen, and Christina Tang. "The Effect of Microenvironment on the Apparent Catalytic Ability of Multifunctional Nanoreactors", *91st ACS Colloids and Surface Science Symposium (2017).*

Teaching Experience

Teaching Assistant

- Introduction to Chemical Engineering — Spring 2018 and 2017
  - Educated students in coding and logic principles with Microsoft Excel and VBA, as well as Python
  - Graded homework, quizzes, and exams and coordinated undergraduate tutors
  - Conducted office hours to engage students and communicate complex ideas effectively
- Thermodynamics — Fall 2017
  - Fostered and promoted students to use coding skills (VBA/Python) to model thermodynamic equilibria
  - Received Student Choice Award for Chemical and Life Science Teaching Assistant of the Year
- Unit Operation Lab — Fall 2016
  - Orchestrated undergraduate student experiments in common chemical engineering processes

Outreach

Annual Volunteer, Future Business Leaders of America, State Leadership Conference — 2015 – Present
- Coordinated and judged student events

Volunteer, Elementary School Outreach at Fox Elementary, Richmond, VA — Fall 2017 – 2019
- Cultivated STEM interest by supervising polymerization reactions conducted by elementary students

Volunteer, Science Museum of Richmond — Spring 2017
- Presented an exhibit on graphene and engaged the public

Physics Tutor, Prep for Success, Richmond, VA — Fall 2013
- Prepared high school students for the AP Physics exam

Volunteer, World Pediatric Project, Richmond, VA — Fall 2011
- Utilized Spanish-speaking skills to engage and entertain sick children and their families

Chapter 9 : References

1. Sheldon, R. A. The e Factor: Fifteen Years On. *Green Chem.* 2007, **9**, 1273–1283.

2. Sheldon, R. A. Fundamentals of Green Chemistry: Efficiency in Reaction Design. *Chem. Soc. Rev.* 2012, **41**, 1437–1451.

3. Lipshutz, B. H.; Ghorai, S. "Designer"-Surfactant-Enabled Cross-Couplings in Water at Room Temperature. *Aldrichimica Acta* 2012, **45**, 3–16.

4. Lipshutz, B. H.; Ghorai, S. Transitioning Organic Synthesis from Organic Solvents to Water. What's Your E Factor? *Green Chem.* 2014, **16**, 3660–3679.

5. La Sorella, G.; Strukul, G.; Scarso, A. Recent Advances in Catalysis in Micellar Media. *Green Chem.* 2015, **17**, 644–683.

6. Petrosko, S. H.; Johnson, R.; White, H.; Mirkin, C. A. Nanoreactors: Small Spaces, Big Implications in Chemistry. *J. Am. Chem. Soc.* 2016, **138**, 7443–7445.

7. Vriezema, D. M.; Aragone, M. C.; Elemans, J. A. A. W.; Cornelissen, J. J. L. M.; Rowan, A. E.; Nolte, R. J. M. Self-Assembled Nanoreactors. *Chem. Rev.* 2005, **105**, 1445–1489.

8. Lu, J.; Dimroth, J.; Weck, M. Compartmentalization of Incompatible Catalytic Transformations for Tandem Catalysis. *J. Am. Chem. Soc.* 2015, **137**, 12984–12989.

9. Li, C. J.; Trost, B. M. Green Chemistry for Chemical Synthesis. *Proc. Natl. Acad. Sci. U. S. A.* 2008, **105**, 13197–13202.

10. Ciulla, M. G.; Zimmermann, S.; Kumar, K. Cascade Reaction Based Synthetic Strategies Targeting Biologically Intriguing Indole Polycycles. *Org. Biomol. Chem.* 2019, **17**, 413–431.

11. Tietze, L. F. Domino Reactions in Organic Synthesis. *Chem. Rev.* 1996, **96**, 115–136.

12. Yang, Y.; Liu, X.; Li, X.; Zhao, J.; Bai, S.; Liu, J.; Yang, Q. A Yolk-Shell Nanoreactor with a Basic Core and an

Acidic Shell for Cascade Reactions. *Angew. Chemie - Int. Ed.* 2012, **51**, 9164–9168.

13. Pang, H.; Gallou, F.; Sohn, H.; Camacho-Bunquin, J.; Delferro, M.; Lipshutz, B. H. Synergistic Effects in Fe Nanoparticles Doped with Ppm Levels of (Pd + Ni). A New Catalyst for Sustainable Nitro Group Reductions. *Green Chem.* 2018, **20**, 130–135.

14. Minkler, S. R. K.; Isley, N. A.; Lippincott, D. J.; Krause, N.; Lipshutz, B. H. Leveraging the Micellar Effect: Gold-Catalyzed Dehydrative Cyclizations in Water at Room Temperature. *Org. Lett.* 2014, **16**, 724–726.

15. Handa, S.; Jin, B.; Bora, P. P.; Wang, Y.; Zhang, X.; Gallou, F.; Reilly, J.; Lipshutz, B. H. Sonogashira Couplings Catalyzed by Fe Nanoparticles Containing Ppm Levels of Reusable Pd, under Mild Aqueous Micellar Conditions. *ACS Catal.* 2019, **9**, 2423–2431.

16. Lipshutz, B. H.; Abela, A. R. Micellar Catalysis of Suzuki-Miyaura Cross-Couplings with Heteroaromatics in Water. *Org. Lett.* 2008, **10**, 5329–5332.

17. Lipshutz, B. H.; Petersen, T. B.; Abela, A. R. Room-Temperature Suzuki-Miyaura Couplings in Water Facilitated by Nonionic Amphiphiles. *Org. Lett.* 2008, **10**, 1333–1336.

18. Lipshutz, B. H.; Ghorai, S.; Leong, W. W. Y.; Taft, B. R.; Krogstad, D. V. Manipulating Micellar Environments for Enhancing Transition Metal-Catalyzed Cross-Couplings in Water at Room Temperature. *J. Org. Chem.* 2011, **76**, 5061–5073.

19. Lipshutz, B. H.; Hageman, M.; Fennewald, J. C.; Linstadt, R.; Slack, E.; Voigtritter, K. Selective Oxidations of Activated Alcohols in Water at Room Temperature. *Chem. Commun.* 2014, **50**, 11378–11381.

20. Feng, J.; Handa, S.; Gallou, F.; Lipshutz, B. H. Safe and Selective Nitro Group Reductions Catalyzed by Sustainable and Recyclable Fe/Ppm Pd Nanoparticles in Water at Room Temperature. *Angew. Chemie - Int. Ed.* 2016, **55**, 8979–8983.

21. Cortes-Clerget, M.; Spink, S. E.; Gallagher, G. P.; Chaisemartin, L.; Filaire, E.; Berthon, J. Y.; Lipshutz, B. H. MC-1. A "Designer" Surfactant Engineered for Peptide Synthesis in Water at Room Temperature. *Green Chem.* 2019, **21**, 2610–2614.

22. Minkler, S. R. K.; Lipshutz, B. H.; Krause, N. Gold Catalysis in Micellar Systems. *Angew. Chemie - Int. Ed.* 2011, **50**, 7820–7823.

23. Lipshutz, B. H.; Gallou, F.; Handa, S. Evolution of Solvents in Organic Chemistry. *ACS Sustain. Chem. Eng.* 2016, **4**, 5838–5849.

24. Lipshutz, B. H.; Aguinaldo, G. T.; Ghorai, S.; Voigtritter, K. Olefin Cross-Metathesis Reactions at Room Temperature Using the Nonionic Amphiphile "PTS": Just Add Water. *Org. Lett.* 2008, **10**, 1325–1328.

25. Klumphu, P.; Lipshutz, B. H. "nok": A Phytosterol-Based Amphiphile Enabling Transition-Metal-Catalyzed Couplings in Water at Room Temperature. *J. Org. Chem.* 2014, **79**, 888–900.

26. Cotanda, P.; Petzetakis, N.; O'reilly, R. K. Catalytic Polymeric Nanoreactors: More than a Solid Supported Catalyst. *MRS Commun.* 2012, **2**, 119–126.

27. Lu, A.; O'Reilly, R. K. Advances in Nanoreactor Technology Using Polymeric Nanostructures. *Curr. Opin. Biotechnol.* 2013, **24**, 639–645.

28. Lempke, L.; Ernst, A.; Kahl, F.; Weberskirch, R.; Krause, N. Sustainable Micellar Gold Catalysis - Poly(2-Oxazolines) as Versatile Amphiphiles. *Adv. Synth. Catal.* 2016, **358**, 1491–1499.

29. Choi, S. H.; Bates, F. S.; Lodge, T. P. Molecular Exchange in Ordered Diblock Copolymer Micelles. *Macromolecules* 2011, **44**, 3594–3604.

30. Cooksey, T. J.; Singh, A.; Le, K. M.; Wang, S.; Kelley, E. G.; He, L.; Vajjala Kesava, S.; Gomez, E. D.; Kidd, B. E.; Madsen, L. A.; *et al.* Tuning Biocompatible Block Copolymer Micelles by Varying Solvent Composition: Core/Corona Structure and Solvent Uptake. *Macromolecules* 2017, **50**, 4322–4334.

31. Lu, A.; Cotanda, P.; Patterson, J. P.; Longbottom, D. A.; O'Reilly, R. K. Aldol Reactions Catalyzed by L-Proline Functionalized Polymeric Nanoreactors in Water. *Chem. Commun.* 2012, **48**, 9699–9701.

32. De Martino, M. T.; Abdelmohsen, L. K. E. A.; Rutjes, F. P. J. T.; Van Hest, J. C. M. Nanoreactors for Green Catalysis. *Beilstein J. Org. Chem.* 2018, **14**, 716–733.

33. Thompson, D. T. Using Gold Nanoparticles for Catalysis. *Nano Today* 2007, **2**, 40–43.

34. Chakraborty, S.; Ansar, S. M.; Stroud, J. G.; Kitchens, C. L. Comparison of Colloidal versus Supported Gold Nanoparticle Catalysis. *J. Phys. Chem. C* 2018, **122**, 7749–7758.

35. Mitsudome, T.; Kaneda, K. Gold Nanoparticle Catalysts for Selective Hydrogenations. *Green Chem.* 2013, **15**, 2636–2654.

36. Zhao, P.; Feng, X.; Huang, D.; Yang, G.; Astruc, D. Basic Concepts and Recent Advances in Nitrophenol Reduction by Gold- and Other Transition Metal Nanoparticles. *Coord. Chem. Rev.* 2015, **287**, 114–136.

37. Deraedt, C.; Salmon, L.; Gatard, S.; Ciganda, R.; Hernandez, R.; Mayor, M.; Astruc, D. Sodium Borohydride Stabilizes Very Active Gold Nanoparticle Catalysts. *Chem. Commun.* 2014, **50**, 14194–14196.

38. Guo, M.; He, J.; Li, Y.; Ma, S.; Sun, X. One-Step Synthesis of Hollow Porous Gold Nanoparticles with Tunable Particle Size for the Reduction of 4-Nitrophenol. *J. Hazard. Mater.* 2016, **310**, 89–97.

39. Zhao, P.; Zhao, P.; Salmon, L.; Liu, N.; Ruiz, J.; Astruc, D. How a Simple 'Clicked' PEGylated 1,2,3-Triazole Ligand Stabilizes Gold Nanoparticles for Multiple Usage. *Chem. Commun.* 2013, **49**, 3218–3220.

40. Huang, D.; Yang, G.; Feng, X.; Lai, X.; Zhao, P. Triazole-Stabilized Gold and Related Noble Metal Nanoparticles for 4-Nitrophenol Reduction. *New J. Chem.* 2015, **39**, 4685–4694.

41. Su, S.; Yue, G.; Huang, D.; Yang, G.; Lai, X.; Zhao, P. Parts per Million Level, Green, and Magnetically-Recoverable Triazole Ligand-Stabilized Au and Pd Nanoparticle Catalysts. *RSC Adv.* 2015, **5**, 44018–44021.

42. Lü, J.; Yang, Y.; Gao, J.; Duan, H.; Lü, C. Thermoresponsive Amphiphilic Block Copolymer-Stablilized Gold Nanoparticles: Synthesis and High Catalytic Properties. *Langmuir* 2018, **34**, 8205–8214.

43. Dai, Y.; Yu, P.; Zhang, X.; Zhuo, R. Gold Nanoparticles Stabilized by Amphiphilic Hyperbranched Polymers for Catalytic Reduction of 4-Nitrophenol. *J. Catal.* 2016, **337**, 65–71.

44. Dai, Y.; Ren, T.; Wang, Y.; Zhang, X. Polyion Complex Micelles to Stabilize Gold Nanoparticles for Catalytic Reduction of 4-Nitrophenol. *Gold Bull.* 2018, **51**, 21–26.

45. Ye, Y.; Jin, M.; Wan, D. One-Pot Synthesis of Porous Monolith-Supported Gold Nanoparticles as an Effective Recyclable Catalyst. *J. Mater. Chem. A* 2015, **3**, 13519–13525.

46. Liu, X.; Liu, F.; Astruc, D.; Lin, W.; Gu, H. Highly-Branched Amphiphilic Organometallic Dendronized Diblock Copolymer: ROMP Synthesis, Self-Assembly and Long-Term Au and Ag Nanoparticle Stabilizer for High-Efficiency Catalysis. *Polymer (Guildf).* 2019, **173**, 1–10.

47. Fenger, R.; Fertitta, E.; Kirmse, H.; Thünemann, A. F.; Rademann, K. Size Dependent Catalysis with CTAB-Stabilized Gold Nanoparticles. *Phys. Chem. Chem. Phys.* 2012, **14**, 9343–9349.

48. Suchomel, P.; Kvitek, L.; Prucek, R.; Panacek, A.; Halder, A.; Vajda, S.; Zboril, R. Simple Size-Controlled Synthesis of Au Nanoparticles and Their Size-Dependent Catalytic Activity. *Sci. Rep.* 2018, **8**, 1–11.

49. Gu, S.; Kaiser, J.; Marzun, G.; Ott, A.; Lu, Y.; Ballauff, M.; Zaccone, A.; Barcikowski, S.; Wagener, P. Ligand-Free Gold Nanoparticles as a Reference Material for Kinetic Modelling of Catalytic Reduction of 4-Nitrophenol. *Catal. Letters* 2015, **145**, 1105–1112.

50. Ansar, S. M.; Kitchens, C. L. Impact of Gold Nanoparticle Stabilizing Ligands on the Colloidal Catalytic Reduction of 4-Nitrophenol. *ACS Catal.* 2016, **6**, 5553–5560.

51. Chakraborty, S.; Kitchens, C. L. Modifying Ligand Chemistry to Enhance Reusability of PH-Responsive Colloidal Gold Nanoparticle Catalyst. *J. Phys. Chem. C* 2019, **123**, 26450–26459.

52. Ansar, S. M.; Chakraborty, S.; Kitchens, C. L. PH-Responsive Mercaptoundecanoic Acid Functionalized Gold Nanoparticles and Applications in Catalysis. *Nanomaterials* 2018, **8**, 1–12.

53. Blanazs, A.; Armes, S. P.; Ryan, A. J. Self-Assembled Block Copolymer Aggregates: From Micelles to Vesicles and Their Biological Applications. *Macromol. Rapid Commun.* 2009, **30**, 267–277.

54. Gu, S.; Wunder, S.; Lu, Y.; Ballauff, M.; Fenger, R.; Rademann, K.; Jaquet, B.; Zaccone, A. Kinetic Analysis of the Catalytic Reduction of 4-Nitrophenol by Metallic Nanoparticles. *J. Phys. Chem. C* 2014, **118**, 18618–18625.

55. Wunder, S.; Lu, Y.; Albrecht, M.; Ballauff, M. Catalytic Activity of Faceted Gold Nanoparticles Studied by a

Model Reaction: Evidence for Substrate-Induced Surface Restructuring. *ACS Catal.* 2011, **1**, 908–916.

56. Wei, W.; Wu, S.; Shen, X.; Zhu, M.; Li, S. Nanoreactor with Core–Shell Architectures Used as Spatiotemporal Compartments for "Undisturbed" Tandem Catalysis. *J. Inorg. Organomet. Polym. Mater.* 2019, **29**, 1235–1242.

57. Sand, H.; Weberskirch, R. Chemoenzymatic One-Pot Reaction of Noncompatible Catalysts: Combining Enzymatic Ester Hydrolysis with Cu(i)/Bipyridine Catalyzed Oxidation in Aqueous Medium. *RSC Adv.* 2017, **7**, 33614–33626.

58. Lu, A.; O'Reilly, R. K. Advances in Nanoreactor Technology Using Polymeric Nanostructures. *Curr. Opin. Biotechnol.* 2013, **24**, 639–645.

59. Peters, R. J. R. W.; Marguet, M.; Marais, S.; Fraaije, M. W.; Van Hest, J. C. M.; Lecommandoux, S. Cascade Reactions in Multicompartmentalized Polymersomes. *Angew. Chemie - Int. Ed.* 2014, **53**, 146–150.

60. Nicolaou, K. C.; Montagnon, T.; Snyder, S. A. Tandem Reactions, Cascade Sequences, and Biomimetic Strategies in Total Synthesis. *Chem. Commun.* 2003, **3**, 551–564.

61. Montolio, S.; Vicent, C.; Aseyev, V.; Alfonso, I.; Burguete, M. I.; Tenhu, H.; García-Verdugo, E.; Luis, S. V. AuNP-Polymeric Ionic Liquid Composite Multicatalytic Nanoreactors for One-Pot Cascade Reactions. *ACS Catal.* 2016, **6**, 7230–7237.

62. Cho, A.; Byun, S.; Kim, B. M. AuPd−Fe3O4 Nanoparticle Catalysts for Highly Selective, One-Pot Cascade Nitro-Reduction and Reductive Amination. *Adv. Synth. Catal.* 2018, **360**, 1253–1261.

63. Poupart, R.; Benlahoues, A.; Le Droumaguet, B.; Grande, D. Porous Gold Nanoparticle-Decorated Nanoreactors Prepared from Smartly Designed Functional Polystyrene-Block-Poly(d, l -Lactide) Diblock Copolymers: Toward Efficient Systems for Catalytic Cascade Reaction Processes. *ACS Appl. Mater. Interfaces* 2017, **9**, 31279–31290.

64. Zuo, C.; Wei, W.; Zhou, Q.; Wu, S.; Li, S. Artificial Active Nanoreactor with Nature-Inspired Sequential Catalytic Ability. *ChemistrySelect* 2017, **2**, 6149–6153.

65. Prathap, K. J.; Wu, Q.; Olsson, R. T.; Dinér, P. Catalytic Reductions and Tandem Reactions of Nitro Compounds Using in Situ Prepared Nickel Boride Catalyst in Nanocellulose Solution. *Org. Lett.* 2017, **19**, 4746–4749.

66. Guo, Y.; Feng, L.; Wang, X.; Zhang, X. Integration of Yolk-Shell Units into a Robust and Highly Reactive Nanoreactor: A Platform for Cascade Reactions. *Chem. Commun.* 2019, **55**, 3093–3096.

67. Miyamura, H.; Kobayashi, S. Tandem Oxidative Processes Catalyzed by Polymer-Incarcerated Multimetallic Nanoclusters with Molecular Oxygen. *Acc. Chem. Res.* 2014, **47**, 1054–1066.

68. Lipshutz, Bruce H.Ghorai, S. Transitioning Organic Synthesis From Organic Solvents to Water. What's Your E-Factor? *Green Chem.* 2014, **16**, 3660–3679.

69. Lu, A.; Moatsou, D.; Hands-Portman, I.; Longbottom, D. A.; O'Reilly, R. K. Recyclable L-Proline Functional Nanoreactors with Temperature-Tuned Activity Based on Core-Shell Nanogels. *ACS Macro Lett.* 2014, **3**, 1235–1239.

70. Schrinner, M.; Polzer, F.; Mei, Y.; Lu, Y.; Haupt, B.; Ballauff, M.; Göldel, A.; Drechsler, M.; Preussner, J.; Glatzel, U. Mechanism of the Formation of Amorphous Gold Nanoparticles within Spherical Polyelectrolyte Brushes. *Macromol. Chem. Phys.* 2007, **208**, 1542–1547.

71. Tang, C.; Amin, D.; Messersmith, P. B.; Anthony, J. E.; Prud'homme, R. K. Polymer Directed Self-Assembly of PH-Responsive Antioxidant Nanoparticles. *Langmuir* 2015, **31**, 3612–3620.

72. D'Addio, S. M.; Prud'homme, R. K. Controlling Drug Nanoparticle Formation by Rapid Precipitation. *Adv. Drug Deliv. Rev.* 2011, **63**, 417–426.

73. Pinkerton, N. M.; Gindy, M. E.; Calero-Ddelc, V. L.; Wolfson, T.; Pagels, R. F.; Adler, D.; Gao, D.; Li, S.; Wang, R.; Zevon, M.; *et al.* Single-Step Assembly of Multimodal Imaging Nanocarriers: MRI and Long-Wavelength Fluorescence Imaging. *Adv. Healthc. Mater.* 2015, **4**, 1376–1385.

74. Zhang, X.; Cardozo, A. F.; Chen, S.; Zhang, W.; Julcour, C.; Lansalot, M.; Blanco, J. F.; Gayet, F.; Delmas, H.; Charleux, B.; *et al.* Core-Shell Nanoreactors for Efficient Aqueous Biphasic Catalysis. *Chem. - A Eur. J.* 2014,

20, 15505–15517.

75. Lu, Y.; Mei, Y.; Ballauff, M.; Drechsler, M. Thermosensitive Core-Shell Particles as Carrier Systems for Metallic Nanoparticles. *J. Phys. Chem. B* 2006, **110**, 3930–3937.

76. Wunder, S.; Lu, Y.; Albrecht, M.; Ballauff, M. Catalytic Activity of Faceted Gold Nanoparticles Studied by a Model Reaction: Evidence for Substrate-Induced Surface Restructuring. *ACS Catal.* 2011, **1**, 908–916.

77. Hervés, P.; Pérez-Lorenzo, M.; Liz-Marzán, L. M.; Dzubiella, J.; Lu, Y.; Ballauff, M. Catalysis by Metallic Nanoparticles in Aqueous Solution: Model Reactions. *Chem. Soc. Rev.* 2012, **41**, 5577.

78. Gindy, M. E.; Panagiotopoulos, A. Z.; Prud'Homme, R. K. Composite Block Copolymer Stabilized Nanoparticles: Simultaneous Encapsulation of Organic Actives and Inorganic Nanostructures. *Langmuir* 2008, **24**, 83–90.

79. Walther, A.; Muller, A. H. E. Janus Particles : Synthesis , Self-Assembly , Physical Properties , and Applications. *Chem. Rev.* 2013, **113**, 5194–5261.

80. Isley, N. A.; Dobarco, S.; Lipshutz, B. H. Installation of Protected Ammonia Equivalents onto Aromatic & Heteroaromatic Rings in Water Enabled by Micellar Catalysis. *Green Chem.* 2014, **16**, 1480–1488.

81. Gall, B.; Bortenschlager, M.; Nuyken, O.; Weberskirch, R. Cascade Reactions in Polymeric Nanoreactors : Mono (Rh) - and Bimetallic (Rh / Ir) Micellar Catalysis in the Hydroaminomethylation of 1-Octene. 2008, 1152–1159.

82. Cotanda, P.; O'Reilly, R. K. Molecular Recognition Driven Catalysis Using Polymeric Nanoreactors. *Chem. Commun.* 2012, **48**, 10280–10282.

83. Lan, Y.; Yang, L.; Zhang, M.; Zhang, W.; Wang, S. Microreactor of Pd Nanoparticles Immobilized Hollow Microspheres for Catalytic Hydrodechlorination of Chlorophenols in Water. *ACS Appl. Mater. Interfaces* 2010, **2**, 127–133.

84. Angioletti-Uberti, S.; Lu, Y.; Ballauff, M.; Dzubiella, J. Theory of Solvation-Controlled Reactions in Stimuli-

Responsive Nanoreactors. *J. Phys. Chem. C* 2015, **119**, 15723–15730.

85. Peter, N.; Tan, B.; Lee, C. H.; Li, P. Green Synthesis of Smart Metal / Polymer Nanocomposite Particles and Their Tuneable Catalytic Activities. 2016.

86. Han, J.; Zhu, Z.; Gian, H.; Wohl, A. R.; Beaman, Charles, J.; Hoye, T. R.; Macosko, C. W. A Simple Confined Impingement Jets Mixer for Flash Nanoprecipitation. *J. Pharm. Sci.* 2012, **101**, 4018–4023.

87. Viegas, A.; Manso, J.; Nobrega, F. L.; Cabrita, E. J. Saturation-Transfer Difference (STD) NMR: A Simple and Fast Method for Ligand Screening and Characterization of Protein Binding. *J. Chem. Educ.* 2011, **88**, 990–994.

88. Momot, K. I.; Kuchel, P. W. Pulsed Field Gradient Nuclear Magnetic Resonance as a Tool for Studying Drug Delivery Systems. *Concepts Magn. Reson.* 2003, **19A**, 51–64.

89. Mun, E. A.; Hannell, C.; Rogers, S. E.; Hole, P.; Williams, A. C.; Khutoryanskiy, V. V. On the Role of Specific Interactions in the Diffusion of Nanoparticles in Aqueous Polymer Solutions. *Langmuir* 2014, **30**, 308–317.

90. Wang, J. H. Self-Diffusion Coefficients of Water. *J. Phys. Chem.* 1965, **69**, 4412–4412.

91. Johnson, B. K.; Prud, R. K. Chemical Processing and Micromixing in Confined Impinging Jets. 2003, **49**.

92. Liu, Y.; Kathan, K.; Saad, W.; Prud, R. K. Ostwald Ripening of β-Carotene Nanoparticles. 2007, **036102**, 8–11.

93. Vaia, R. A.; Maguire, J. F. Polymer Nanocomposites with Prescribed Morphology: Going beyond Nanoparticle-Filled Polymers. *Chem. Mater.* 2007, **19**, 2736–2751.

94. Ghosh, S. K.; Nath, S.; Kundu, S.; Esumi, K.; Pal, T. Solvent and Ligand Effects on the Localized Surface Plasmon Resonance (LSPR) of Gold Colloids. *J. Phys. Chem. B* 2004, **108**, 13963–13971.

95. Lange, H.; Juárez, B. H.; Carl, A.; Richter, M.; Bastús, N. G.; Weller, H.; Thomsen, C.; Von Klitzing, R.; Knorr, A. Tunable Plasmon Coupling in Distance-Controlled Gold Nanoparticles. *Langmuir* 2012, **28**, 8862–8866.

96. Tang, C.; Sosa, C. L.; Pagels, R. F.; Priestley, R. D.; Prud'Homme, R. K. Efficient Preparation of Size Tunable PEGylated Gold Nanoparticles. *J. Mater. Chem. B* 2016, **4**, 4813–4817.

97. Pagels, R. F.; Edelstein, J.; Tang, C.; Prud'homme, R. K. Controlling and Predicting Nanoparticle Formation by Block Copolymer Directed Rapid Precipitations. *Nano Lett.* 2018, **18**, 1139–1144.

98. Tang, C.; Prud'homme, R. K. Targeted Theragnostic Nanoparticles Via Flash Nanoprecipitation: Principles of Material Selection. In *Polymer Nanoparticles for Nanomedicines*; Springer International Publishing: Cham, 2016; pp. 55–85.

99. Tadele, K.; Verma, S.; Nadagouda, M. N.; Gonzalez, M. A.; Varma, R. S. A Rapid Flow Strategy for the Oxidative Cyanation of Secondary and Tertiary Amines via C-H Activation. *Sci. Rep.* 2017, 6–10.

100. Nigra, M. M.; Ha, J. M.; Katz, A. Identification of Site Requirements for Reduction of 4-Nitrophenol Using Gold Nanoparticle Catalysts. *Catal. Sci. Technol.* 2013, **3**, 2976–2983.

101. Zhang, M.; Liu, L.; Wu, C.; Fu, G.; Zhao, H.; He, B. Synthesis, Characterization and Application of Well-Defined Environmentally Responsive Polymer Brushes on the Surface of Colloid Particles. *Polymer (Guildf).* 2007, **48**, 1989–1997.

102. Menumerov, E.; Hughes, R. A.; Neretina, S. Catalytic Reduction of 4-Nitrophenol: A Quantitative Assessment of the Role of Dissolved Oxygen in Determining the Induction Time. *Nano Lett.* 2016, **16**, 7791–7797.

103. D'Addio, S. M.; Saad, W.; Ansell, S. M.; Squiers, J. J.; Adamson, D. H.; Herrera-Alonso, M.; Wohl, A. R.; Hoye, T. R.; MacOsko, C. W.; Mayer, L. D.; *et al.* Effects of Block Copolymer Properties on Nanocarrier Protection from in Vivo Clearance. *J. Control. Release* 2012, **162**, 208–217.

104. Budijono, S. J.; Russ, B.; Saad, W.; Adamson, D. H.; Prud'homme, R. K. Block Copolymer Surface Coverage on Nanoparticles. *Colloids Surfaces A Physicochem. Eng. Asp.* 2010, **360**, 105–110.

105. Chang, Y. C.; Chen, D. H. Catalytic Reduction of 4-Nitrophenol by Magnetically Recoverable Au Nanocatalyst. *J. Hazard. Mater.* 2009, **165**, 664–669.

106. Ncube, P.; Bingwa, N.; Baloyi, H.; Meijboom, R. Catalytic Activity of Palladium and Gold Dendrimer-Encapsulated Nanoparticles for Methylene Blue Reduction: A Kinetic Analysis. *Appl. Catal. A Gen.* 2015, **495**, 63–71.

107. Narayan, S.; Muldoon, J.; Finn, M. G.; Fokin, V. V.; Kolb, H. C.; Sharpless, K. B. "On Water": Unique Reactivity of Organic Compounds in Aqueous Suspension. *Angew. Chemie - Int. Ed.* 2005, **44**, 3275–3279.

108. Liu, X.; Mu, S.; Long, Y.; Qiu, G.; Ling, Q.; Gu, H.; Lin, W. Gold Nanoparticles Stabilized by 1,2,3-Triazolyl Dendronized Polymers as Highly Efficient Nanoreactors for the Reduction of 4-Nitrophenol. *Catal. Letters* 2019, **149**, 544–551.

109. Mei, Y.; Lu, Y.; Polzer, F.; Ballauff, M.; Drechsler, M. Catalytic Activity of Palladium Nanoparticles Encapsulated in Spherical Poly Electrolyte Brushes and Core-Shell Microgels. *Chem. Mater.* 2007, **19**, 1062–1069.

110. Harrison, A.; Vuong, T.; Zeevi, M.; Hittel, B.; Wi, S.; Tang, C. Rapid Self-Assembly of Metal/Polymer Nanocomposite Particles as Nanoreactors and Their Kinetic Characterization. *Nanomaterials* 2019, **9**, 318.

111. Teimouri, M.; Khosravi-Nejad, F.; Attar, F.; Saboury, A. A.; Kostova, I.; Benelli, G.; Falahati, M. Gold Nanoparticles Fabrication by Plant Extracts: Synthesis, Characterization, Degradation of 4-Nitrophenol from Industrial Wastewater, and Insecticidal Activity – A Review. *J. Clean. Prod.* 2018, **184**, 740–753.

112. Kong, X. K.; Sun, Z. Y.; Chen, M.; Chen, C. Le; Chen, Q. W. Metal-Free Catalytic Reduction of 4-Nitrophenol to 4-Aminophenol by N-Doped Graphene. *Energy Environ. Sci.* 2013, **6**, 3260–3266.

113. Vaidya, M. J.; Kulkarni, S. M.; Chaudhari, R. V. Synthesis of P-Aminophenol by Catalytic Hydrogenation of p-Nitrophenol. *Org. Process Res. Dev.* 2003, **7**, 202–208.

114. Cotanda, P.; Petzetakis, N.; O'reilly, R. K. Catalytic Polymeric Nanoreactors: More than a Solid Supported Catalyst. *MRS Commun.* 2012, **2**, 119–126.

115. Dabbagh, A.; Mahmoodian, R.; Johan, B.; Abdullah, J. Low-Melting-Point Polymeric Nanoshells for Thermal-Triggered Drug Release under Hyperthermia Condition Low-Melting-Point Polymeric Nanoshells for Thermal-Triggered Drug Release under Hyperthermia Condition. 2015.

116. Wang, Z.; Tan, B.; Hussain, I.; Schaeffer, N.; Wyatt, M. F.; Brust, M.; Cooper, A. I. Design of Polymeric Stabilizers for Size-Controlled Synthesis of Monodisperse Gold Nanoparticles in Water. *Langmuir* 2007, **23**,

885–895.

117. Hegetschweiler, A.; Kraus, T.; Staudt, T. Colloidal Analysis of Particles Extracted from Microalloyed Steel. *Metall. Ital.* 2017, **109**, 23–28.

118. Pamies, R.; Cifre, J. G. H.; Espín, V. F.; Collado-González, M.; Baños, F. G. D.; De La Torre, J. G. Aggregation Behaviour of Gold Nanoparticles in Saline Aqueous Media. *J. Nanoparticle Res.* 2014, **16**.

119. Cheng, W.; Wang, E. Size-Dependent Phase Transfer of Gold Nanoparticles from Water into Toluene by Tetraoctylammonium Cations: A Wholly Electrostatic Interaction. *J. Phys. Chem. B* 2004, **108**, 24–26.

120. Gittins, D. I.; Caruso, F. Spontaneous Phase Transfer of Nanoparticulate Metals from Organic to Aqueous Media. *Angew. Chemie - Int. Ed.* 2001, **40**, 3001–3004.

121. Gu, S.; Kaiser, J.; Marzun, G.; Ott, A.; Lu, Y.; Ballauff, M.; Zaccone, A.; Barcikowski, S.; Wagener, P. Ligand-Free Gold Nanoparticles as a Reference Material for Kinetic Modelling of Catalytic Reduction of 4-Nitrophenol. *Catal. Letters* 2015, **145**, 1105–1112.

122. Neal, R. D.; Inoue, Y.; Hughes, R. A.; Neretina, S. Catalytic Reduction of 4-Nitrophenol by Gold Catalysts: The Influence of Borohydride Concentration on the Induction Time. *J. Phys. Chem. C* 2019, **123**, 12894–12901.

123. Gregor, L.; Reilly, A. K.; Dickstein, T. A.; Mazhar, S.; Bram, S.; Morgan, D. G.; Losovyj, Y.; Pink, M.; Stein, B. D.; Matveeva, V. G.; *et al.* Facile Synthesis of Magnetically Recoverable Pd and Ru Catalysts for 4-Nitrophenol Reduction: Identifying Key Factors. *ACS Omega* 2018, **3**, 14717–14725.

124. Liu, Y.; Xu, L.; Liu, X.; Cao, M. Hybrids of Gold Nanoparticles with Core-Shell Hyperbranched Polymers: Synthesis, Characterization, and Their High Catalytic Activity for Reduction of 4-Nitrophenol. *Catalysts* 2015, **6**.

125. Gao, D.; Zhang, X.; Dai, X.; Qin, Y.; Duan, A.; Yu, Y.; Zhuo, H.; Zhao, H.; Zhang, P.; Jiang, Y.; *et al.* Morphology-Selective Synthesis of Active and Durable Gold Catalysts with High Catalytic Performance in the Reduction of 4-Nitrophenol. *Nano Res.* 2016, **9**, 3099–3115.

126. Chen, Z.; Cui, Z. M.; Cao, C. Y.; He, W. D.; Jiang, L.; Song, W. G. Temperature-Responsive Smart Nanoreactors: Poly(N-Isopropylacrylamide)- Coated Au@mesoporous-SiO2 Hollow Nanospheres. *Langmuir* 2012, **28**, 13452–13458.

127. Liu, Y.; Li, M.; Chen, G. A New Type of Raspberry-like Polymer Composite Sub-Microspheres with Tunable Gold Nanoparticles Coverage and Their Enhanced Catalytic Properties. *J. Mater. Chem. A* 2013, **1**, 930–937.

128. Wang, L.; Yang, Q.; Cui, Y.; Gao, D.; Kang, J.; Sun, H.; Zhu, L.; Chen, S. Highly Stable and Biocompatible Dendrimer-Encapsulated Gold Nanoparticle Catalysts for the Reduction of 4-Nitrophenol. *New J. Chem.* 2017, **41**, 8399–8406.

129. Wang, S.; Zhang, J.; Yuan, P.; Sun, Q.; Jia, Y.; Yan, W.; Chen, Z.; Xu, Q. Au Nanoparticle Decorated N-Containing Polymer Spheres: Additive-Free Synthesis and Remarkable Catalytic Behavior for Reduction of 4-Nitrophenol. *J. Mater. Sci.* 2015, **50**, 1323–1332.

130. Peng, P.; Shi, B.; Jia, L.; Li, B. Relationship between Hansen Solubility Parameters of ABS and Its Homopolymer Components of PAN, PB, and PS. *J. Macromol. Sci. Part B Phys.* 2010, **49**, 864–869.

131. Hansen, C. M. *Hansen Solubility Parameters: A User's Handbook*; Second.; Taylor and Francis Group, LLC., 2007.

132. Batista, M. M.; Guirardello, R.; Krähenbühl, M. A. Determination of the Solubility Parameters of Biodiesel from Vegetable Oils. *Energy and Fuels* 2013, **27**, 7497–7509.

133. Antonels, N. C.; Meijboom, R. Preparation of Well-Defined Dendrimer Encapsulated Ruthenium Nanoparticles and Their Evaluation in the Reduction of 4-Nitrophenol According to the Langmuir-Hinshelwood Approach. *Langmuir* 2013, **29**, 13433–13442.

134. Blanco, E.; Atienzar, P.; Hernández, P.; Quintana, C. The Langmuir-Hinshelwood Approach for Kinetic Evaluation of Cucurbit[7]Uril-Capped Gold Nanoparticles in the Reduction of the Antimicrobial Nitrofurantoin. *Phys. Chem. Chem. Phys.* 2017, **19**, 18913–18923.

135. Rautiainen, S.; Simakova, O.; Guo, H.; Leino, A. R.; Kordás, K.; Murzin, D.; Leskelä, M.; Repo, T. Solvent Controlled Catalysis: Synthesis of Aldehyde, Acid or Ester by Selective Oxidation of Benzyl Alcohol with

Gold Nanoparticles on Alumina. *Appl. Catal. A Gen.* 2014, **485**, 202–206.

136. Bekhradnia, A. R.; Zahir, F.; Arshadi, S. Selective Oxidation of Organic Compounds Using Pyridinium-1-Sulfonate Fluorochromate, C5H5NSO3H [CrO3F] (PSFC). *Monatshefte fur Chemie* 2008, **139**, 521–523.

137. Zhu, J.; Wang, P. C.; Lu, M. Selective Oxidation of Benzyl Alcohol under Solvent-Free Condition with Gold Nanoparticles Encapsulated in Metal-Organic Framework. *Appl. Catal. A Gen.* 2014, **477**, 125–131.

138. Passos, M. L.; Ribiero, C. P. *Innovation in Food Engineering : New Techniques and Products*; CRC Press, 2009.

139. Santonastaso, M.; Freakley, S. J.; Miedziak, P. J.; Brett, G. L.; Edwards, J. K.; Hutchings, G. J. Oxidation of Benzyl Alcohol Using in Situ Generated Hydrogen Peroxide. *Org. Process Res. Dev.* 2014, **18**, 1455–1460.

140. Göksu, H.; Burhan, H.; Mustafov, S. D.; Şen, F. Oxidation of Benzyl Alcohol Compounds in the Presence of Carbon Hybrid Supported Platinum Nanoparticles (Pt@CHs) in Oxygen Atmosphere. *Sci. Rep.* 2020, **10**, 1–8.

141. Nagy, G.; Beck, A.; Sáfrán, G.; Schay, Z.; Liu, S.; Li, T.; Qiao, B.; Wang, J.; Lázár, K. Nanodisperse Gold Catalysts in Oxidation of Benzyl Alcohol: Comparison of Various Supports under Different Conditions. *React. Kinet. Mech. Catal.* 2019, **128**, 71–95.

142. Tsunoyama, H.; Sakurai, H.; Negishi, Y.; Tsukuda, T. Size-Specific Catalytic Activity of Polymer-Stabilized Gold Nanoclusters for Aerobic Alcohol Oxidation in Water. *J. Am. Chem. Soc.* 2005, **127**, 9374–9375.

143. Buonerba, A.; Cuomo, C.; Ortega Sánchez, S.; Canton, P.; Grassi, A. Gold Nanoparticles Incarcerated in Nanoporous Syndiotactic Polystyrene Matrices as New and Efficient Catalysts for Alcohol Oxidations. *Chem. - A Eur. J.* 2012, **18**, 709–715.

144. Ferraz, C. P.; Garcia, M. A. S.; Teixeira-Neto, É.; Rossi, L. M. Oxidation of Benzyl Alcohol Catalyzed by Gold Nanoparticles under Alkaline Conditions: Weak vs. Strong Bases. *RSC Adv.* 2016, **6**, 25279–25285.

145. Sand, H.; Weberskirch, R. Bipyridine-Functionalized Amphiphilic Block Copolymers as Support Materials for the Aerobic Oxidation of Primary Alcohols in Aqueous Media. *RSC Adv.* 2015, **5**, 38235–38242.

146. Xu, Z.; Lu, X. A Novel [3+2] Cycloaddition Approach to Nitrogen Heterocycles via Phosphine-Catalyzed

Reactions of 2,3-Butadienoates or 2-Butynoates and Dimethyl Acetylenedicarboxylate with Imines: A Convenient Synthesis of Pentabromopseudilin. *J. Org. Chem.* 1998, **63**, 5031–5041.

147. Zheng, Y.; Ma, K.; Li, H.; Li, J.; He, J.; Sun, X.; Li, R.; Ma, J. One Pot Synthesis of Imines from Aromatic Nitro Compounds with a Novel Ni/SiO2 Magnetic Catalyst. *Catal. Letters* 2009, **128**, 465–474.

148. Vicini, P.; Geronikaki, A.; Incerti, M.; Busonera, B.; Poni, G.; Cabras, C. A.; La Colla, P. Synthesis and Biological Evaluation of Benzo[d]Isothiazole, Benzothiazole and Thiazole Schiff Bases. *Bioorganic Med. Chem.* 2003, **11**, 4785–4789.

149. Huang, J.; Yu, L.; He, L.; Liu, Y. M.; Cao, Y.; Fan, K. N. Direct One-Pot Reductive Imination of Nitroarenes Using Aldehydes and Carbon Monoxide by Titania Supported Gold Nanoparticles at Room Temperature. *Green Chem.* 2011, **13**, 2672–2677.

150. Layer, R. W. The Chemistry of Imines. *Chem. Rev.* 1963, **63**, 489–510.

151. Bomann, M. D.; Guch, I. C.; DiMare, M. A Mild, Pyridine-Borane-Based Reductive Animation Protocol. *J. Org. Chem.* 1995, **60**, 5995–5996.

152. Guzen, K. P.; Guarezemini, A. S.; Órfão, A. T. G.; Cella, R.; Pereira, C. M. P.; Stefani, H. A. Eco-Friendly Synthesis of Imines by Ultrasound Irradiation. *Tetrahedron Lett.* 2007, **48**, 1845–1848.

153. Zhou, X.; Li, X.; Jiao, L.; Huo, H.; Li, R. Programmed Synthesis Palladium Supported on Fe3O4@C: An Efficient and Heterogeneous Recyclable Catalyst for One-Pot Reductive Amination of Aldehydes with Nitroarenes in Aqueous Reaction Medium. *Catal. Letters* 2015, **145**, 1591–1599.

154. Levit, S. L.; Yang, H.; Tang, C. Rapid Self-Assembly of Polymer Nanoparticles for Synergistic Codelivery of Paclitaxel and Lapatinib via Flash Nanoprecipitation. *Nanomaterials* 2020, **10**, 1–17.

155. Harrison, A.; Zeevi, M. P.; Vasey, C. L.; Nguyen, M. D.; Tang, C. Accelerated Reaction Rates within Self-Assembled Polymer Nanoreactors with Tunable Hydrophobic Microenvironments. 2020, 1–17.

156. Gaborskia, T. R.; Snyder, J. L.; Striemer, C. C.; Fang, D. Z.; Hoffman, M.; Fauchet, P. M.; McGrath, J. L. High

Performance Separation of Nanoparticles with Ultrathin Porous Nanocrystalline Silicon Membranes. *ACS Nano* 2010, **4**, 6973–6981.

157. Shokrolahi, A.; Zali, A.; Keshavarz, M. H. Reductive Amination of Aldehydes and Ketones by NaBH 4 Using Carbon-Based Solid Acid (CBSA) as Catalyst. *Green Chem. Lett. Rev.* 2011, **4**, 195–203.

158. Afzal Khan, S.; Hamayun, M.; Ahmed, S. Degradation of 4-Aminophenol by Newly Isolated Pseudomonas Sp. Strain ST-4. *Enzyme Microb. Technol.* 2006, **38**, 10–13.

159. Kalbasi, R. J.; Mazaheri, O. Facile One-Pot Tandem Reductive Amination of Aldehydes from Nitroarenes over a Hierarchical ZSM-5 Zeolite Containing Palladium Nanoparticles. *New J. Chem.* 2016, **40**, 9627–9637.

160. Ergen, S.; Nişanci, B.; Metin, Ö. One-Pot Reductive Amination of Aldehydes with Nitroarenes Using Formic Acid as the Hydrogen Donor and Mesoporous Graphitic Carbon Nitride Supported AgPd Alloy Nanoparticles as the Heterogeneous Catalyst. *New J. Chem.* 2018, **42**, 10000–10006.

161. Tang, C. H.; He, L.; Liu, Y. M.; Cao, Y.; He, H. Y.; Fan, K. N. Direct One-Pot Reductive N-Alkylation of Nitroarenes by Using Alcohols with Supported Gold Catalysts. *Chem. - A Eur. J.* 2011, **17**, 7172–7177.

162. Nagi Reddy, K. S.; Reddy, K. P.; Sabitha, G. Green Approach for the Domino Reduction/Reductive Amination of Nitroarenes and Chemoselective Reduction of Aldehydes Using Fe/Aq. Citric Acid/Montmorillonite K10. *ChemistrySelect* 2018, **3**, 13670–13674.